This is to certify that the

thesis entitled

AN INVESTIGATION ON THE RETROFITMENT OF AN INDUSTRIAL ROBOTIC MANIPULATOR WITH A COMPOSITE ARM: DESIGN, ANALYSIS, AND FABRICATION

presented by

ALLEN M. MAGOLAN

has been accepted towards fulfillment
of the requirements for

MASTER OF SCIENCE degree in MECHANICAL ENGRG.

G. V. Gandhi

Major professor

Date 31 July 1989

AN INVESTIGATION ON THE RETROFITMENT OF AN INDUSTRIAL ROBOTIC MANIPULATOR WITH A COMPOSITE ARM: DESIGN, ANALYSIS, AND FABRICATION

By

Allen M. Magolan

A THESIS

Submitted to
Michigan State University
in partial fulfillment of the requirements
for the degree of

MASTER OF SCIENCE

Department of Mechanical Engineering

1989

IND

The dyna
which fe
aterial
relative
aluminum
to yield
istics de
relative
forearms
atch st
was fabr
process
using th
percent
natural
The robo
equivale

ABSTRACT

INVESTIGATION ON THE RETROFITMENT OF AN INDUSTRIAL ROBOTIC MANIPULATOR WITH A COMPOSITE ARM: DESIGN, ANALYSIS, AND FABRICATION

By

Allen M. Magolan

The dynamic performance of industrial robotic manipulators which feature structural components fabricated in composite materials yield superior performance characteristics relative to traditional manipulator designs employing aluminum structural components. Composites can be tailored to yield desired stiffness, mass, and damping characteristics depending upon the required application. To evaluate relative dynamic performance between aluminum and composite forearms, a composite laminate sequence was synthesized to match static equivalent stiffnesses. A composite forearm was fabricated for retrofitment on a General Electric P-50 process robot employing graphite/epoxy prepreg material using the hand lay-up technique. The composite arm had 57 percent less mass than the aluminum arm, a higher first natural frequency, and superior damping characteristics. The robot featuring the composite forearm exhibited equivalent performance characteristics.

to my love

I give th
fresh po
help and
give tha
my advis
thanks t
thanks t
Air Indus
lay-up, I
for the e
Mike Mcph
and I giv
Universit
all of th

ACKNOWLEDGEMENTS

I give thanks to Chun-Ying Lee for his endless knowledge and fresh points of view, I give thanks to Sung-Bok Choi for his help and ideas, I give thanks to my father for his money, I give thanks to my family for their support, I give thanks to my advisor Dr. Mukesh Gandhi for his big pictures, I give thanks to Dr. Brian Thompson for his suggestions, I give thanks to Dave Graves, Gary, Tim, Jean, and Jerry of Auto Air Industries for their knowledge and help with composite lay-up, I give thanks to Tom at the MSU Physics Machine Shop for the excellent machining of the arm, I give thanks to Mike McPherson for the great help with the MEL VAX computer, and I give thanks to all of the friends I made at the University of Michigan and Michigan State University, for all of the fun times.

TABLE OF CONTENTS

Table 2.1
current i
and const

Table 2.2
unidirect
metals [8

Table 2.3
for Herc
fabric c
units in
properti

Table 2.

Table 2.
applied
numerica

Table 2.
experime
aluminu

Table 2.
313.9 N
sequence
fabric).

Table 3.
fabrica

Table 4.
loads f

Table 4.
and com

Table 4.
aluminu

LIST OF TABLES

Table 4.
composit
cured si
Air Indu

Table 4.
frequenc
configur
the half
fundamen

Table 4.6
forearms

Table 4.
bar, the
forearm.

Table 4.8
forearms.

Table 5.1
(angles
position

Table 5.2
aluminum
velocity
end-effec

Table 5.3
displace
unloading

Table 5.4
and compo

Table 5.5
and compo
paths.

Table 5.6
with alum
response

Table 5.7
aluminum
response

Table 5.8
with alum
response

Table 5.
aluminum
response

LIST OF FIGURES

LIST OF FIGURES

Th

cating,

Electric

composit

characte

the comp

composit

shoot an

those of

mass of

1.1 Mo

Th

enhanced

The equa

dynamic

Where (x

[M] is t

the stif

modal re

field as

Referrin

CHAPTER 1

INTRODUCTION

The project undertaken consisted of designing, fabricating, and testing a composite forearm for a General Electric P-50 robotic manipulator. After fabricating the composite arm, tests were conducted to compare performance characteristics such as overshoot and settling-time between the composite arm and the original aluminum arm. By using composite materials for the forearm of the GE P-50, overshoot and settling-time during maneuvers were equivalent to those of the P-50 with the original aluminum arm, while the mass of the forearm was reduced by 60 percent.

1.1 MOTIVATION OF TOPIC

The performance of robotic manipulators can be enhanced by fabricating members with composite materials. The equations of motion for a finite element analysis of a dynamic system are (from Choi [1]),

$$[M]\{\ddot{x}\} + [C]\{\dot{x}\} + [K]\{x\} = \{F\} - [M]\{P_R\},$$

where $\{x\}$ is a row vector containing nodal displacements, $[M]$ is the mass matrix, $[C]$ is the damping matrix, $[K]$ is the stiffness matrix, $\{F\}$ is the sum of external forces and nodal reaction forces, and $\{P_R\}$ is the discrete velocity field associated with the rigid body motion of each node. Referring to this equation, it is clear that decreasing the

mass red
indicate
properti
structur

In

robots c
to incre
hazardou
composit
employed
lightwei
and yet
In each
invaluab

In

for high
military
responsi
being in
of opera
restrict
upon the
systems.
developm
for the

mass reduces the inertial loading. This characteristic indicates that the principal design variables are the properties of the link materials and the geometry of the structural members.

In assembly and manufacturing environments, current robots could be replaced by robots employing composite arms to increase productivity through faster maneuvers. In hazardous environments, such as fire-fighting, lightweight composite robots tolerant of high temperatures could be employed to relieve human dangers. In space applications, lightweight composite robots could be launched into space, and yet be strong enough to manipulate multi-ton satellites. In each of these areas, composite manipulators can become invaluable workhorses.

Intense competition in the international marketplace for high-performance machines and equipment in advanced military, aerospace, and manufacturing environments has been responsible for the evolution of more stringent criteria being imposed on robotic systems. Typically, higher speeds of operation are demanded, power consumption is often restricted, and generally tighter tolerances are imposed upon the output characteristics of these high-performance systems. While significant progress has been made in the development of viable methodologies and also technologies for the many subsystems of robotic devices, the absence of a

vi

be

of

th

ro

re

1.

fa

we

Co

st

in

th

is

se

Li

an

re

re

as

An

viable approach for developing lightweight robot arms has been recognized as being a major impediment to the evolution of the next generation of robotic systems [2-6]. This thesis addresses the complete development of a lightweight robot arm and includes the methodology and technology required for the development.

1.2 LITERATURE SURVEY

The current generation of robotic systems are fabricated with articulating members possessing a payload-weight to arm-weight ratio of approximately 1:20 [4]. Consequently, these members are characterized by high stiffnesses, massive weights, and also large moments of inertia which severely restrict the dynamic performance of these robotic systems. If superior performance characteristics are to be achieved, such as higher speeds and shorter settling-times, then from a mechanical-design viewpoint, lightweight structural members must be designed, engineered, and fabricated.

Design methodologies for predicting the dynamic response of this new generation of robotic systems will be required to mathematically model these systems as an assemblage of articulating interconnecting flexible bodies [7-12]. Several methodologies have been proposed for analyzing this class of articulating mechanical systems, and

these ar

Upon rev

vigorous

establis

generati

stiffnes

On

arms wit

approach

materia

ties fo

for spe

specifi

number,

fiber c

stiffne

mass de

than co

longer

I

Fiber c

member

the err

correct

send s

these are highlighted in two recent survey papers [13, 14]. Upon reviewing these papers, it is clearly evident that a vigorous research thrust is currently in progress to establish viable methodologies for designing the next generation of robot arms which will be characterized by high stiffness-to-weight ratios.

One design approach involves the fabrication of robot arms with geometrically optimized shapes [15, 16]. A second approach requires the arm to be fabricated from composite materials [17], which opens a new realm of design possibilities for robotic manipulators. Composites can be tailored for specified characteristics required by the component specifications through the many design variables such as ply number, ply angle, fiber volume fraction, and even different fiber or matrix combinations. Composites can have higher stiffnesses and strengths than conventional materials. The mass densities of fiberous polymeric composites are less than conventional metallic materials, and fatigue life is longer than that of other materials [18].

Improvements can be made in all areas of robotics. Fiber optics could be used in composite links to determine member deflections. By sending signals to the controller, the error due to payload and inertial forces can be corrected. For transient vibrations, the controller could send signals to either actuators or smart structure members

for dyn

charact

T

robotic

geometr

actuato

be enha

materia

lighter

and hig

structu

Naganat

Kinemat

studied

Tesar p

implemen

controll

Le

signific

[30]. S

algorith

optimum

of emplo

Ramirez

dynamic

for dynamic tailoring of the robot, changing the frequency characteristics of the members [19].

The current status and overview of research within robotics has been discussed by Waldron [20]. Subsystems of geometric structure designs, design of manipulator links, actuator selections, control algorithms, and sensors can all be enhanced through current research programs using advanced materials. The structural geometry can be designed with lighter, composite links, offering higher end-point accuracy and higher speed [21]. Tesar and Waldron studied robot structures for improved kinematics and compliance [22, 23]. Naganathan investigated the coupling effects between kinematics and flexibility [24], and compliance effects were studied by ElMaraghy and Kazerooni [25-27]. Stauffer and Tesar presented the latest concepts and applications implemented in robotic technology including sensors, controllers, mechanisms, automation, and modeling [28, 29].

Leu showed that the chain drives of a robot were significantly more compliant than the links and bearings [30]. Sung, Saravanos, Thompson, and Liao suggested algorithms for determining composite design variables for optimum performance [31-34]. Sung discussed the advantages of employing composites for high-speed robotics [35]. Ramirez fabricated a composite robot arm but did not present dynamic experimental data [36]. By maintaining the

effectiv

using co

deflecti

Su

elastic

complete

Evans in

controll

Wang, an

flexible

Ro

proposed

and mani

service

by Nakan

Ge

determin

tailorin

characte

Robotics

booths,

able to

a loss

well in

effective static stiffness (EI) and reducing the mass by using composite materials, Gandhi showed that smaller deflections can be obtained in dynamic systems [37].

Sunada and Turcic developed analytic models for elastic members of dynamic systems [38-40]. Turcic completed the study with experimental measurements [41]. Evans interfaced a personal computer to a P-50 robot for controller design [42]. Cannon, Sangveraphunsiri, Usoro, Wang, and Matsuno studied the control of manipulators with flexible members [43-47].

Robotic manipulators with advanced materials were also proposed for human-like environments such as micro-surgery and manipulator aids for the handicapped. An example of a service environment for robotic applications was presented by Nakano [48].

General composite studies included methodologies for determining optimal properties. Liao presented the idea of tailoring composite materials to have optimal damping characteristics according to certain constraints [49]. Robotics used in hazardous environments such as paint booths, high-temperature ovens, and chemical plants must be able to perform under hostile operating environments without a loss in performance. Many composite materials perform well in moisture, temperature, and chemical environments.

Lee stu
istics
differe

G
structu
method
implemer
manufact
differe
tivity
producti
consider
bonding

1.3 TH
IM

In
deflecti
using co
Figure
retrofi
epoxy b
project,
composit

Lee studied the variance of modulus and damping characteristics for various materials and configurations under different temperatures [50].

Glance reviewed the ability to analyze composite structures before fabrication using the finite element method [51]. Menges presented ideas for design and implementation of composite components [52]. Composite manufacturing research included studies conducted on many different composite manufacturing techniques and productivity [53-56]. Economic issues were discussed for various production methods of composites [57-59]. Many have considered other fabrication requirements such as the bonding and drilling of composite materials [60-67].

1.3 THESIS STATEMENT AND CONTRIBUTIONS - IMPROVING THE RESPONSE OF THE GE P-50

In a previous study by Choi, dynamic end-point deflections of the GE P-50 robot were reduced 60 percent by using composite materials for a portion of the forearm [1]. Figure 1.1 displays the previous project where the P-50 was retrofitted with a multi-piece arm consisting of a graphite-epoxy box beam and aluminum bearing housings. In this project, the entire forearm was replaced with a one-piece composite arm.

Figure
multi-

Piece
and 1.
using
With a
design,
materia
Project
will be

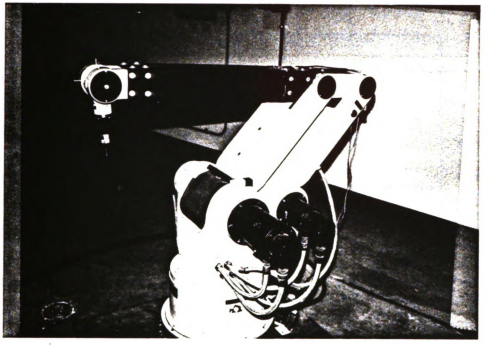

Figure 1.1. Previous project of GE P-50 retrofitted with a multi-piece aluminum/composite forearm [1].

Dynamic results for the P-50 robot with the multi-piece arm unloaded and with payload are shown in Figures 1.2 and 1.3. Note the reduction in deflections of the robot by using composite materials. Improved results are anticipated with a one-piece graphite-epoxy arm. Issues concerning design, analysis, and fabrication employing composite materials for the entire forearm will be presented in this project. Also, the dynamic end-point response of the robot will be studied.

Figure
maneuve

Figure
maneuve

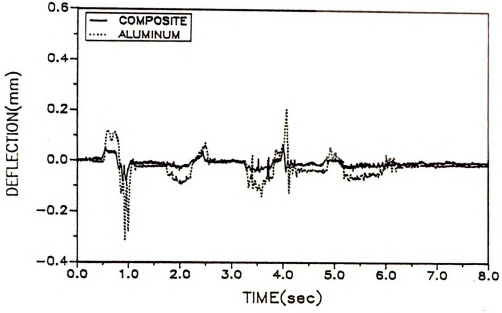

Figure 1.2. End-point deflections of P-50 during a maneuver. Previous project without payload [1].

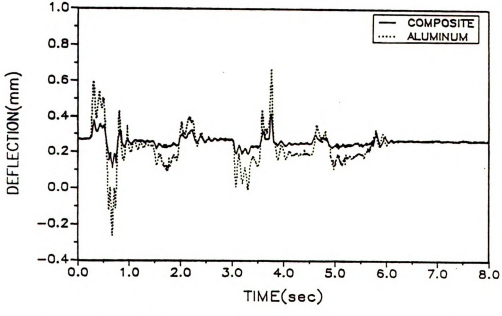

Figure 1.3. End-point deflections of P-50 during a maneuver. Previous project with 7.7 kg payload [1].

Co

since ea

distinct

the mate

previous

entire s

project

the bas

and anal

testing

robot ar

the ori

1.4 S

C

and man

discuss

issues.

enginee

From a

is used

laminae

require

C

composi

Composite parts must be designed for fabrication, since each manufacturing process imparts significantly distinct stiffness, damping, and mass characteristics due to the material qualities associated with each process. Of the previous literature survey, very few researchers covered the entire span of composite design and manufacture [68]. This project was a complete study of a composite robot arm, from the basic design possibilities, the fabrication techniques, and analysis parameters, to the actual fabrication and testing of a one-piece composite forearm. The result was a robot arm with similar dynamic response characteristics as the original commercial arm, and 60 percent less mass.

1.4 SUMMARY OF CHAPTERS

Chapter Two discusses composite materials, mechanics, and manufacturing. Methods of fabrication are briefly discussed, with an emphasis on design-for-manufacture issues. Industrial robots are also reviewed, and based on engineering constraints, design guidelines are obtained. From a geometric model, a commercial finite element package is used to find the laminate sequence of graphite/epoxy laminae for the composite arm considering the performance requirements.

Chapter Three documents the fabrication of the composite arm. Manufacturing details of the fabrication

process

encount

composi

C

arms in

static

C

robotic

robot.

frequen

scribed

present

C

butions

propose

process are presented, along with problems and difficulties encountered in the fabrication and machining of the composite forearm.

Chapter Four contains experiments conducted on the arms in isolation from the robot structure. Effective static stiffnesses and natural frequencies are compared.

Chapter Five contains experiments conducted on the robotic system with the composite forearm installed on the robot. Tests include static response with hysteresis, frequency response, and response of the robot under prescribed maneuvers. Comparisons with the aluminum arm are presented.

Chapter Six presents a summary of the results, contributions of the study, problems and recommendations, and proposed areas of study.

M

compos

materia

employe

2.1 I

C

describe

materia

ways to

properti

fiberous

with an

a materi

interact

materia

textbook

from man

R

use of c

materia

commonly

CHAPTER 2

COMPOSITE ROBOT ARM DESIGN

Many factors must be considered in the design of composite-based parts. The following sections on composite materials and industrial robots review the ideas that were employed for the fabrication of the composite robot arm.

2.1 INTRODUCTION TO COMPOSITE MATERIALS

Composite materials for structural applications can be described as (1) consisting of two or more distinct materials, (2) mixing the separate materials in prescribed ways to achieve optimum properties, and (3) resulting in properties superior to the original materials [69]. In fiberous polymeric composites, high-strength fibers combine with an environmentally protective polymer matrix to produce a material that has both high-strength and durability. The interaction of the two materials results in a more desirable material as a whole. Many composites handbooks and textbooks supply information on composite materials ranging from manufacturing to material analysis [69-78].

Recently, there has been a dramatic increase in the use of composite materials where, previously, conventional materials have been used [59, 70]. Composite materials are commonly found in aircraft, automobiles, and sporting goods.

This tre

which o

to sign

althoug

convent

reducti

result

D

impleme

In orde

manufac

propert

2.2 M

D

T

depends

manufac

affects

The mar

part of

integra

P

fabrica

This trend can be attributed mostly to the weight reduction which often occurs by employing composite materials, leading to significantly superior performance. Furthermore, although composite materials may be more expensive than conventional materials, the benefits such as weight reduction, resistance to fatigue, and higher stiffness result in overall advantages.

Dynamic performance enhancements are anticipated by implementing composite materials for a robotic manipulator. In order to present a cohesive document, a basic review of manufacturing methods and the analysis of stiffness properties for composite materials will be presented.

2.2 MANUFACTURING OF COMPOSITES: DESIGN-FOR-MANUFACTURE ISSUES

The dynamic performance of a composite structure depends upon the fabrication procedure employed to manufacture the structure, since the fabrication procedure affects the mass, stiffness and damping characteristics. The manufacturing process must be considered as an integral part of design, and the design must be considered as an integral part of the manufacturing process.

Primary issues to review for determining a proper fabrication procedure are investment cost, component

property specifications, and production volume. Gandhi [68] suggests the methodology shown in Figure 2.1 to design-for-manufacture composite components. Variables in the methodology are material, geometry, and fabrication selection. Margolis presented composite fabricating economics, where processing costs are of greatest importance in the commercial industries [59]. Figure 2.2 presents the relation of cost, production, and performance as specific demands of fabrication. In general, high-performance composites result in low production rates and high costs. Composite structures can be manufactured using a variety of methods, presented in Table 2.1 in order of production volume.

Tooling costs for most composite production techniques are expensive. Due to the inherent abrasive nature of composites, tool wear is significant, thus requiring stronger, more abrasion resistant surfaces of higher costs. For processes such as injection molding and SMC, estimates for molds of the composite robot arm exceeded $100,000. In this project, only one composite arm was to be fabricated, and the lowest fabrication cost was sought.

Composite materials are designed on micromechanical and macromechanical levels. Micromechanical options include fiber volume fraction, matrix density, fiber diameter, and fiber density. Macromechanical options include fiber types,

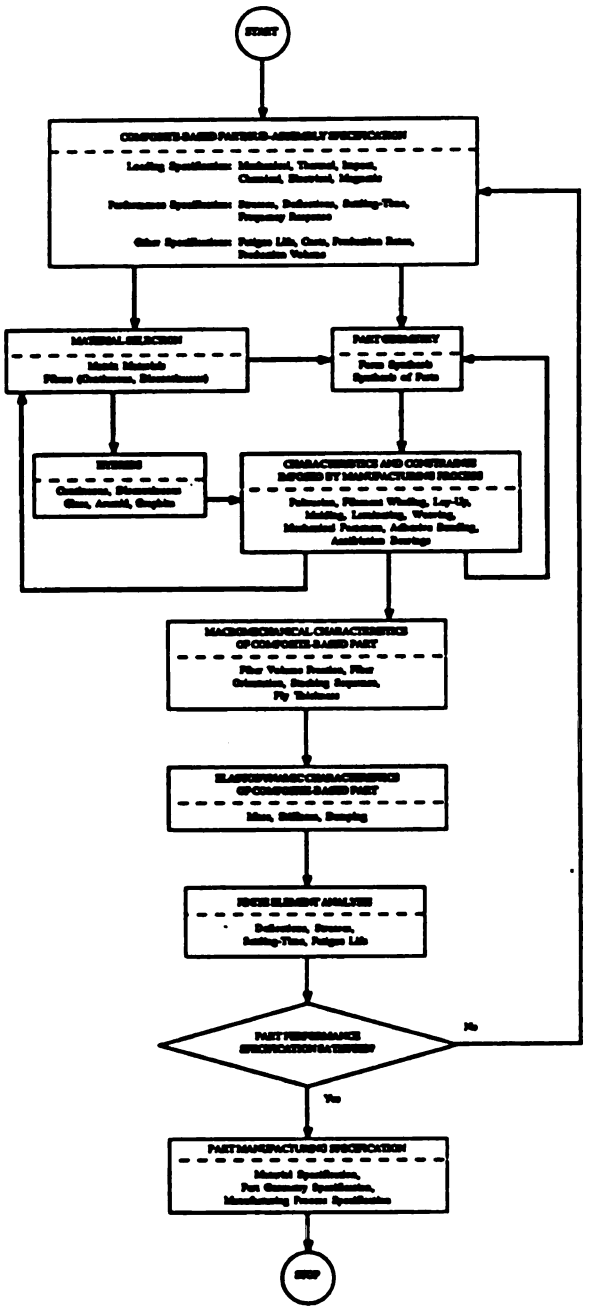

Figure 2.1. Design-for-manufacture methodology for composite-based parts [68].

fiber orientation, stacking sequence, and ply thickness. Figure 2.3 diagrams how manufacturing processes are dependent on fiber selection. For example, most molding

Fig
per
aer

pr

th

pr

pl

hi

gr

ex

ad

us

or

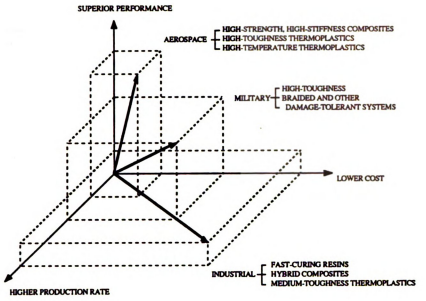

Figure 2.2. Diverse costs, production rates, and performance characteristics of composite-based systems for aerospace, military, and industrial environments [68].

processes cannot specially orient continuous fibers within the component.

For large production runs, the injection molding process is common. This process typically uses thermoplastic matrices and chopped fibers which are injected under high pressure into a cavity. Due to their abrasive nature, graphite fibers are rarely used, since this results in excessive damage to the molding equipment and mold. The advantages of injection molding include fast cycle-times and use of unskilled labor. Disadvantages include random fiber orientation and high equipment costs [73].

Table 2
industr
goods [

Proces	
Inject moldi	
Bulk formi (SMC)	
RRIM a SRIM	
Filam Windi	
Lay-u	

(SMC)

high q

by ins

faces

throug

accele

fibers

Materi

Table 2.1. Composite fabrication methods popular in current industries such as transportation, defense, and consumer goods [73, abridged listing].

Process	Prod. Volume	Fiber	Matrix	Comment
Injection molding	High	Chopped glass	Thermo-plastic	Very fast process. Large press required.
Bulk forming (SMC)	High	Glass Kevlar	Thermo-set or thermo-plastic	Continuous or chopped, random fiber orientation.
RRIM and SRIM	Medium	Glass	Urethane	Continuous or chopped fibers with preform mat.
Filament winding	Medium	Glass Kevlar Graphite	Thermo-set	Limited to cylindrical shapes.
Lay-up	Low	Glass Kevlar Graphite	Thermo-set	Any shape, size, or material property desired.

The bulk forming process with sheet molded compound (SMC) is also used in the automotive industry because of the high quality surface finish [73]. Bulk forming is initiated by inserting a measured quantity of SMC between two heated faces of a mold. The mold is then closed, forcing the SMC throughout the cavities of the mold. The heat of the mold accelerates the curing process. Typical materials are glass fibers and thermoset matrices, although many different materials have been used.

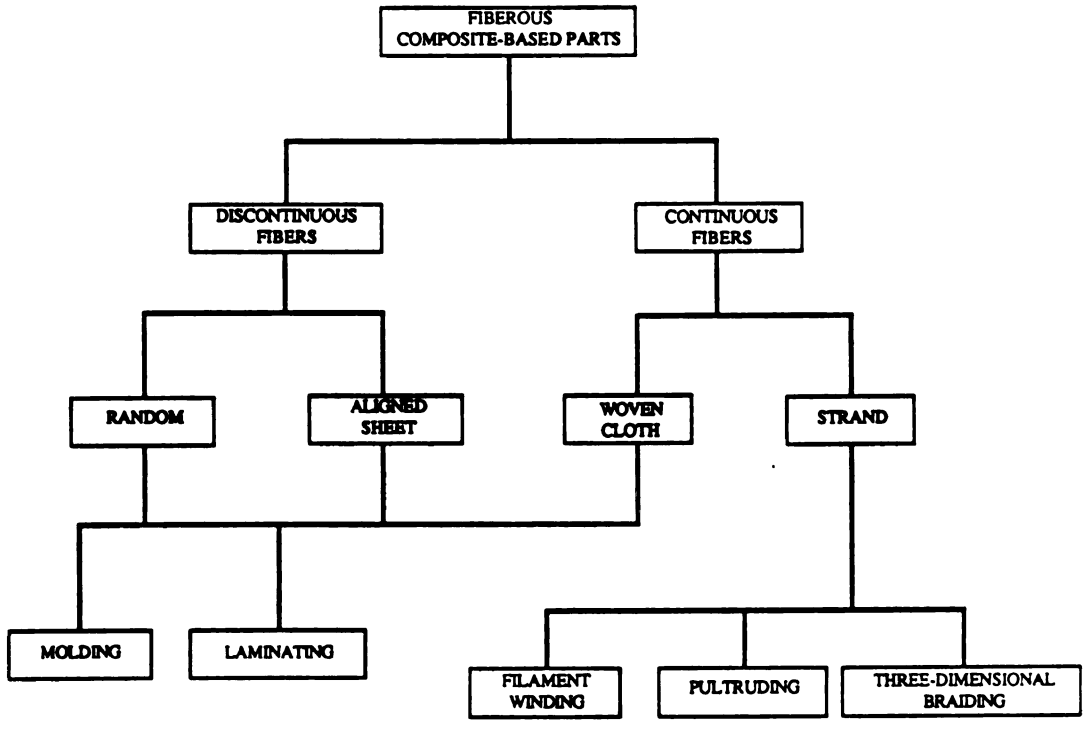

Figure 2.3. Impact of fiber selection upon the choice of manufacturing process [68].

Reinforced reaction injection molding (RRIM) is not a high volume process, although cycle times can be two minutes or less. Many automotive manufacturers use this process and structural RIM (SRIM) to produce dent-forgiving body panels and light-weight reinforcing structures. The urethane material is obtained through a reaction of isocyanate and polyol, two low viscosity chemicals [79]. Reinforcing fibers can be either injected with the chemicals, or can be inserted into the mold as a preform [54, 80]. The two chemicals are mixed just prior to entering the mold. Within seconds, the mold is filled and the polyurethane curing process begins. After a minute or so, the part in a

pre-hardened state can be removed from the mold and post-cured in an oven.

Filament winding is a process that lays ribbons or strands of fibers impregnated with resin onto a moving spindle [71]. The circular spindle maintains the desired shape, as a second mechanism guides the fibers over its surface with a prescribed tension and motion. Winding machines vary in complexity, but component geometries are limited to axisymmetric shapes. One significant advantage is the preferred orientation and use of continuous fibers. The optimal winding angle for torsional or axial loading can be determined, decreasing the amount of material used. This process can be expensive primarily due to the large capital investment costs [55, 71, 81].

Lay-up can be performed by robots for simple panels, although most commonly by manual labor [56, 73]. Quality control and part consistency exist as problems of the method, so cleanliness should be monitored and proper non-destructive tests should be employed. Low costs are involved with hand lay-up; the major factors being the mold cost and the autoclave use and operation costs [71]. In general, lay-up is a slow process, where molding processes imply high production rates.

Advantages of the lay-up technique included mold and

compone

shell-l

lay-up

arm. A

of the

fabrica

numerou

back on

resins

enviro

differ

glass,

2.2 pr

betwee

metals

longit

Table
tiona

Type
B(4) AS/ Kev Scot

component complexity and the ability to create very strong shell-like structures such as aircraft panels. Thus the lay-up technique was chosen here for making the composite arm. Auto Air Industries [82] assisted in the fabrication of the composite robot arm, with details of the actual fabrication presented in Chapter 3. Auto Air supplied numerous ideas in the fabrication of the robot arm, falling back on their years of experience with composites.

Proper material selection was also required. Epoxy resins commonly used for lay-up are very durable to chemical environments and temperatures up to 150°C [83]. Many different fibers are available, the four most common are glass, Kevlar (a DuPont aramid), graphite, and boron. Table 2.2 presents a comparison of stiffness-to-weight ratios between fiber/epoxy composite materials and traditional metals. The ratio was determined by dividing the longitudinal modulus by the mass density (per unit volume).

Table 2.2. The stiffness-to-weight ratios for unidirectional fibers in epoxy matrices [75], and metals [84].

Type	Material	Ratio
B(4)/5505	Boron	102 GPa/kg
AS/3501	Graphite	86
Kevlar	Aramid	52
Scotchply	Glass	21
	Steel	27 GPa/kg
	Titanium	26
	Aluminum	25
	Cast Iron	14

Glass/epoxy yields nearly the same stiffness-to-weight ratio as aluminum, so a part originally made of aluminum could be designed using glass/epoxy. If the stiffness properties matched between the parts, the masses would not differ either. For glass/epoxy composites used in the auto industry, marginal stiffnesses are required for shape stability, resulting in parts softer than aluminum, but of less weight.

The graphite/epoxy combination produced by several manufacturers had a high stiffness-to-mass ratio. A robot arm employing graphite/epoxy composites would have reduced mass by maintaining the stiffness properties inferred from the original aluminum arm. Continuous graphite fibers and an epoxy matrix were chosen as the materials for the laminates primarily due to their superior properties over glass/epoxy and Kevlar/epoxy, and lower cost than boron/epoxy.

For the high-strength, low production, and low weight requirements of the project, a graphite/epoxy material was the best choice of composite materials. For higher production volumes, consideration could be made for hybridization, using a combination of glass and graphite fibers. Hybridization, which has been studied in several texts [85-88], would also increase the impact resistance of the arm over a graphite/epoxy configuration. In high moisture situations,

the ele

corrode

graphit

reactio

T

of comp

lay-up

2.3 Y

T

manufa

of com

impreg

stiffn

the cr

longit

2.4).

anisot

differ

the ma

the sa

the cy

[59],

Figure

the electrically conductive graphite/epoxy material would corrode. By properly fabricating a hybrid of glass and graphite to break the electrical path, electrolytic reactions that cause corrosion would be inhibited [65].

The next step is to consider the material properties of composites, in the form of a laminate, produced by the lay-up technique.

2.3 MECHANICS OF COMPOSITE LAMINATES

The composite materials utilized for the robot arm manufactured by Hercules Incorporated [89]. They consiste of continuous graphite fibers of various configurations impregnated with an epoxy resin (Hercules 3501-6). The stiffness of a unidirectional composite is the greatest in the on-axis configuration, when the graphite fibers (the longitudinal axis) align with the material axis (Figure 2.4). Unidirectional fibers (Hercules AS4) exhibit drastic anisotropy; the longitudinal and transverse stiffnesses differ by a factor of ten. By orienting the fibers off of the material axis (the off-axis configuration, Figure 2.5), the same load carrying strength requires more material than the original configuration. Using the notation from Hull [69], the longitudinal stiffness, Q11, of AS4 is shown in Figure 2.6 as a function of fiber angle.

Figure
in the

Figure
in the

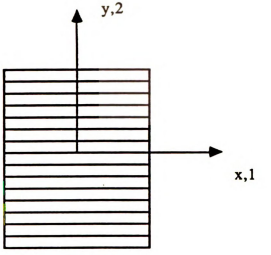

Figure 2.4. Unidirectional (AS4) graphite/epoxy represented in the on-axis configuration.

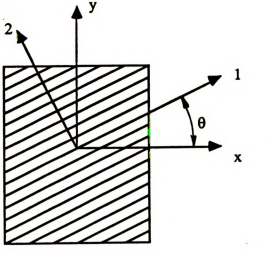

Figure 2.5. Unidirectional (AS4) graphite/epoxy represented in the off-axis configuration.

STIFFNESS Q11 (GPa)

Figure
(AS4)

2.7, c
woven
aligne
the wo
natior
90°.
is sh
fabri
unidi
than
compo

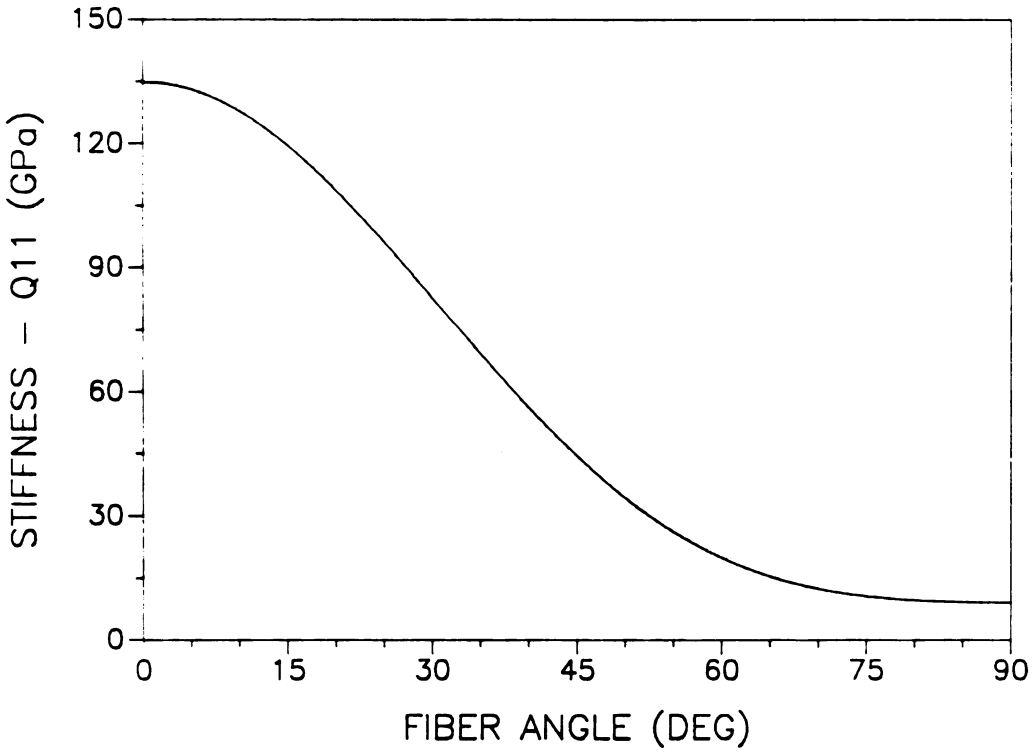

Figure 2.6. Stiffness versus ply angle for unidirectional (AS4) graphite/epoxy.

Woven fabric (Hercules A370-5H), depicted in Figure 2.7, consists of two sets of unidirectional graphite fibers woven together and impregnated with epoxy resin. One set is aligned at 0° and the other at 90°. The characteristics of the woven fabric reduce the potential for free-edge delamination when woven fabric is included in the laminate [82, 90]. The longitudinal stiffness, Q11, of the woven fabric is shown in Figure 2.8. Although the stiffness of the woven fabric for the on-axis configuration is less than the unidirectional composite, the transverse stiffness is higher than the transverse stiffness of the unidirectional composite. During fabrication, this results in easy

applic

unidir

Figure
repres

100

80

60

40

20

STRENGTH (GPa)

Figure
(A370-

application of the woven fabric compared to the unidirectional pre-preg.

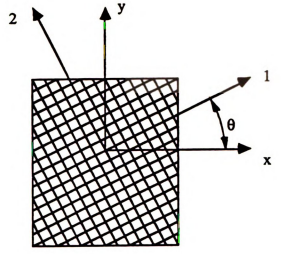

Figure 2.7. Woven fabric (A370-5H) graphite/epoxy represented in the off-axis configuration.

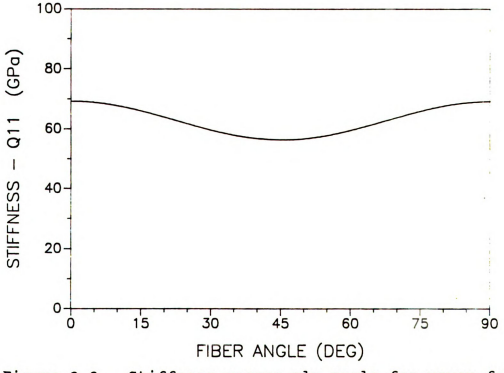

Figure 2.8. Stiffness versus ply angle for woven fabric (A370-5H) graphite/epoxy.

app

uni

Fig
repr

STRENGTH - Q11 (GPa)

Figu
(A37

application of the woven fabric compared to the unidirectional pre-preg.

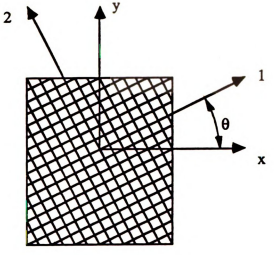

Figure 2.7. Woven fabric (A370-5H) graphite/epoxy represented in the off-axis configuration.

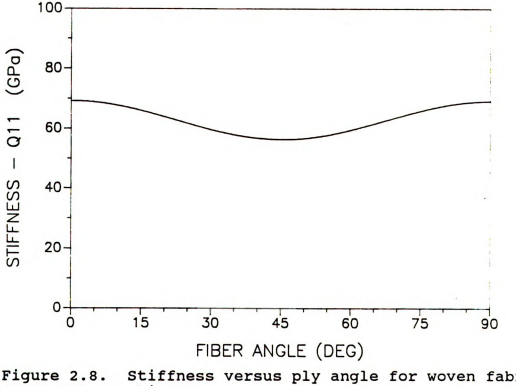

Figure 2.8. Stiffness versus ply angle for woven fabric (A370-5H) graphite/epoxy.

layers

lamina

materi

textbo

includ

thickn

used f

materi

Compos

engine

In com

and Po

materi

behavi

Unidir

Table

the des

stiffn

strain

stiffn

Composite shell-like structures consist of multiple layers of composite laminae (or plies). The classical laminate theory (CLT), which assumes that the composite material is elastic, can be found in most composite textbooks [69, 77, 78]. Other assumptions for the CLT include perfect bonding between layers, small laminate thickness, and small displacements. The CLT analysis is used for shell-like structures, where deformation of the material thickness (normal to the surface) is neglected. Composite materials can be represented by the four engineering constants obtained by material tests:

E1	Longitudinal Modulus
E2	Transverse Modulus
v12	Transverse Poisson's Ratio
G12	Transverse Shear Modulus

In conventional materials such as aluminum, only the modulus and Poisson's ratio are required to fully describe the material. Furthermore, the methods for predicting the behavior of composite materials are more complex.

The engineering constants, or material properties, for unidirectional and woven fabric composites are listed in Table 2.3. The engineering constants are easily applied to the design of conventional materials. For composites, stiffness components are required to relate stresses to strains. The material properties, transformed into the stiffness properties [Q] as shown by Vinson [78] are

Table
Hercul
compos
[89].
stiffn

E1	
E2	
v1	
G1	
v1	
Q1	
Q2	
Q1	
Q6	
U	
U	
U	
U	
U	

The i

Table 2.3. Published engineering material constants for Hercules graphite/epoxy unidirectional and woven fabric composites (nd = non-dimensional, otherwise units in GPa) [89]. Also, calculated stiffness properties and invariant stiffness properties.

Hercules Composite Materials		
	AS4/3501-6	A370-5H/3501-6
E1	134.00	69.00
E2	9.00	69.00
v12 (nd)	0.30	0.05
G12	7.00	20.00
v12 (nd)	0.02	0.05
Q11	134.81	69.17
Q22	9.05	69.17
Q12	2.72	3.46
Q66	7.00	20.00
U1	58.13	62.74
U2	62.88	0.00
U3	13.80	6.43
U4	16.52	9.89
U5	20.80	26.43

$$v21=v12*E2/E1$$

$$Q11=E1/(1-v12*v21)$$

$$Q22=E2/(1-v12*v21)$$

$$Q12=v21*E2/(1-v12*v21)$$

$$Q66=G12.$$

The invariant stiffness properties {U} are

$$U1=(3Q11+3Q22+2Q12+4Q66)/8$$

$$U2=(Q11-Q22)/2$$

$$U3=(Q11+Q22-2Q12-4Q66)/8$$

$$U4=(Q11+Q22+6Q12-4Q66)/8$$

$$U5=(Q11+Q22-2Q12-4Q66)/8.$$

The in

proper

lamina

nesses

proper

in Tab

are co

functi

stiffn

As an

The eq

are EA

the fi

matrix

flexur

implie

easily

The invariants can be used to determine the stiffness properties of a composite laminate consisting of numerous lamina of various combinations of materials, ply thicknesses, and ply angles. The stiffness and invariant properties for the graphite/epoxy materials are also listed in Table 2.3.

For off-axis orientations, the stiffness properties are combinations of invariants U2 and U3 and cosine functions of the fiber angle. The extensional and flexural stiffness matrices are defined in Tsai [75] as:

$$A_{ij} = \int_h Qij \, dz,$$

$$D_{ij} = \int_h Qij \, z^2 dz.$$

As an example, the first entry in each matrix is:

$$A_{11} = \int_h Q11 \, dz = \int_h [U1 + U2\cos 2\theta + U3\cos 4\theta] \, dz,$$

$$D_{11} = \int_h Q11 \, z^2 dz = \int_h [U1 + U2\cos 2\theta + U3\cos 4\theta] \, z^2 dz.$$

The equivalent moduli for in-plane and flexural stiffnesses are $EA)_i = b/a_{11}$ and $EI)_f = b/d_{11}$, respectively, where a_{11} is the first entry in the inverse of the extensional stiffness matrix and d_{11} is the first entry in the inverse of the flexural stiffness matrix (where matrix inversion is implied). So the analysis of simple beams can be completed easily using the above in-plane and flexural stiffnesses.

For more complex structures, such as two dimensional

plat

beam

geom

stre

prope

mater

publi

part

preve

final

integ

metho

obtai

2.4

means

probl

be pr

use o

human

outpu

the

gripp

plates, a more rigorous analysis is required. Analyses for beams, plates, and shells exist in literature for simple geometries [78], and topics such as cylindrical bending and strength theories have been studied [90-92].

The manufacturing method also influences the material properties of composites. Proper material preparation and material curing should be carefully monitored to obtain the published values of the material manufacturer. Prior to part cure, debulking removes excess air from thick lay-ups, preventing a high laminate void content. Considerations for final machining are critical to final part strength and integrity. Only by executing the proper manufacturing method with the proper material can the desired results be obtained.

2.4 BACKGROUND ON INDUSTRIAL ROBOTS

In the past, the industrial robot was regarded as a means of automation which would solve technical and economic problems in the handling of rapidly changing tasks. It can be programmed to perform tasks under automatic control. The use of robots has increased due to the efforts being made to humanize the working environment and to increase production output [93]. Robotic systems can be assumed to consist of the following five sub-systems: kinematic structure, grippers, control system, actuators, and sensors.

2.4.1 KINEMATIC STRUCTURE

The kinematics of the GE P-50 robotic manipulator represent a parallel mechanism with five degrees-of-freedom. The axes of motion presented in Figure 2.9 include (1) base rotation, (2) upper arm motion, (3) forearm motion, (4) wrist bend, and (5) wrist twist. Transformation equations were developed in [94], and tip acceleration was determined as a function of the five (time-dependent) degrees-of-freedom. The vertical work envelope of the robot is shown in Figure 2.10, about a base rotation of 270°.

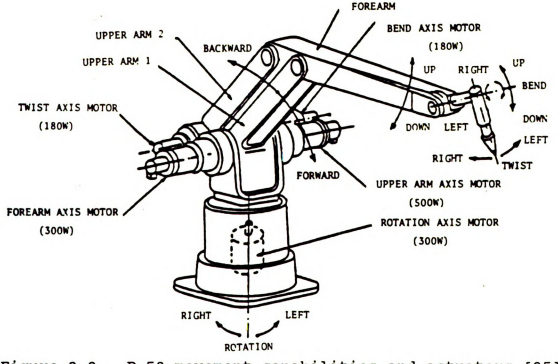

Figure 2.9. P-50 movement capabilities and actuators [95].

Figur

2.4.2

proje

attac

typic

inter

error

be ma

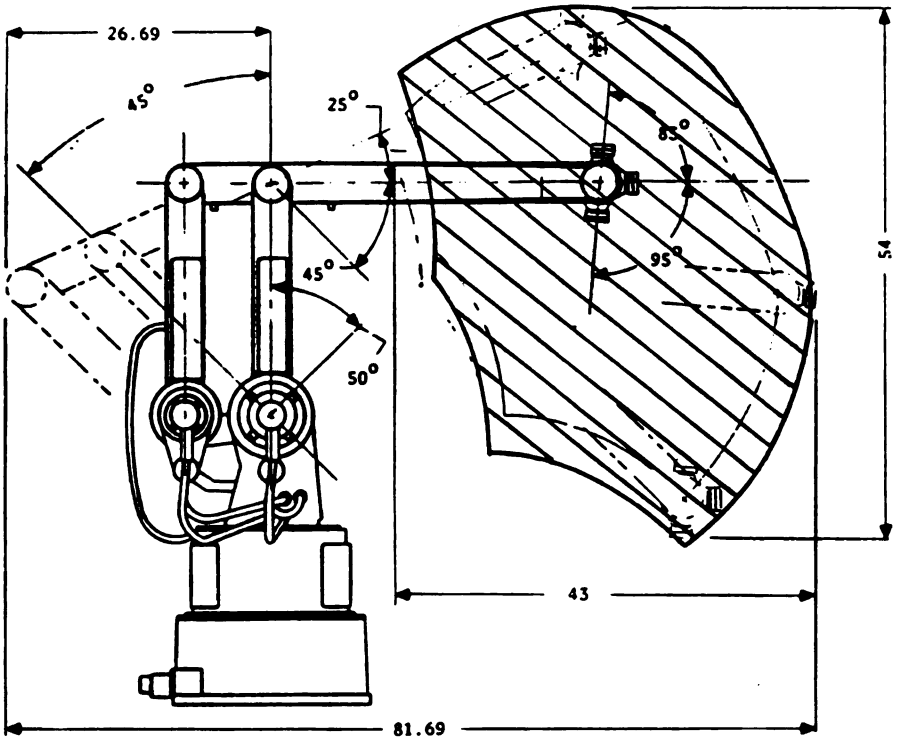

Figure 2.10. P-50 vertical work envelope [95].

2.4.2 END-EFFECTOR

The end-effector of the robotic manipulator in this project does not implement a gripper, only a payload attachment point as in Figure 2.11. Industrial robots will typically have a gripper, a machine tool, or a spray gun for interaction with the environment. Here, only the end-point error will be of interest, and measurements of the P-50 will be made using a dial gage, strain gages, and accelerometers.

Figur
and p

2.4.3

deter

robot

diffe

the a

seque

contr

using

panel

The p

Figure 2.11. P-50 robotic manipulator with end-effector and payload.

2.4.3 CONTROL SYSTEM

The versatility and flexibility of any robot is determined by the capabilities of its control system. The robot and the control system are rarely supplied by different manufacturers [42]. The control system provides the actuators with proper signals for desired motion sequences within the limits of kinematic design. The P-50 controller is a point-to-point system, and is programmed using a teach box. The teach box is a portable control panel separated from the P-50 controller unit by a cable. The P-50 controller, the teach box, and the programming

langua

code.

accur

stora

contr

as lo

posit

Durin

diffi

obsta

value

proce

as li

was d

Hitac

dynam

paren

were

geome

contr

proje

language are hard-wired and in permanently stored computer code.

In general, point-to-point systems have higher accuracy than continuous-path systems due to the reduced storage and computation requirements. Point-to-point controllers are typically used for handling operations such as loading and unloading of materials, where only the final position is of interest and the path is not a concern. During the motions, the actual path of the end-point is difficult to predict so each routine should be tested for obstacle avoidance. The computer provides desired position values from user data, measures actual position values, and processes the error using a control algorithm with data such as link speeds and dwell times to signal the actuators.

Although the robot, which is the focus of this thesis, was distributed by General Electric, it was manufactured by Hitachi of Japan. Colleagues within the Machinery Elasto-dynamics Laboratory attempted to contact Hitachi USA and the parent company in Japan, but specifications of the robot were not obtained. All required information (such as arm geometry) was determined through measurements, and the control system was understood to be a "black box" for this project.

The "black box" characteristics were developed for

rigi

fore

were

woul

If a

the

Sect

shoul

indep

2.4.4

robot

Hydra

carry

diffi

due t

power

actua

locat

sizes

rigid body dynamics of the robot structure. Although the forearm mass was modified for the project, no alterations were made to the controller. The rigid body controller would encounter problems if arm flexibility was significant. If access to the controller was possible, one could modify the algorithm to accommodate flexible links as mentioned in Section 1.2. To assure repeatability of the robot, the arm should have equal or greater static stiffness, which is independent of the controller.

2.4.4 ACTUATORS

Robot actuators, or drive motors, for industrial robots are either hydraulic, pneumatic, or electric. Hydraulic actuators are not clean, but offer large load-carrying abilities. Pneumatic actuators are loud and difficult to control. They are commonly used for grippers, due to their light weight. Electric motors have limited power transfer, but are the most reliable of the three actuator types. The P-50 actuators are electric motors, located on the robot as shown in Figure 2.9. The motor sizes are listed in Table 2.4.

Table

M
B
U
F
B
T

2.4.5

runs,
encod
very
optic
Figur
Senso
and c
but a

2.4.6

end-e
is th
mecha
are t
of th

Table 2.4. P-50 motor sizes [95].

Motion	Motor Size (Watts)
Base	300
Upper Arm	500
Forearm	300
Bend	180
Twist	180

2.4.5 SENSORS

Robot sensors include limit switches for link over-runs, tachometers for velocity indication, and rotary encoders for link position determination. The P-50 is a very accurate manipulator because of the high resolution optical encoders and tachometers incorporated in the joints. Figure 2.12 presents a typical robotic welding application. Sensors for the work-space environment such as weld control and conveyor timing are not incorporated in this project, but are used throughout the robotic industry.

2.4.6 POSITIONING ERROR AND REPEATABILITY

The robot positioning error is the deviation of the end-effector from the desired motion. The resulting motion is the actual motion developed during a maneuver. From a mechanical-systems viewpoint, the principle error sources are the clearance in the joints and the inherent flexibility of these joints, the mass and stiffness characteristics of

Figur
applic

the st

flexib

effect

cycle

the hy

the p-

2.4.7

enhanc

increa

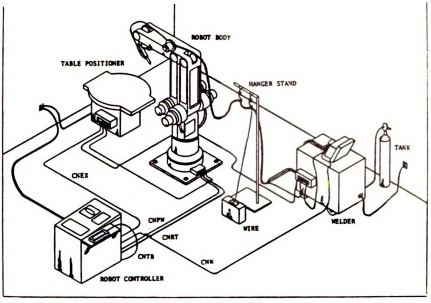

Figure 2.12. P-50 robotic manipulator in a typical welding application.

the structural members of the robot, and the inertia and flexibility in the drive-train.

Repeatability of a robot determines how close the end-effector will be to a particular point in space for any cycle of a maneuver [95], the principle error source being the hysteresis of the robotic system. The repeatability of the P-50 is 0.2 mm.

2.4.7 ROBOT SUMMARY

The robot is a useful tool in many fields. By enhancing the performance of the robot, productivity can be increased. The next section considers the requirements

impos

2.5

desig
impor
consi
for e
produ
Upon
and m
techn

weigh
deter
arm a
accor
arm,
Furth
the s
Creat
possi

Shown

imposed upon the design of a composite robot arm.

2.5 CONCEPTUAL DESIGN PHASE

Different methods and materials are available to the design engineer for producing composite components. An important first step was to create design concepts. Then consider all possible designs, and determine pros and cons for each. Design and manufacture are coupled so that costs, production, and material must be included in the analysis. Upon reaching a preliminary design, manufacturing method, and material type, the design was analyzed using modeling techniques.

The composite arm must conform to the geometric and weight constraints of the GE P-50 robotic manipulator as determined by studying the original two-piece cast aluminum arm and specifications. For the composite arm, accommodations should be made for the chain paths within the arm, and the work envelope should not be altered. Furthermore, the structural static stiffness should remain the same for appropriate dynamic comparisons. Concepts created by a colleague will be used to explore design possibilities [94].

The robot arm can be separated into three sections as shown in Figure 2.13. Section A is the bearing section,

requ

and

consi

secti

parti

confi

Figur
secti

be se

form

possi

loads

required to have adequate strength for controlling the arm and housing the bearings. Section B is the main section, consisting of a load-bearing beam. Section C is the end section. By accommodating certain designs for each particular requirement, we can obtain the ideal arm configuration.

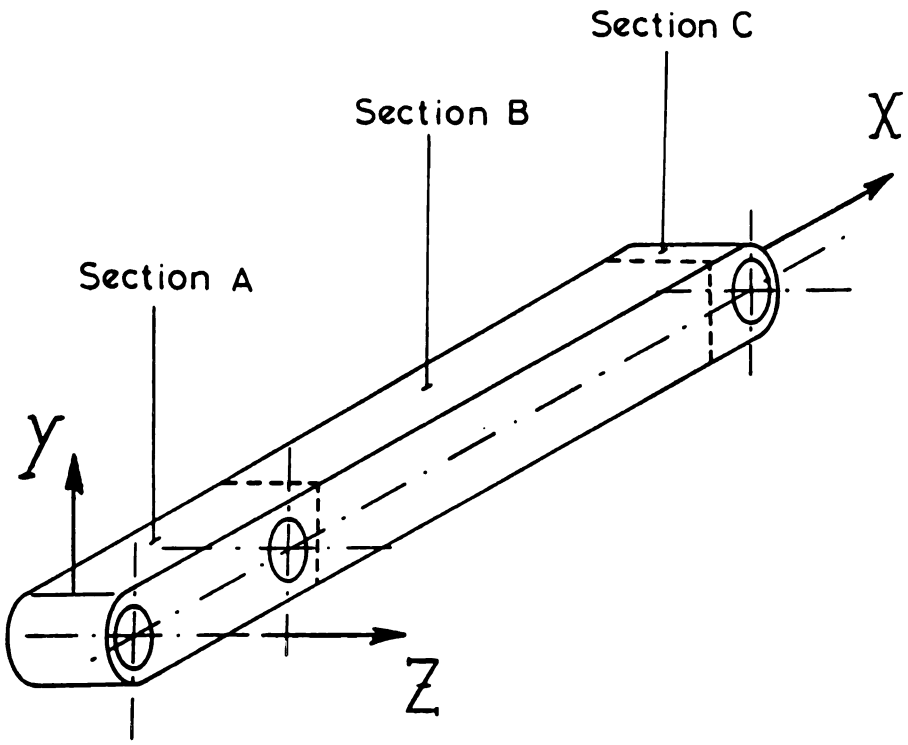

Figure 2.13. Three major sections of forearm: bearing section, main section, and end section [94].

For example, in Figure 2.14, the bearing section could be separately molded from SMC in two pieces, then bonded to form a rigid member. In Figure 2.15, many different design possibilities exist for the main section. If torsional loads will be encountered, the circular section would be

Figur

Figur

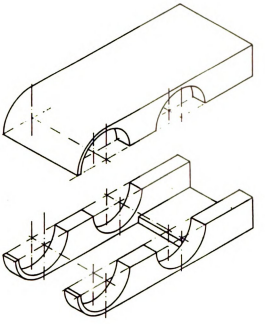

Figure 2.14. Bearing section molded in two pieces [94].

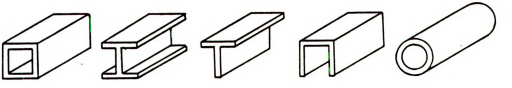

Figure 2.15. Main section geometry options [94].

cho

cri

are

app

tog

mas

cro

met

in

by

usi

chosen. If horizontal and vertical loading would be critical, the box section would be used. And if the loads are in the vertical plane, an I-beam may be most appropriate.

The assembly of sections could then be bonded or wound together in Figure 2.16 using composites. Alternatively, if mass production was considered, Figure 2.17 shows a constant cross-section arm that can be produced using pultrusion methods. Figure 2.18 implies that strength can be obtained in the bearing section and light weight in the main section by combining two pultruded sections of different sizes. By using three different pieces (Figure 2.19), each section

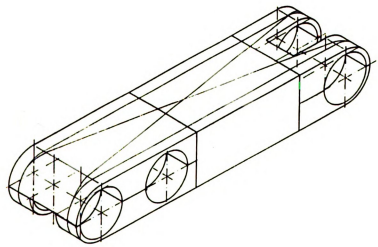

Figure 2.16. Assembly of sections using adhesives or filament winding [94].

coul

comb

opti

sect

tubu

fina

robo

diff

tubu

fabr

Fig

could be optimally designed for reducing weight, and then be combined for a perfect result. The main section could be optimized in shape, where Figure 2.19 presents an I-beam section for vertical loads, and Figure 2.20 presents a tubular section for torsional loads.

Many concepts should be considered before choosing a final design. Figure 2.21 is an elaborate design for a robot arm which might perform well but would be very difficult to fabricate using composite materials. The tubular section of Figure 2.20 would be appropriate to fabricate using the winding method.

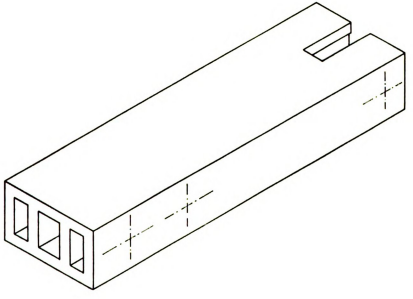

Figure 2.17. Forearm of constant cross-section [94].

Fig

Figur
separ
carry

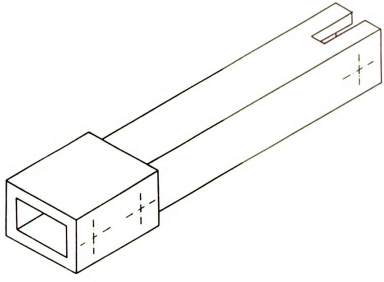

Figure 2.18. Two-piece arm [94].

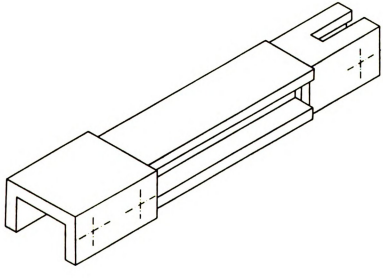

Figure 2.19. Three piece arm. All three sections designed separately. Main section is I-beam for vertical load-carrying ability [94].

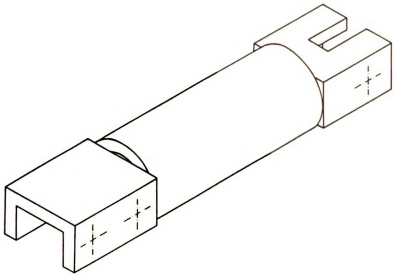

Figure 2.20. Three piece arm. Main section is tubular for torsional rigidity [94].

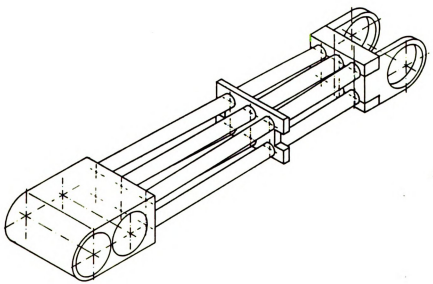

Figure 2.21. Multi-component arm. Elaborate design to accommodate a specific need [94].

the

inclu

the

bear

alum

groo

Pote

exis

Alte

the

compo

Figu

roun

pres

to t

groo

A box-beam, constant cross-section geometry similar to the original forearm was chosen for the project. The design included clearance for the chain paths along the length of the arm, and fabrication using the hand lay-up technique.

Another consideration is the accommodation of the bearings. Figure 2.22 is a section through a bearing in the aluminum arm. Note that the retaining ring is fixed in a groove, preventing the bearing from moving axially. Potential for delamination and high stress concentrations exists in composite materials with such grooves. Alternatives include bolting an aluminum bearing housing to the composite arm (Figure 2.23), or fabricating the composite laminate around an aluminum bearing housing, as in Figure 2.24. These, however, require extra surface area for mounting as shown in Figure 2.25. The chosen design is presented in Figure 2.26. A bearing retaining ring bonded to the inside wall of the arm eliminates any need for holes, grooves, or large mounting surfaces on the composite arm.

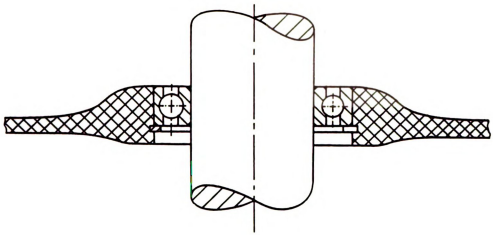

Figure 2.22. Cross-section of aluminum arm bearing housing [94].

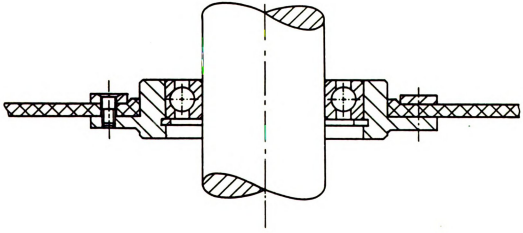

Figure 2.23. Cross-section of composite arm with aluminum bearing housing bolted to arm [94].

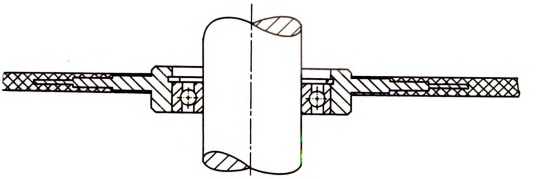

Figure 2.24. Cross-section of composite arm with aluminum bearing housing fabricated within composite arm [94].

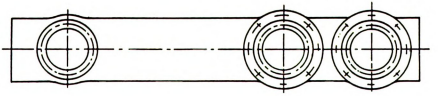

Figure 2.25. Composite arm detailing the enlarged mounting surface required for aluminum bearing housings [94].

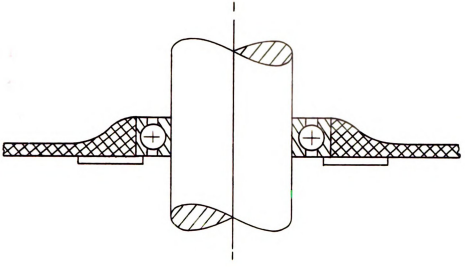

Figure 2.26. Cross-section of composite arm with chosen design: metal retaining ring bonded to inner surface.

With a well posed design problem, taking into account all design factors and assumptions, the modeling and analysis can be initiated.

2.6 FINITE ELEMENT ANALYSIS

The purpose of the finite element analysis (FEA) is to determine the laminate sequence for the composite arm such that it has the same effective stiffness as the aluminum arm. Finite element analyses can determine displacements and stresses in proposed designs before prototypes are manufactured.

Using analytic methods, the study of a simple Euler-Bernoulli beam is straightforward. Effects such as load-displacement relations and natural frequencies and mode shapes can be observed. Analytic results should compare closely with results from experiments through careful execution. For more complex problems such as the analysis of three-dimensional beams and plates with complex shapes and loadings, the finite element method can be developed to solve for displacements and mode shapes. Although many books on the finite element method exist [96-98], the analysis of a structure such as the robot arm is a complex problem.

Furthermore, as found in Section 2.3, much of the theory for mechanics of composites is developed for simple beams, plates, and shells. Therefore, the theory cannot be applied to the analysis of the robot arm. Numerous FEA packages are commercially available. Most can solve three dimensional problems that include effects such as composite laminates in the form of anisotropic shells and solids. In general, the FEA packages can also analyze a dynamic problem such as a beam in motion, although this capability is limited, especially for systems of components such as a robotic manipulator. Using the analysis model, one can try different geometries, ply sequences, and simulated loads to evaluate design performance.

Using the finite element method, the geometry is approximated using elements chosen for the analysis to correctly simulate the actual problem. For example, the analysis of a beverage can would employ three-dimensional thin-shell elements with the isotropic properties of aluminum.

Triangular and quadrilateral (rectangular) elements presented in Figure 2.27 are two different types of shell elements available in most commercial packages. Both types of elements are characterized by the order of the element, where Figure 2.27 presents linear and quadratic order elements. The element order is determined by the approximation functions used to describe the geometry and displacements of the element. Thus, the order is also directly related to the accuracy desired. Linear elements deform linearly, and in Figure 2.28, the deflections of a cantilever beam determined from linear elements will not accurately represent the deformed shape. The exact solution to Figure 2.28 is a fourth-order polynomial, so improved accuracy can be obtained using high-order elements, which also exhibit higher rates of convergence than linear elements.

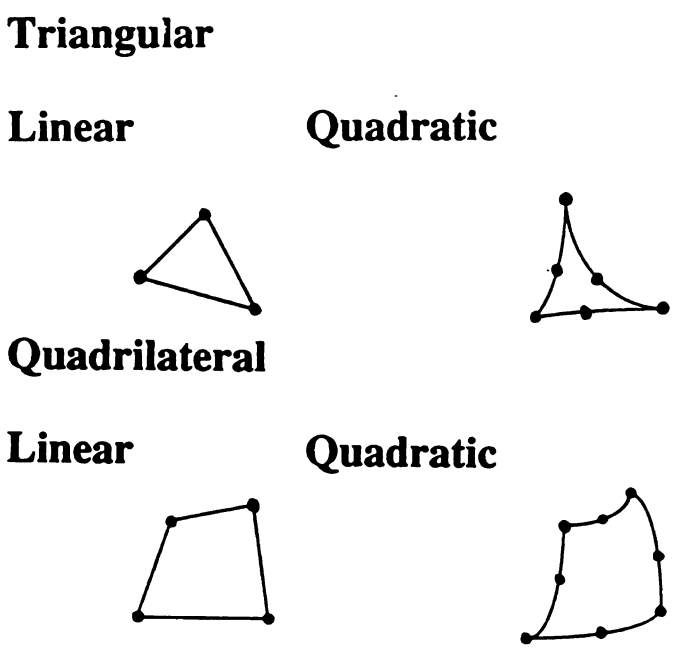

Figure 2.27. Triangular and quadrilateral elements.

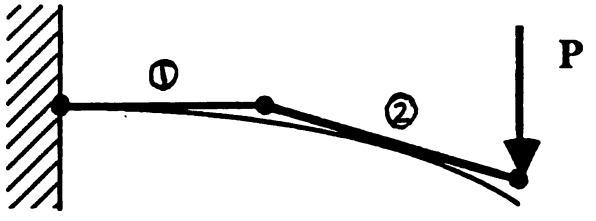

Figure 2.28. Finite element model of a cantilevered beam employing two linear beam elements.

Other important ideas include element connectivity, element distortion, and geometry approximations. In Figure 2.29, the element normal which comes out of the page, follows the right-hand rule using local nodal coordinates

one through four. The model must have consistent connectivity of all of its elements, such as all element normals outward from the center of the structure. Figure 2.30 presents highly distorted elements which should be avoided to assure accuracy of solution. Non-symmetric triangular meshes in symmetric structures will result in non-symmetric and misleading solutions. As a recommendation, Figure 2.31 depicts the use of quadrilateral elements in triangular and circular geometries.

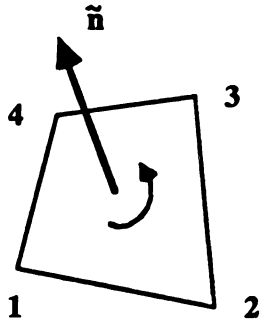

Figure 2.29. Element connectivity with outward normal, ñ.

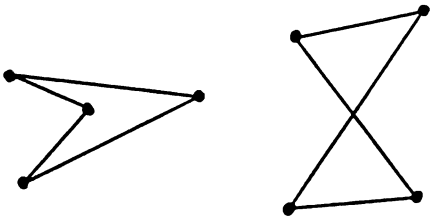

Figure 2.30. Highly distorted and twisted elements.

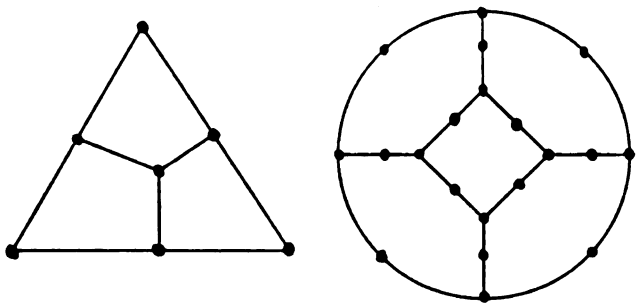

Figure 2.31. Use of quadrilateral elements for triangular and circular geometries.

The finite element modeler also discovers that each problem is different, and familiarity with the model is crucial. Mesh generation and mesh refinement are necessary skills the modeler must develop. Few rules apply to mesh generation, where any two modelers will usually conceive different meshes for the same problem. Figure 2.32 is an example that illustrates the effect of mesh refinement on a cantilever block with a stress concentration. Note that Figures 2.32(b) and 2.32(c) require the same computation time, but Figure 2.32(b) obtains a better solution in the area of interest.

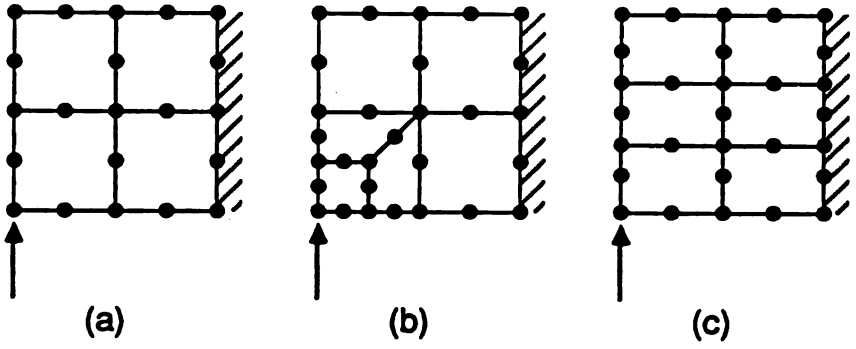

Figure 2.32. Cantilever block with stress concentration:
(a) 4 elements, 21 nodes, 12.5 sec,
(b) 6 elements, 29 nodes, 16.3 sec,
(c) 6 elements, 29 nodes, 16.3 sec.

The robot arm was analyzed with NISA II, a commercial finite element package developed by Engineering Mechanics Research Corporation [99]. Inputs for the model included static and eigenvalue analysis type, shell element type, element connectivity, nodal locations, material type(s), and loading case(s). The element and nodal data were derived primarily through a pre-processor. The pre-processor determined nodal locations and element connectivity automatically from a geometric model. Further refinements by hand were then required to sufficiently model the arm for the final mesh of Figure 2.33.

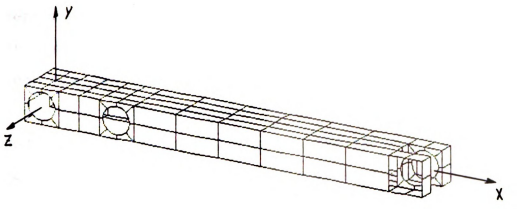

Figure 2.33. Finite element model of P-50 forearm. Note the orientation of the coordinate system, with the x-axis along the length of the arm and the y-axis vertical to the arm.

The geometrical characteristics were obtained from the shape and dimensions of the original arm. The model consisted of 188 three dimensional quadratic shell elements with six degrees-of-freedom per node and eight nodes per element for a total of 3750 degrees-of-freedom. The NISA II element included bending and membrane deformation effects and transverse shear deformation. The element did not provide rotational stiffness about the normal, $\hat{n}$, but in bending load cases, difficulties in numerical computations were not encountered. The only requirements for the FEA model were resultant nodal displacements, although strains and stresses could also be computed from the model.

The finite element model was verified by comparing the

deflection of the actual aluminum arm to that of the finite element model. The apparatus and procedure for the experiment can be found in Section 4.1. The deflections between the two were compared by enforcing identical loading and boundary conditions. The results of the comparison are listed in Table 2.5 and plotted in Figure 2.34. The complex geometry, including bearing openings and tapered edges, intuitively reduced the accuracy of the model, although experimental and numerical results were within 5 percent of each other. Static loads in the vertical and horizontal planes, and a torsional load, shown imposed on the model in Figure 2.35 display the versatility of FEA modeling.

Table 2.5. Deflection of the aluminum arm due to applied vertical static loads. Experimental and numerical values.

	Deflection (mm)	
Load (N)	Experiment	F.E.M.
0.0	0.00	0.000
88.2	0.09	-
96.0	0.10	-
129.7	0.13	0.132
217.9	0.22	-
225.7	0.23	-
313.9	0.33	0.320

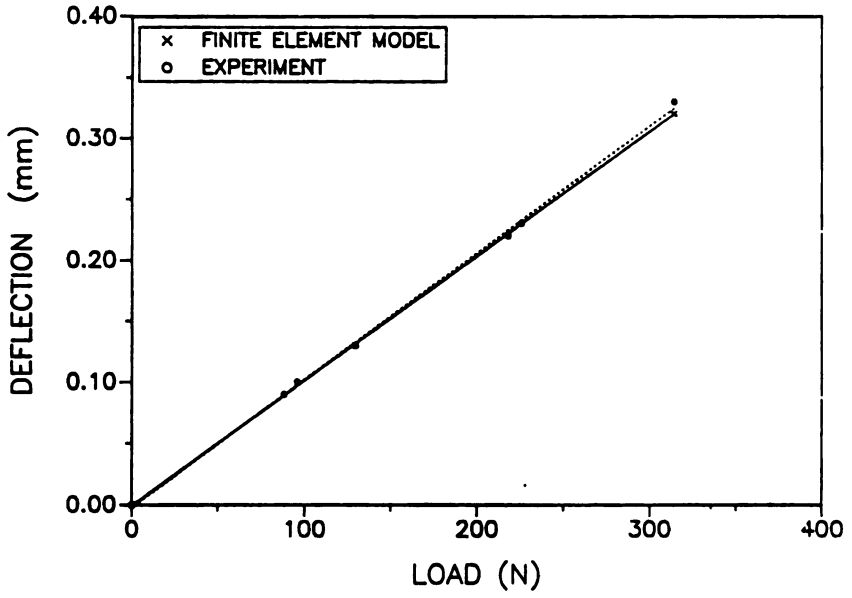

Figure 2.34. Deflection of the aluminum arm as a function of applied static load in the -z direction applied on the end of the arm. Experimental and numerical results.

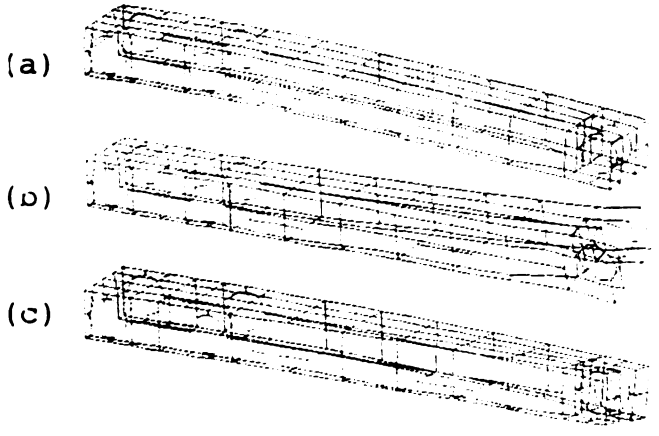

Figure 2.35. Finite element solutions for (a) vertical, (b) horizontal, and (c) torsional static loads.

Comparisons of an eigenvalue analysis using the FEA package and frequency response experiments described in Section 4.2 found the first natural frequencies of the model and actual arm to be within one percent of each other, both indicating the first twisting mode. The eigenvalue analysis

detected a second twisting mode, but the experiments did not. This was likely because the aluminum forearm was a two-piece casting. The joint was not considered in the FEA model which added torsional rigidity to the arm. Table 2.6 lists the comparative results. The first three free-free non-zero mode shapes are presented in Figure 2.36.

Table 2.6. Comparison between frequency response experiments and numerical eigenvalue analysis for the aluminum forearm.

	Natural Frequency (Hz) and Mode Shape		
Experiment	1. Twist		2. Bending
	276		398
Numerical	1. Twist	2. Double Twist	3. Bending
	274	346	403

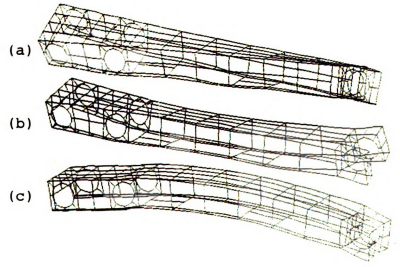

Figure 2.36. Finite element solutions for the eigenvalue analysis. Mode shapes are (1) twisting, (2) double twising, and (3) bending.

The FEA model was subsequently modified to incorporate anisotropic material properties using a composite element supplied by the package. Data required for the computation included stiffness values of the composite, number of laminae (plies), and orientations of each ply with respect to a user supplied coordinate direction. The NISA II composite element assumptions include the previous deformation effects, and assumed perfect bonding between each layer. To avoid confusion and aid in manufacturing, a symmetric lay-up was used. To determine the lay-up for fabrication, many iterations of solving the model were needed to determine the best stacking sequence for the composite laminate with the above design constraints and a 313.9 N vertical load.

Table 2.7 presents composite laminate sequences evaluated using the FEA model. Unidirectional and woven fabric composites were discussed in Section 2.3. The unidirectional material was chosen due to the high stiffness in the longitudinal direction. Several layers of woven fabric material were required in the lay-up to prevent delamination along free edges. The laminate sequence for the composite model having the same effective stiffness as the aluminum model was:

$$[45w/0/0]_3 \quad [0]_8 \quad [0/0/45w]_3$$

where the 45w represents woven fabric oriented 45° to the principal material axis (the x-axis), and the 0 represents

unidirectional material oriented along the principal axis. Through careful fabrication, good results are anticipated.

Table 2.7. Deflection due to applied static load of 313.9 N for the aluminum arm and various stacking sequences of graphite/epoxy composite (w = woven fabric).

Material	Deflection (mm)	Thickness (mm)
Aluminum	0.320	7.00
Composite - Stacking Sequence		
$[0]_{36}$	0.251	4.57
$([\pm 45/0/0]_4[0]_2)_s$	0.307	4.57
$([45w/0/0]_4[0]_2)_s$	0.280	5.18
$([0w/0/0]_3[0]_4)_s$	0.341	4.52
$([45w/0/0]_3[0]_4)_s$	0.320	4.52

2.7 REMARKS ON COMPOSITE ARM DESIGN

Many different concepts were considered for the design of the composite robot arm. Certain manufacturing processes were specific for certain types of composite materials. Advanced materials theory was required to predict the properties of composite laminates. Using proper modeling techniques, designs were easily tested before fabrication of the composte robot arm.

a co

are

prod

perf

of r

prev

sub-

as s

The

asse

fat

cas

GE

fab

exe

Sec

pur

imp

wou

Con

lay

CHAPTER 3

FABRICATION OF COMPOSITE ARM

The design and fabrication of a composite robot arm is a complex undertaking. Many different methods and materials are available to the design engineer for analyzing and producing composite components. Composites can improve the performance of high-speed machinery and reduce deflections of robotic manipulators where conventional materials were previously applied. Parts which are currently fabricated as sub-assemblies in monolithic materials could be fabricated as single parts in composite materials (part consolidation). The higher cost of composites can be justified by reduced assembly and machining costs, and improved performance and fatigue life. The original aluminum arm was a two-piece casting which conforms to the geometric constraints of the GE P-50 Robotic Manipulator. One composite arm is to be fabricated, so the fabrication process should be carefully executed.

The hand lay-up fabrication process selected in Section 2.2 required minimal investment costs, the major purchase being the aluminum mold. The fabrication process implied that each layer of the chosen laminate sequence would be applied by hand onto the mold. The final laminate contained 20 unidirectional layers and six woven fabric layers. The laminate was cured in an autoclave according to

manufacurers specifications and removed from the mold. Machining of the arm was required for the bearing housings and robot member interfaces.

3.1 MOLD DESIGN

The design of the mold was attributed to Auto Air's Dave Graves who had many years of experience in the field of hand lay-up [82]. The mold, shown in Figure 3.1, was an 18-piece male mold which was disassembled (Figure 3.2) and removed from the arm after curing through small openings in the arm. Correct dimensions of the mold were verified with the original aluminum arm.

Local dimensions such as width and height were taken from the aluminum arm. Mold expansion during the cure cycle was accounted for in the overall length of the mold. The bearing surface dimensions could not be molded exactly, so six bearing bosses, 2.9 inches in diameter, were used as undersized molds. This required machining 0.1 inch off of each bearing surfaces to the recommended 0.001 inch interference fit [100]. For the lay-up, the bearing areas were filled with woven fabric scraps (Figure 3.3) to prevent the unidirectional fibers from being machined and to avoid delamination.

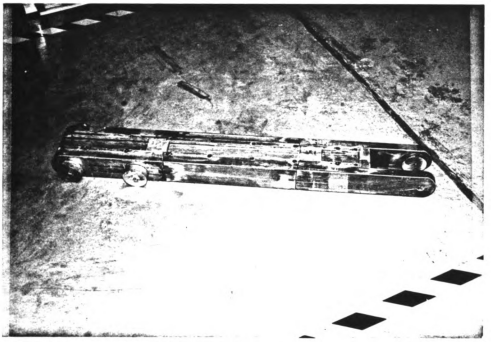

Figure 3.1. Photograph of assembled mold.

Figure 3.2. Photograph of disassembled mold.

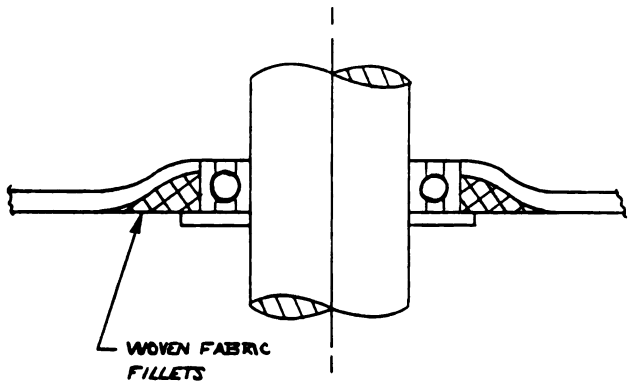

Figure 3.3. Cross-section of composite arm showing the location of the fillets.

Prior to lay-up, the mold pieces were coated with Epoxical liquid release compound, manufactured by USG Industries. The release compound aided in the removal of the mold after curing. These pieces were then assembled using hex head bolts and pull dowels. Pull dowels were used on the bearing bosses for easy removal. The bolts and pull dowels were also coated with the release agent, and covered with plastic tape. Gaps between mold sections were then filled using TP-903 tooling polyester, manufactured by Akemi Plastics, Incorporated. At this point, the mold was ready for lay-up.

3.2 FABRICATION - COMPOSITE LAY-UP

The mold was first warmed in an oven at 100°C for 30 minutes. The bearing fillets and the very first layer were easy to apply using the heated mold. Since the aluminum mold was warm, the material adhered to the mold, even though it was coated with the release agent.

Figure 3.4 shows the locations of the fillets. As mentioned earlier, the fillets were added using scrap material to be machined for the bearing surfaces. By using filler material, the unidirectional layers were not cut by the machining, retaining the strength of the laminate. This method also prevented delamination during machining. The bearing surface width of 16 mm was obtained from enlarging the laminate thickness of 4.4 mm using the filler material applied in a random manner around the bearing bosses. A

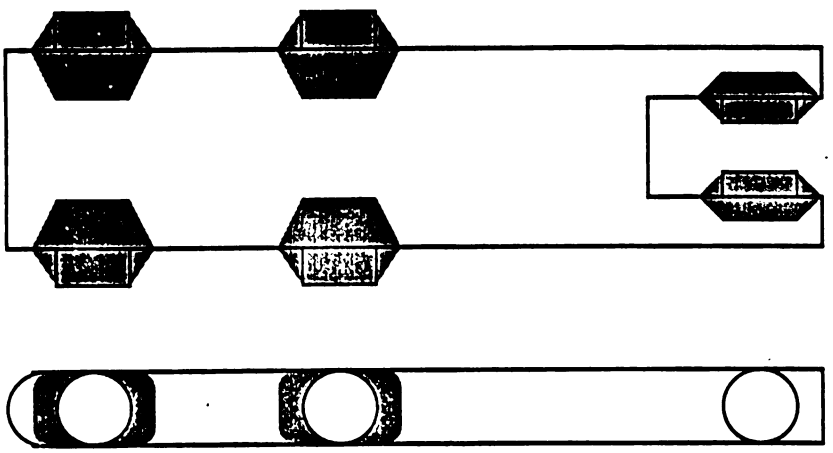

Figure 3.4. Location of fillets on the mold designed to create bearing surfaces.

number of important issues for working with composite materials will now be pointed out.

The epoxy resin (Hercules 3501-6) used in the composite material has a 0°C shelf life of six months. At 22°C, the shelf life is ten days. So the composite material remained in freezer storage until required. Every two days, a small supply of material was cut from the unidirectional and woven fabric rolls, and the rolls were placed back in the freezers. Care was taken not to expose the material to moisture, and the material was not handled when frozen. This resulted in a delay time between material preparation and actual lay-up. A safety suggestion for applying the pre-preg was to wear gloves during handling. Hand lotion was used extensively instead of gloves because the pre-preg was much easier to apply without gloves. Lab coats and hair nets were worn to prevent contamination of the laminate. Fabrication was performed in a clean room at Auto Air, isolated from the rest of the building. The actual application of the layers is a skill to learn. The author first completed a ten-layer glass/epoxy arm to practice the lay-up technique (with inexpensive material).

The unidirectional layers were applied in pairs to reduce fabrication time. The application of unidirectional layers is shown in Figure 3.5. The fiber angle for the unidirectional layers was 0° to the x-axis (along the length

of the arm). The unidirectional material had brown paper as a backing material. During the lay-up, this paper was left on the pre-preg because although the strength in the fiber direction was high, the pre-preg easily pulled apart in the transverse direction (see Figure 3.6). As each piece of the unidirectional material was applied, the brown paper was removed. At times, the pre-preg would not stick to the laminate sufficiently, so a heat gun was used to warm the material enough to make it sticky. The heat gun was used conservatively, however, because epoxy cures under heat. The quality of the final cure was affected each time the heat gun was applied.

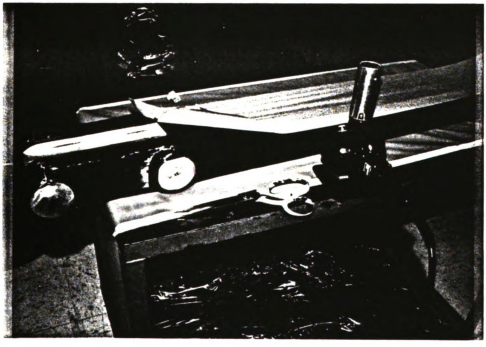

Figure 3.5. Unidirectional pre-preg applied to arm.

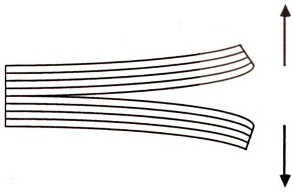

Figure 3.6. Tearing of unidirectional material in the transverse direction.

Figures 3.7 and 3.8 show difficulties in applying the unidirectional pre-preg over contoured surfaces. Figure 3.7 is a view of the bottom of the laminate at a bearing section. Note that a cut across a layer of fibers was directly beneath the bearing opening. The gaps were butt-joined and staggered to eliminate any possible weak points in the laminate. Minor cuts in the material such as this were expected through the lamination process, although the main section contains no cuts, gaps, or joints. Fiber angle along most of the arm was within 1° of the 0° design orientation.

Figure 3.8 presents the contoured bearing surfaces, where unidirectional material split along the fibers, revealing the woven fabric layers below. Small pieces of pre-preg were added over the gaps. Figure 3.9 shows the unidirectional pre-preg applied at the end section for the right fork. First, flaps were folded from the sides over the end and trimmed. Then tabs from the top and bottom surfaces were folded over each other on the end. Finally, a separate rectangular piece of material was applied inside the end section, between the two forks. A two inch wide belt of pre-preg was then applied over the graphite septum between the end forks. Additional pieces were added to cover gaps.

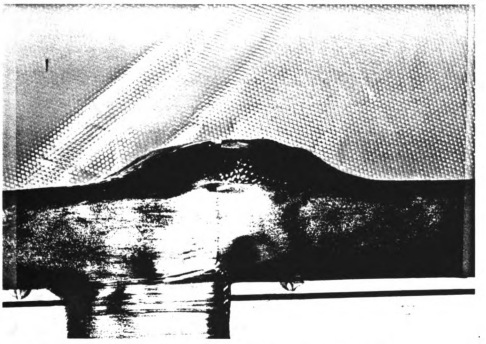

Figure 3.7. Lay-up of unidirectional pre-preg beneath the bearing opening.

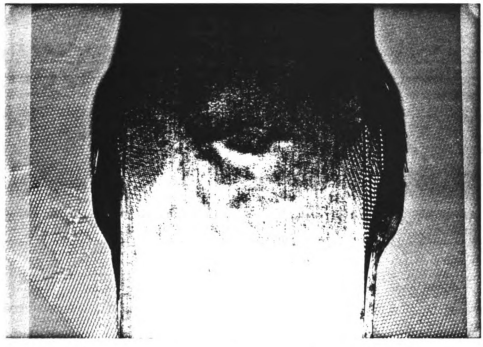

Figure 3.8. Contours on surface created gaps in the unidirectional pre-preg lay-up.

Figure 3.9. Unidirectional material applied at end section.

The woven fabric pre-preg was much easier to apply because the 0°/90° weave held together. Also, the material would stretch along the bias (Figure 3.10), the diagonal of the weave, which allowed curved surfaces to be fully covered. The woven fabric was oriented at 45° for all six layers. The main reason for using the woven fabric was not only for ease of fabrication, but also to prevent splitting, delamination, and edge-effects of the unidirectional material. Figures 3.11 to 3.13 show the application of the woven fabric at the end section. Figure 3.14 of the bearing section shows that at some locations, cuts in the woven fabric were required, although for the final layer (Figure 3.15), minimal cuts were made. It was difficult to control the fiber angle of the woven fabric for the entire arm since the bias disoriented fibers over contoured surfaces. Careful accounting was kept on the laminate sequence using a lay-up checklist as the arm was constructed (Table 3.1).

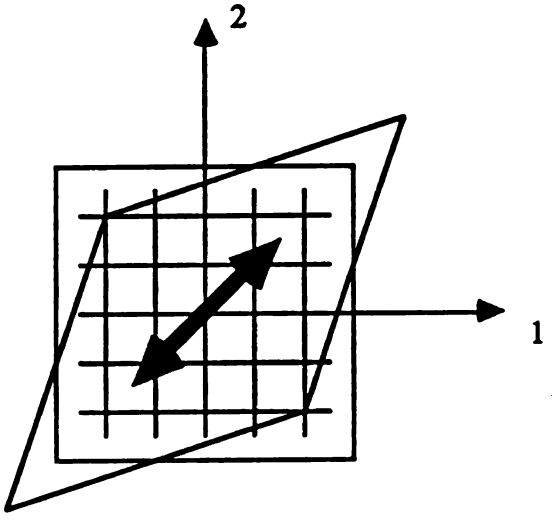

Figure 3.10. Bias of woven fabric.

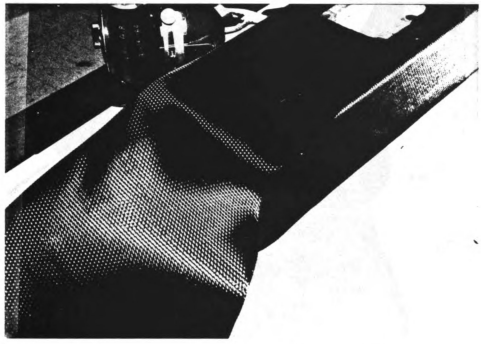

Figure 3.11. Lay-up material loosely on part.

Figure 3.12. Work with one section at a time.

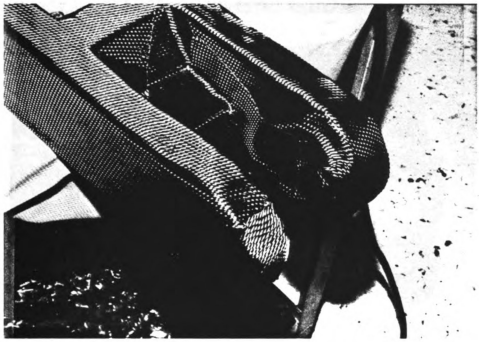

Figure 3.13. Be sure all edges are down securely. Trim edges as required.

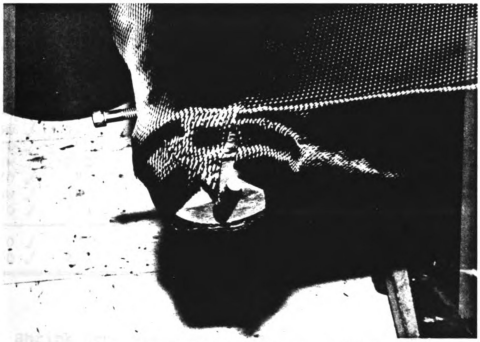

Figure 3.14. Cuts in woven fabric around bearing section.

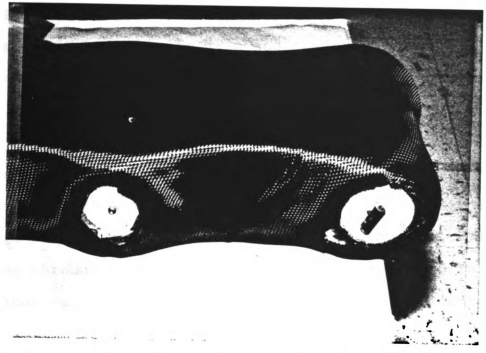

Figure 3.15. Final layer of woven fabric. Very few cuts were made.

Table 3.1. Laminate sequence checklist for fabrication.

Laminate Sequence Check-off List					
Layer	Date	Hours	Layer	Date	Hours
45w ✓	2/1	3.5	0/0 ✓	"	
0/0 ✓	"		0/0 ✓	2/6	3.5
45w ✓	2/2	4.5			
0/0 ✓	"		0/0 ✓	"	
45w ✓	"		45w ✓	"	
0/0 ✓	2/3	4.0	0/0 ✓	2/7	5.0
			45w ✓	"	
0/0 ✓	"		0/0 ✓	"	
0/0 ✓	2/4	4.5	45w ✓	"	

Shrink tape was used to secure layers of prepreg in tight corners when pressure from hands was not adequate.

The shrink tape contracts under heat from the heat gun. By wrapping the shrink tape over loose areas and securing, the heat gun would shrink the wrap and compress the layers onto the laminate.

Each night, the mold was bagged and debulked at room temperature to remove excess air from the pre-preg laminate (sequence of Figures 3.16 to 3.18). The void content is the measure of air pockets present in a cured laminate. Fibers passing through voids are not supported by surround resin. The fiber may buckle or crack, creating stress concentrations in the resin [73]. By applying a vacuum, the pre-preg material compressed, creating a thinner pre-cure laminate and insuring a low void content in the cured laminate.

Figure 3.16. Debulking bag prepared for vacuum.

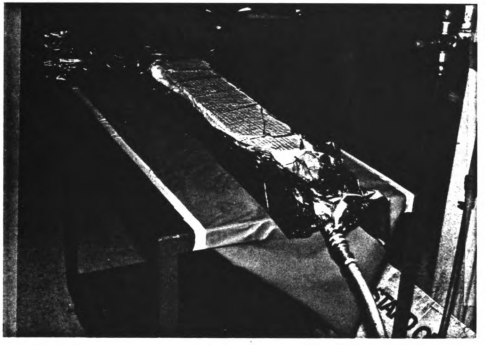

Figure 3.17. Debulking bag under 30 psi vacuum.

Figure 3.18. Detail showing the pulling effect at the end section between the two forks.

The debulking process consisted of wrapping the laminate in scrap backing material (obtained from the woven fabric roll). Next, the laminate was inserted into the bag. An air bleeder cloth was included to allow air from the far side of the bag to escape through the spicket, which connects to a vacuum hose. The bag was then applied a vacuum of 30 psi for the whole night. By morning, the laminate was packed tight and resin was observed on the surface of the laminate.

An important finding was that a wrinkle in the vacuum bag would result in a mark or a wrinkle in the laminate. As the lay-up progressed, the significance of a wrinkle-free vacuum bag increased. At the end section, a large quantity of bagging material was required to prevent the material from pulling away from the end section. The resident expert at Auto Air assisted in removing wrinkles in the autoclave vacuum bag and prepared the dual spicket bag properly for the autoclave. A significant amount of resin flowed from the laminate during cure, which can clog the vacuum lines. The dual spicket configuration insured proper vacuum during the cure process.

3.3 AUTOCLAVE CURING

The pre-preg material was cured according to the manufacturers specifications [89] for the 3501-6 resin, with

the cure cycle shown in Figure 3.19. The material property specifications should be obtained through proper implementation of the prescribed cure cycle. Also cured were test panels of unidirectional and woven fabric composites. The test panels were then used to determine the material properties of the cured laminate which are listed in Section 4.1.

A modern autoclave consists of a heating and cooling system within a pressurized container. The system parameters of temperature and pressure are micro-processor controlled, although vacuum of the bagged part may require manual control. The MSU Composite Materials and Structures Center (CMSC) autoclave is shown in Figure 3.20. The test panels for determining material properties were cured at MSU. The small size restricted maximum part length to two feet. Since the robot arm would not fit in the MSU-CMSC autoclave, Auto Air Industries cured the arm. The Auto Air autoclave is shown in Figure 3.21, in which the 1989 MSU SAE student formula race car was cured.

After autoclaving, the mold was removed from the composite arm in steps. First, the bottom mold plate was removed through the rear opening at the bearing section, then the top mold plate was removed. Through the opening in the bottom of the composite arm, the left and right side mold plates were removed in pieces. Lastly, the miscellaneous pieces were taken from the arm. Large amounts

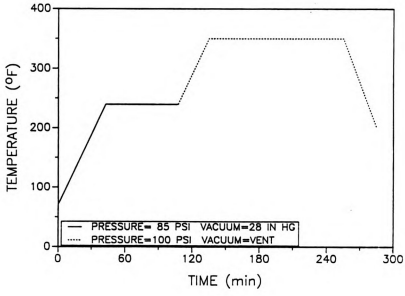

Figure 3.19. Cure cycle for 3501-6 epoxy.

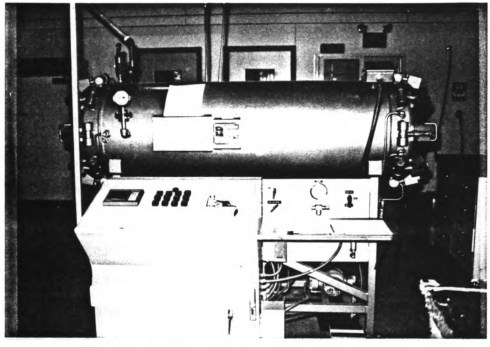

Figure 3.20. Photograph of MSU-CMSC autoclave.

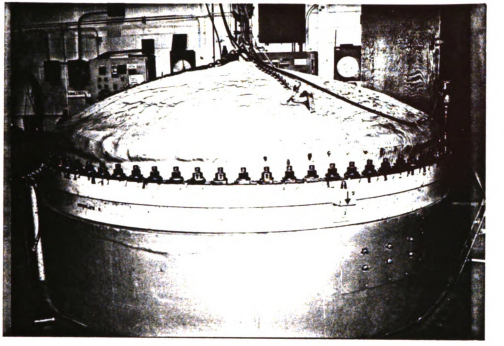

Figure 3.21. Photograph of Auto Air Industries autoclave.

of resin had seeped through cracks into the mold, and in several places, the composite laminate overlapped access areas and covered bolt heads, which created difficulties in disassembling the mold. The bolt heads were revealed and access areas were enlarged as required for disassembly using a grinding wheel.

The difference in the thermal expansion coefficients between the aluminum mold and the composite laminate affected the final dimensions of the cured part. As discussed in Section 3.1, an expansion coefficient was used in determining the length of the mold. Aluminum expands under heat, i.e., it has a positive coefficient of thermal

expansion of 23.0E-06/K. Unidirectional graphite epoxy has a slightly negative coefficient of thermal expansion of -0.9E-06/K. Under this competing effect, tremendous forces were generated between the mold and the laminate during the cure cycle. Upon mold removal, it was found that several of the pull dowels that retain the bearing bosses were sheared.

Before machining, the arm was post-cured with the test specimens for final cross linking of the polymer chains. The post-cure cycle was 180°C for three hours, with ambient pressure and no vacuum.

3.4 MACHINING THE COMPOSITE ARM

Serious problems can be encountered in machining composite materials. In particular, the graphite-epoxy was a very abrasive material. Tool wear and composite delamination result from improper machining. Studies were conducted to determine the best tool shapes and materials suitable for machining composites [66]. Possible tool materials included carbide, ceramic, and diamond inserts. The graphite/epoxy bearing housing test specimen (Figure 3.22) was fabricated to determine problems with properly fitting the bearing and obtaining an adequate surface finish from machining.

The bearing housing test specimen was fabricated from

material scraps of Fiberite Hy-E 1034C continuous fiber graphite/epoxy prepreg, with a $[0/90]_{10}$ lay-up sequence. Two 1" wide pre-preg strips were wrapped around the boss for each layer in the body, so the test specimen contained a significant amount of unidirectional fiber in the boss area. Using the specifications of Figure 3.23, the specimen was machined by the Michigan State University Physics Department Machine Shop. It was anticipated that the Physics machine shop would also machine the composite forearm, so they were given the bearing housing test specimen to practice with since only one composite arm was fabricated.

First, the height was machined off of the specimen using a carbide boring rasp. Accuracy over this area was

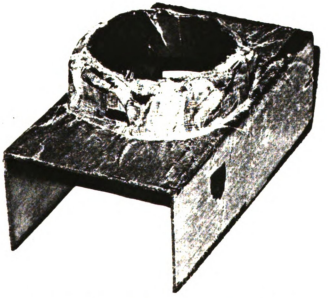

Figure 3.22. Bearing housing test specimen.

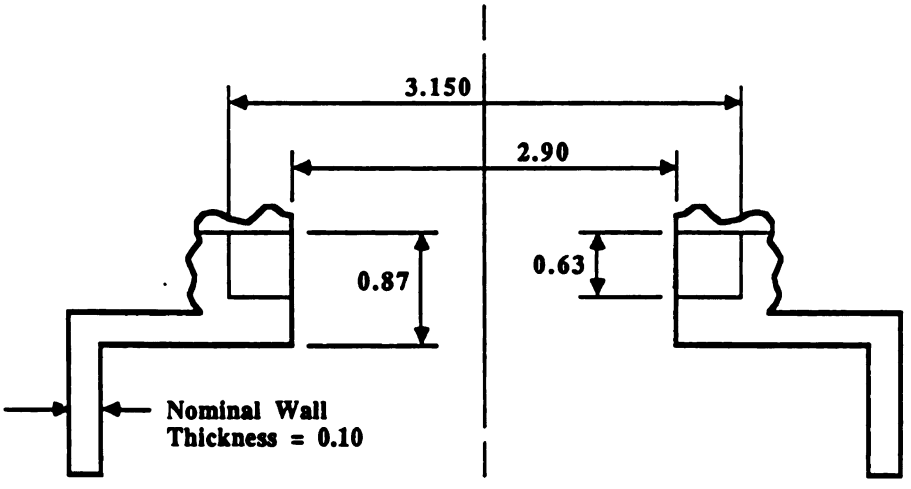

Figure 3.23. Bearing housing test specimen machining specifications.

not required, so the tolerance was easily maintained at ±0.01". The bearing surface was machined using an all-carbide tool which experienced significant wear. The required dimension for the bearing surface was 0.001" interference fit for a 3.150" diameter bearing [100]. The bore was machined initially from a diameter of 2.9" to 3.0". Significant tool wear was noted, and the tool was sharpened. The diameter was then opened up to 3.140" with verified error using calipers. The tool had worn down enough for significant error in the diameter. Another cut was made with the resharpened tool to bring the diameter within 0.004" of the required 0.001" interference fit.

For the final cut, the tool was resharpened. After the cut was made, it was found that the tool required so much pressure just to initiate cutting that the final diameter was 0.001" clearance, or 0.002" too far. The error was attributed to the amount of unidirectional composite present in the boss area, which resulted in very stiff material properties, and to the insufficient toughness of the carbide tool. The delamination of the unidirectional fibers was also observed as in Figure 3.24. To avoid these problems in machining the composite arm, woven fabric was randomly applied in the boss area, and a diamond-tipped tool was used for machining.

Before machining the composite arm, TP-903 polyester filler material, manufactured by Akemi Plastics, was applied to the end section to accommodate the end-effector (Figure 3.25). This detail was overlooked during mold design and fabrication, although negligible mass was added to the arm. The end section width was then ground from between the two forks by Auto Air using a 1" diameter white stone grinding wheel.

The arm was then fastened in a machining jig for the required cuts. A diamond insert fixed to a carbide boring bar was used to machine the end section. Proper machining

Figure 3.24. Delamination near bearing surface.

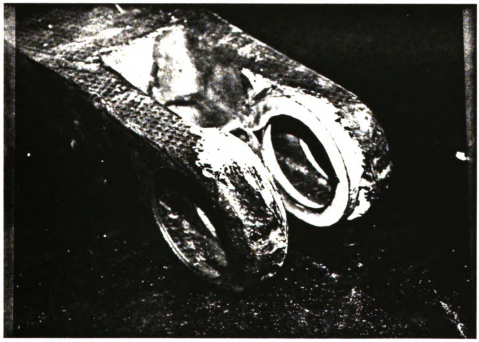

Figure 3.25. Polyester filler on end section.

was required to fit the end-effector parts supplied by General Electric such as the bend-axis bearings. The dimensions of the cuts are shown in Figure 3.26. Note the location of the epoxy filler material. No tool wear was noticed on the diamond insert, and the proper dimensions were obtained. The bearing section was then machined to accommodate the NSK 7010-ATYG bearings using the diamond tool.

Important manufacturing considerations in machining composites were discovered from machining the composite arm. Water baths should always be used for graphite/epoxy composites, since the fine graphite fibers were a dangerous breathing hazard. Surface finishes cannot be specified for

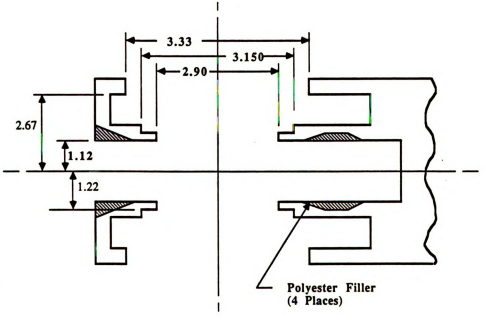

Figure 3.26. Machining instructions for the end section.

composites, which allow for only one final cut. The bearing surface finishes were completed using a fine-grit hone, although the final surface finish was clearly not as smooth as typical machined metal surfaces.

The final step in preparing the arm was the addition of the bearing retaining rings (Figure 3.27). The retaining rings were used to prevent axial movement. The retaining rings were bonded in place using Miller-Stephenson Versamid-140 Polyamid Resin manufactured by Henkel Corporation, and Epon Resin 828 manufactured by Shell Chemical Corporation. The resin mass mixture ratio was 1.0:0.8. After applying the resin mixture and clamping the rings in place, the epoxy was cured at 100°C for two hours.

With the fabrication and machining steps completed, testing was conducted to determine the validity of the analysis and fabrication phases.

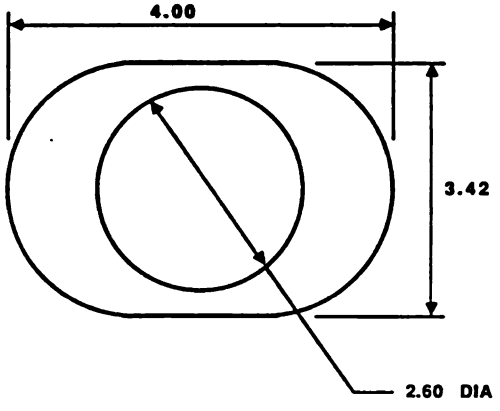

Figure 3.27. Bearing retaining ring.

CHAPTER 4

EXPERIMENTAL INVESTIGATION OF FOREARMS

Experiments were conducted on the aluminum and composite forearms isolated from the robotic manipulator. The composite arm had a mass of 3.7 kg, or 57 percent less than the aluminum arm (8.7 kg). The effective stiffnesses for both arms, determined through static testing, were intended to be equivalent. The natural frequencies of each forearm were determined through frequency response testing. Calibration constants were obtained in the following experiments to determine arm deflections from strain readings of the dynamic experiments of Chapter 5.

4.1 STATIC TESTING

The objective of the static testing was to determine the effective stiffness of the GE P-50 aluminum forearm and the composite forearm in the x-y plane (axes defined by Figure 2.33). The effective stiffnesses of the finite element model and the actual aluminum arm detailed in Section 2.6 were within five percent of each other. The design intentions were to create a composite arm which would have the same effective stiffness, so the two arms could be appropriately compared in a dynamic environment.

4.1.1 EXPERIMENTAL APPARATUS AND PROCEDURE

The static tests were performed with time-invariant loads using a static fixture mounted on a large, cast iron table presented in Figure 4.1. The fixture was prepared by the Michigan State University Physics Machine Shop. It consisted of one inch thick steel walls with stainless steel retaining pins. The experimental equipment is diagrammed in Figure 4.2. Deflections were measured using a Mitutoyo Model 2046-01 dial gage with 0.01 mm resolution. A set of four Micro-Measurements Model WD-DY-250BG-350 strain gages with a gage factor of 3.27 were arranged in a full bridge pattern and bonded to the arm for measurements of strain. The locations of the strain gages are shown in Figure 4.3. Values of strain were determined using a Measurements Group Model P-3500 Digital Strain Indicator with 1 $\mu\varepsilon$ resolution. For dynamic strain calibrations, a Measurements Group Model 2100 Strain Gage Conditioner and Amplifier System was used in the static tests in combination with a Beckman Model 3010 Digital Multimeter.

Figure 4.1. Static fixture for forearm testing.

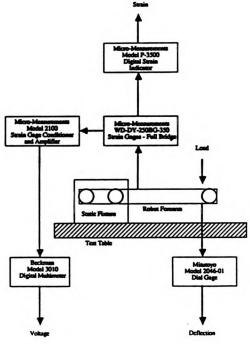

Figure 4.2. Experimental apparatus for forearm testing.

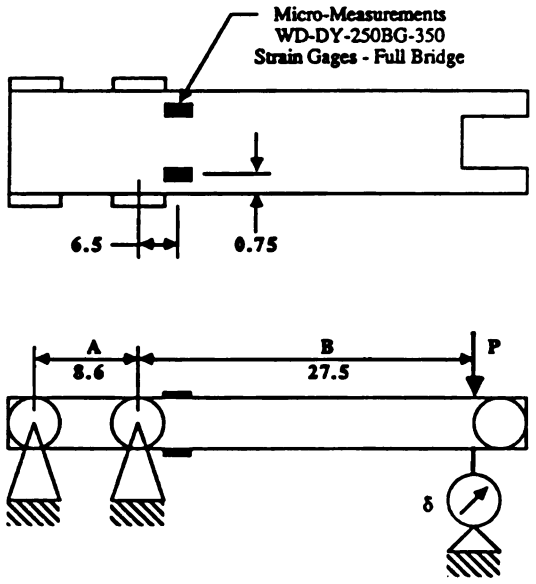

Figure 4.3. Full-bridge strain gage locations. Identical for aluminum and composite forearms.

To obtain the effective stiffness, the transverse arm deflection as a function of the load was determined for both arms. Three weights, using various combinations for a total of six loads, were applied as static loads on the end of the arm. Strain and deflection were recorded over five trials and averaged. Then voltage readings from the conditioner were found by a second set of tests using the same loading conditions.

4.1.2 EXPERIMENTAL RESULTS

As noted in Chapter 2, the finite element analysis and the experimental results for the aluminum arm were within

five percent of each other. The composite lay-up sequence was determined using the finite element model for effective stiffness equivalent to the aluminum arm and fabricated as described in Chapter 3.

Tables 4.1 and 4.2 list load, deflection, and strain for the aluminum and composite arms which were averaged over five loading cycles. Figure 4.4 shows deflection due to the prescribed static loads for the aluminum and composite arms obtained by the least squares method using the averaged values of Table 4.1. This graph shows that the composite arm had less effective stiffness. Using the equation for an overhanging beam,

$$EI = P\ B^2\ (A + B)\ /\ 3\ \delta,$$

with the parameters defined in Figure 4.3, the effective stiffesses were determined for each arm (Table 4.3). The composite arm had 38 percent less effective stiffness, which may be due to several factors. Possible causes were (1) incorrect composite FEM formulation, (2) inappropriate boundary conditions for analysis, (3) fabrication errors, and (4) cure procedure errors or faulty material errors.

Table 4.1. Averaged deflection values due to static loads for the aluminum and composite forearms.

	Deflection (mm)	
Load (N)	Aluminum	Composite
0.0	0.00	0.00
88.2	0.09	0.15
96.0	0.10	0.17
129.7	0.13	0.22
217.9	0.22	0.37
225.7	0.23	0.39
313.9	0.33	0.53

Table 4.2. Deflection versus strain for the aluminum and composite arms as measured.

Aluminum Arm		Composite Arm	
Strain ($\mu\epsilon$)	Defl. (mm)	Strain ($\mu\epsilon$)	Defl. (mm)
0.0	0.00	0.0	0.0
41.0	0.09	50.5	0.15
46.0	0.10	53.5	0.17
59.0	0.13	71.5	0.22
99.0	0.22	117.5	0.37
104.0	0.23	125.0	0.39
144.0	0.33	174.0	0.53

Table 4.3. Effective static stiffness for the aluminum and composite arms.

Effective Static Stiffness ($N \cdot mm^2$)	
Aluminum	141.7
Composite	88.2

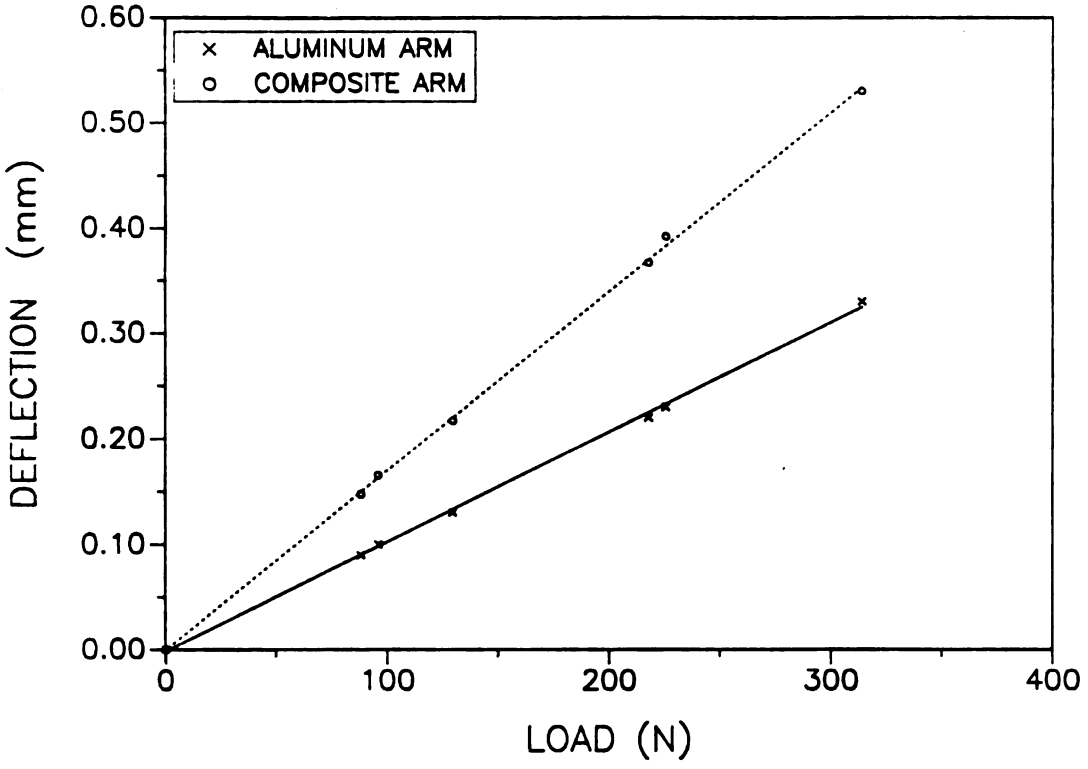

Figure 4.4. Deflection of forearm due to prescribed static loads.

Factors that influence finite element accuracy include element formulation, mesh formulation, boundary conditions, and computational errors. Since the aluminum model compared well, the finite element formulation errors were small.

Inappropriate boundary conditions may have been a likely source for error, since the openings on the composite arm for the bearing section have very complex stress patterns. The unidirectional material in the area of the openings may not have been properly oriented. One possible solution would be to model the arm as a cantilevered beam, neglecting the stiffness of the bearing section as shown in Figure 4.5.

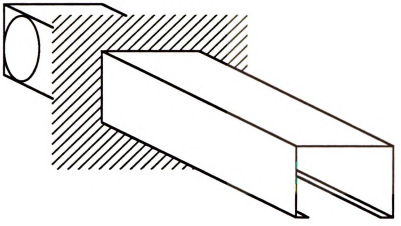

Figure 4.5. Arm modeled as cantilever beam, neglecting bearing section.

Fabrication error sources include misalignment of fibers and unclean application. The author fabricated the arm with great care in cleanliness and lay-up order, so fabrication errors were small.

The material quality and cure procedure were found to be major sources of error. Table 4.4 lists the material properties of the Hercules material (1) as published, (2) from test panels cured at the Michigan State University Composite Materials and Structures Center, and (3) from test panels cured simultaneously with the composite arm by Auto Air Industries. Note that the values given by the manufacturer were the greatest, specimens cured at MSU were the next highest, and specimens cured at Auto Air with the composite arm were the lowest. The published material

properties could only be obtained under ideal conditions specified by Hercules; obviously not achieved in either of cases (2) or (3). Note a 10 to 15 percent reduction in modulus between cases (2) and (3), possibly due to an incorrect cure cycle or aged material. The material properties implemented by the FEM program were of the specimens cured at MSU. Accordingly, the composite arm would be expected to have less stiffness than anticipated by the FEM simulation.

Table 4.4. Published values (1), cured at MSU Composite Materials and Structures Center (2), and cured simultaneously with composite arm (3) at Auto Air Industries (values in GPa).

AS4/3501-6 Unidirectional			
	1	2	3
E1	138.0	132.0	110.0
E2	9.0	10.1	8.1
G12	8.0	7.9	7.4
A370-5H/3501-6 Woven Fabric			
E1	69.0	58.7	51.8
E2	69.0	58.0	52.4
G12	8.0	7.2	6.1

Another result of the testing was the relationship of strain versus deflection (Figure 4.6). Using the combination of Figures 4.4 and 4.6, the relationship between strain and load may be obtained.

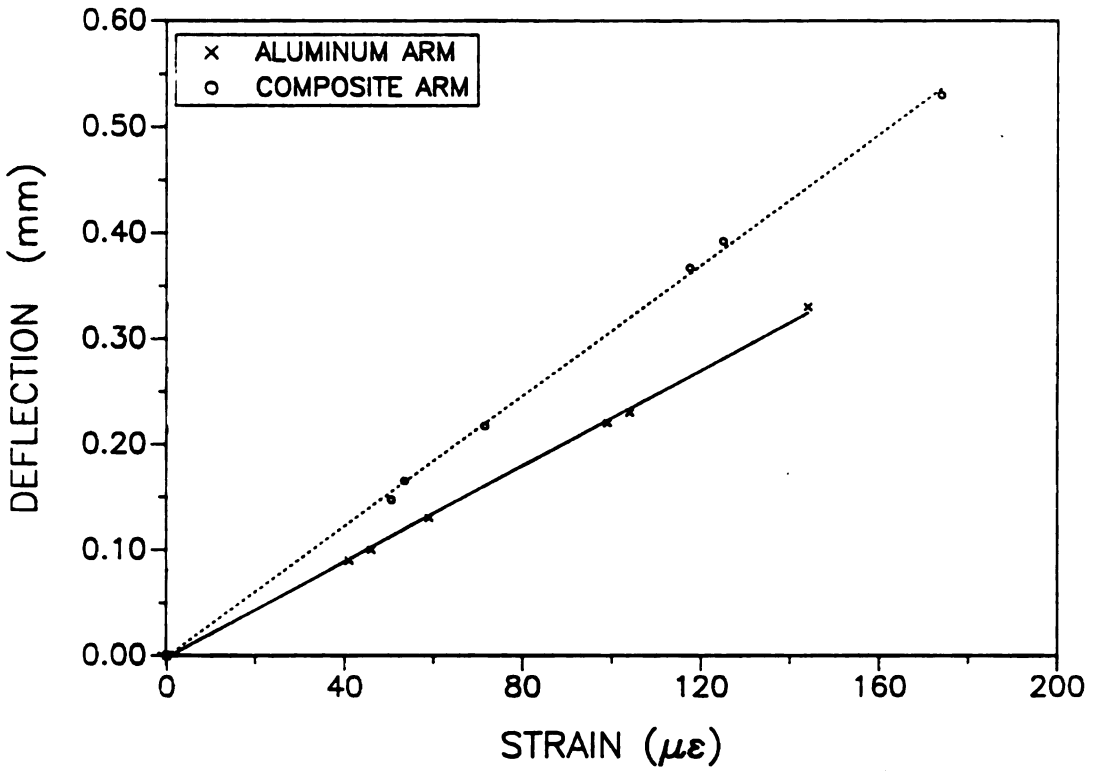

Figure 4.6. Deflection versus strain for aluminum and composite arms.

Strain calibration constants were also determined using the static fixture. Measurements were taken using the strain conditioner, which would also be used for dynamic robot testing. Figure 4.7 shows the relationship of the voltage output from the strain conditioner to the deflection of the arm. Strain conditioner readings from the dynamic robot testing would be implemented in Chapter 5, using this graph to convert voltage to arm deflection.

A clear advantage for using composites can be seen by comparing the stiffness-per-unit-mass between the aluminum and composite arms. Figure 4.8 reinforces the fact that by

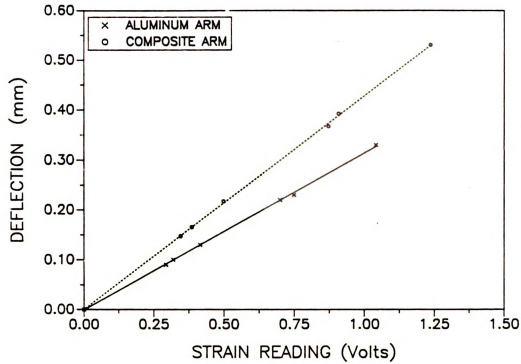

Figure 4.7. Deflection versus strain conditioner voltage output for the aluminum and composite forearms.

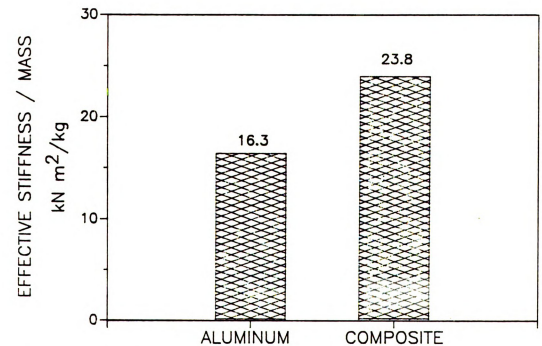

Figure 4.8. Stiffness-per-unit-mass of aluminum and composite forearms.

using composite materials, lighter and stiffer components can be fabricated.

4.2 FREQUENCY RESPONSE TESTING

An alternative method to obtain bending stiffness characteristics is to analyze the frequency response of the arm. Dynamic characteristics are obtained through frequency response testing.

4.2.1 EXPERIMENTAL APPARATUS AND PROCEDURE

The arms were supported for the free-free tests using foam blocks (see Figure 4.9). The foam blocks allowed sufficient rigid body motion upon excitation for the

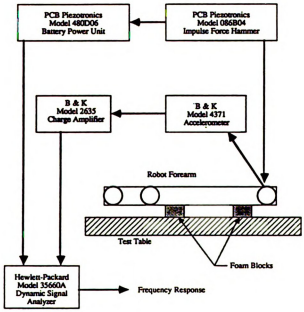

Figure 4.9. Experimental apparatus for frequency response testing.

free-free analysis. Rubber band hangers provided the same frequency response as foam but required a lengthy set-up and adjustment period prior to testing, so they were not used.

The frequency response and the fundamental frequencies of vibration were determined using the impulse testing method [101, 102], which requires an impulsive force input with measured response output. The transfer function between the input and output was then determined using a signal analyzer and converted into the frequency domain.

A Hewlett-Packard Model 35660A dynamic signal analyzer was used to compute the frequency response for the experiments. The excitation hammer was a PCB Piezotronics Model 086B04 Impulse Force Hammer with PCB Model 480D06 Battery Power Unit. The vibration was first measured using the strain gages and conditioner described in Section 4.1.1, but the first mode (twisting mode) was not found because a twist in the beam would not create a sufficient change in the strain reading due to the full-bridge arrangement. So the response was measured using a Bruel & Kjaer Model 4371 Accelerometer with a B&K Model 2635 Charge Amplifier.

4.2.2 EXPERIMENTAL RESULTS

The frequency responses for the aluminum and composite arms are presented in Figure 4.10, with the responses

averaged over ten trials using the RMS option on the signal analyzer. Note that the first two natural frequencies of the composite arm are higher than those for the aluminum arm, with values presented in Table 4.5.

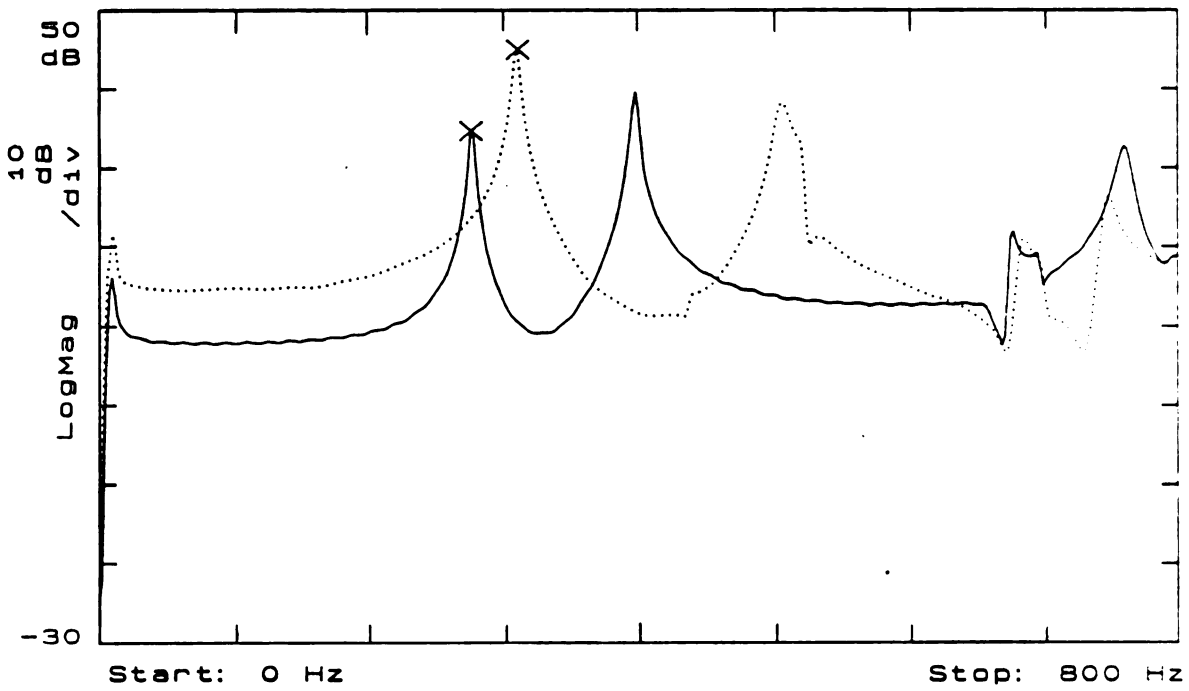

Figure 4.10. Frequency response of aluminum (solid) and composite (dotted) arms in a free-free configuration. Marked peaks represent twisting mode frequency. The left-most peaks represent the rigid body response due to the free-free configuration.

Table 4.5. First two fundamental frequencies from frequency response of the arms in free-free configurations. *Damping ratio was determined using the half power bandwidth method about the first fundamental frequency.

	Twisting Mode	Bending Mode	Damping Ratio*
Aluminum	276 Hz	398 Hz	0.0053
Composite	310 Hz	506 Hz	0.0061
Increase	13 %	27 %	15 %

It was anticipated that the robot would perform better with the composite arm because of less inertial loading as indicated by the above results. Thus higher maneuver speeds may be possible. Using the composite arm under the same operating speed, the required torques would be less. Also note that the damping ratio for the composite arm increased by 15 percent. Unidirectional graphite/epoxy composites have only slightly higher damping characteristics than aluminum, although for other angles, damping characteristics of graphite/epoxy are significantly higher.

4.3 MASS MOMENT OF INERTIA TESTING

The objective of this section is to compare the mass moment of inertia of the aluminum and composite forearms. The mass moment of inertia quantitatively represents the resistance for changes in rotational motions about the z-axis for the forearms. In general for any robot, the speed and accuracy of the robot can be improved by reducing the mass and the mass moment of inertia of the links.

The mass moments of inertia for the robot arms were calculated using the equation for the slender rod approximation: $I = ml^2/12 = 0.29$ kg m^2. The values, listed in Table 4.6, relied on the slender rod approximation. Experimental tests were undertaken to experimentally obtain improved values.

Table 4.6. Calculated mass moments of inertia for the forearms using the slender rod approximation.

Mass Moments of Inertia $kg \cdot m^2$	
Aluminum Arm	Composite Arm
0.84	0.35

4.3.1 EXPERIMENTAL APPARATUS AND PROCEDURE

To experimentally find the mass moment of inertia for arbitrary objects, the moment of inertia must be known for some other measurable object or specimen [103]. In this case, the mass moments of inertia for the arms were found through algebraic relations to a slender rod.

The bar used in the experiment has a mass of 1.8 kg, a length of 1.4 m, and an aspect ratio (width/length) of 0.04. Since the bar had a small aspect ratio, it was modeled as a slender rod, which had the mass moment of inertia: $I = ml^2/12 = 0.29\ kg \cdot m^2$. The bar was first suspended by a wire 0.5 m long about the bar's center of mass. Then the bar was rotated, which twisted the wire like a rotational spring. Upon release of the bar from rest, the period of oscillation was timed using a watch with 0.1 s resolution and averaged over five oscillations for an average of 21.8 s. Similarly, the periods of oscillation were found for the aluminum and composite arms to be 40.2 and 26.3 respectively (Table 4.7).

Table 4.7. Averaged periods of oscillation for the bar, the P-50 aluminum forearm, and the composite forearm.

Period of Oscillation (sec)		
Bar	Aluminum Arm	Composite Arm
21.8	40.2	26.3

4.3.2 EXPERIMENTAL RESULTS

Using the following equation where T represents the period of oscillation and I represents the mass moment of inertia,

$$I_{arm} = I_{bar} \left[\frac{T_{arm}}{T_{bar}} \right]^2 ,$$

the moments of inertia for the arms were related to the moment of inertia for the bar. Using this equation, the moments of inertia were calculated from the experimental comparison, with the values listed in Table 4.8.

These tests indicated that the mass moment of inertia of the composite arm was 58 percent less than the aluminum arm. This illustrates the potential reduction in energy required to maneuver the composite arm. Upon a stopping command, the torque required to stop the arm would be less.

Table 4.8. Measured mass moments of inertia for the forearms.

Mass Moments of Inertia $kg \cdot m^2$	
Aluminum Arm	Composite Arm
0.99	0.42

As an observation, the measured values (Table 4.8) for the arms were higher than the values calculated by the slender rod approximation (Table 4.6). This discrepancy was anticipated since each arm had mass distributed away from the longitudinal axis, which violated the slender rod approximation.

4.4 SUMMARY OF RESULTS

The mass of the composite forearm was 57 percent less than the aluminum arm. The static tests indicated that the static stiffness of the composite forearm was 38 percent less than the aluminum arm. From the frequency analysis, the fundamental frequency of the composite forearm was 13 percent higher than the original aluminum arm. The composite arm also exhibited enhanced damping characteristics. Finally, the mass moment of inertia of the composite arm was 58 percent less than the aluminum arm.

CHAPTER 5

EXPERIMENTAL INVESTIGATION OF ROBOTIC SYSTEMS

The P-50 robot, retrofitted with the composite arm (Figure 5.1), was tested in static and dynamic environments. The static experiments included static loading and unloading to determine the hysteresis in the system. Impulse testing determined the frequency response of the system. Transient vibration determined the fundamental frequencies for the system which were then compared with the frequency response data. The experiments conducted during robot maneuvers included recording robot tachometer values to verify forearm and upper arm positions. Absolute acceleration at the end-effector was recorded to evaluate dynamic performance, and

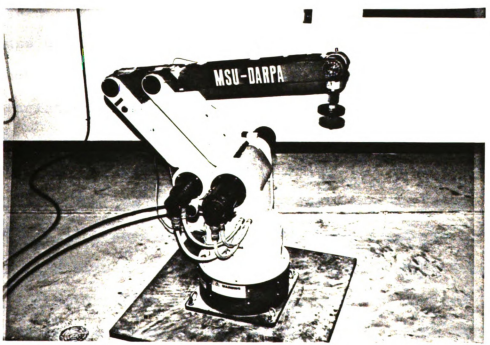

Figure 5.1. P-50 robot retrofitted with the composite arm.

strain in the forearm was recorded to evaluate the elastodynamic behavior.

The objective of the static tests was to compare positioning error characteristics between the P-50 robotic manipulator and the P-50 robot retrofitted with a composite forearm. Industrial robots comprise of an assemblage of different subassemblies, which all contribute to the positioning error. The positioning error is the deviation between the desired motion and the actual motion developed during a maneuver. The robot was evaluated at four configurations, given in Table 5.1, and graphically represented in Figure 5.2. Base rotation was not considered in the testing, so Figure 5.2 documents the vertical work-space envelope. Upon examining the figure, it is evident that the configurations were chosen in the work space to examine the response of the robot at the boundaries of the envelope. Although the robot is a five degree-of-freedom manipulator, only variations in forearm and upper arm positions were considered.

The objective of the dynamic tests was to compare the relative performance between the P-50 robot and the P-50 retrofitted with a composite forearm by evaluating acceleration characteristics at the end-effector and elastodynamic behavior of the forearm during articulation. From the dynamic response of the P-50, stiffness, damping, inertial,

Table 5.1. Prescribed angles for test configurations (angles in degrees). Configuration 1 is the zero position for the GE P-50 robot.

Configuration	Upper Arm θ_1	Forearm θ_2
1	133	2
2	133	22
3	90	0
4	44.5	-32

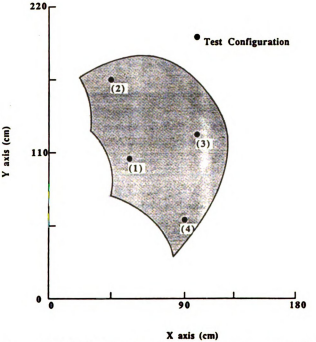

Figure 5.2. Vertical work envelope and test configurations.

and overshoot characteristics of the robotic system can be inferred.

Dynamic testing was performed on both robotic systems subjected to identical motions by running programmed

maneuvers of the P-50. The maneuvers, or test programs, are presented in Table 5.2. All three dynamic test programs initiated motion from configuration 1 (of Table 5.1), proceeded through configurations 2, 3, and 4, and ended the maneuver at configuration 1. For example, test program A, with a speed of 95 cm/sec, proceeded to each sequential configuration, pausing for 0.8 sec at each configuration. The tests were easily repeatable, resulting in a controlled experiment with little testing error.

Table 5.2. Test programs for the P-50 robot with aluminum and composite forearms. Speed is the velocity tangent to the trajectory described by the end-effector.

Test Program	Speed (cm/s)	Payload (kg)	Dwell Time (sec)
A	95	0.0	0.8
B	95	7.7	0.8
C	65	0.0	0.8

5.1 STATIC TESTING

The static testing was conducted to compare, quantitatively, the hysteresis characteristics and principal error sources of the P-50 robotic manipulator with those of the P-50 retrofitted with a composite forearm. Two types of hysteresis exist in the system. Material hysteresis is the measure of energy loss due to loading-unloading cycles on

the material. Viscoelastic materials such as polymers exhibit this characteristic. Metals behave elastically, with no energy loss after loading-unloading cycles. material hysteresis is a negligible effect compared to the linkage hysteresis. Robotic systems contain the second type of hysteresis, which is the non-linear behavior of the system due to contributions of the chain clearances, bearing clearances, gear backlash, and motor shaft viscous friction. From a mechanical-systems standpoint, the principal error sources are the clearance in the joints, the mass and stiffness characteristics of the structural members, and the inertia and flexibility in the drive-train.

5.1.1 EXPERIMENTAL APPARATUS AND PROCEDURE

Figure 5.3 schematically represents the equipment used for the static testing. Displacements were measured at the end-effector for each loading and unloading step using a Mitutoyo Model 2046-01 dial gage with 0.01 mm resolution. Simultaneously, voltage readings from the full-bridge Micro-Measurements Model WD-DY-250BG-350 strain gage arrangement and Micro-Measurements Model 2100 strain gage conditioner and amplifier, described in Section 4.1, were used to determine the amount of arm deflection which contributed to the total end-effector displacement. The voltage was converted to forearm deflection using the calibration constants determined in Section 4.1.

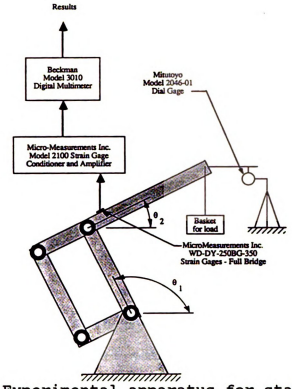

Figure 5.3. Experimental apparatus for static testing.

The tests were performed by loading the robotic manipulator at the end-effector with weights lowered into a basket. The loading procedure was to sequentially apply a set of eight 8.9 N weights, which resulted in a monotonically increasing load up to a maximum of 71.2 N. The loading procedure was then reversed for unloading. By loading the robotic manipulator at the wrist-assembly of the end-effector rather than the actual payload attachment location, displacements due to the chain drive for the bend and twist axes were eliminated from the measurements. The procedure was repeated at each of the four test configurations of Table 5.1 to obtain average values of deflection.

5.1.2 EXPERIMENTAL RESULTS

It is evident from Figure 5.4 and Table 5.3 for configuration 1 that the maximum displacement was reduced by 28 percent by employing the graphite-epoxy composite fore-arm, even though the loading curves shown in the figure are identical up to the 28 N load. Typically, joint displacements in robotic systems are the principle contributors to the total displacement. Figure 5.5 presents the amounts of arm deflection and joint displacements as tested in the P-50 for configuration 1 with the composite arm. The total displacement results were obtained from the dial gage readings. The deflections due to the stiffness of the arm were determined from the strain readings during the tests, by converting voltage to deflection using the calibration constants determined in Section 4.1. The deflections of the arm increased in a linear fashion, while the joint displacements increased non-linearly.

The total displacements for the composite and aluminum systems increased in similar fashions up to the 28 N load. Under large loads, the aluminum arm displaced significantly more than the composite arm. Hysteresis curves for the other configurations are presented in Figures 5.6, 5.7, and 5.8. The static friction in the joints was overcome upon imposing certain threshold loads, which are different for all robotic systems.

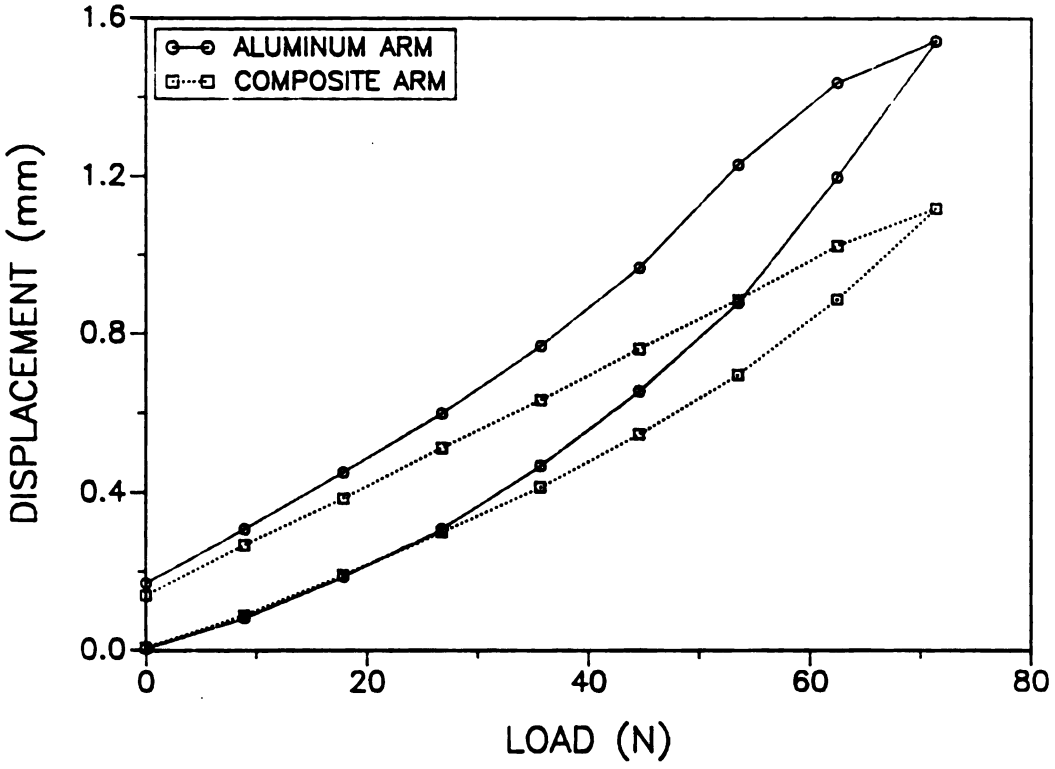

Figure 5.4. Displacement of end-effector due to static loading and unloading. Configuration 1.

Table 5.3. Loading sequence and corresponding displacements for configuration 1 (L = loading, UL = unloading). Averaged over three sequences.

Payload (N)	Displacement (mm)			
	Aluminum		Composite	
	L	UL	L	UL
0.00	0.000	0.165	0.000	0.132
8.92	0.078	0.302	0.083	0.260
17.84	0.183	0.446	0.186	0.378
26.75	0.304	0.595	0.294	0.506
35.67	0.464	0.765	0.408	0.627
44.59	0.653	0.964	0.542	0.756
53.51	0.874	1.225	0.692	0.880
62.43	1.193	1.432	0.881	1.017
71.36	1.537		1.111	

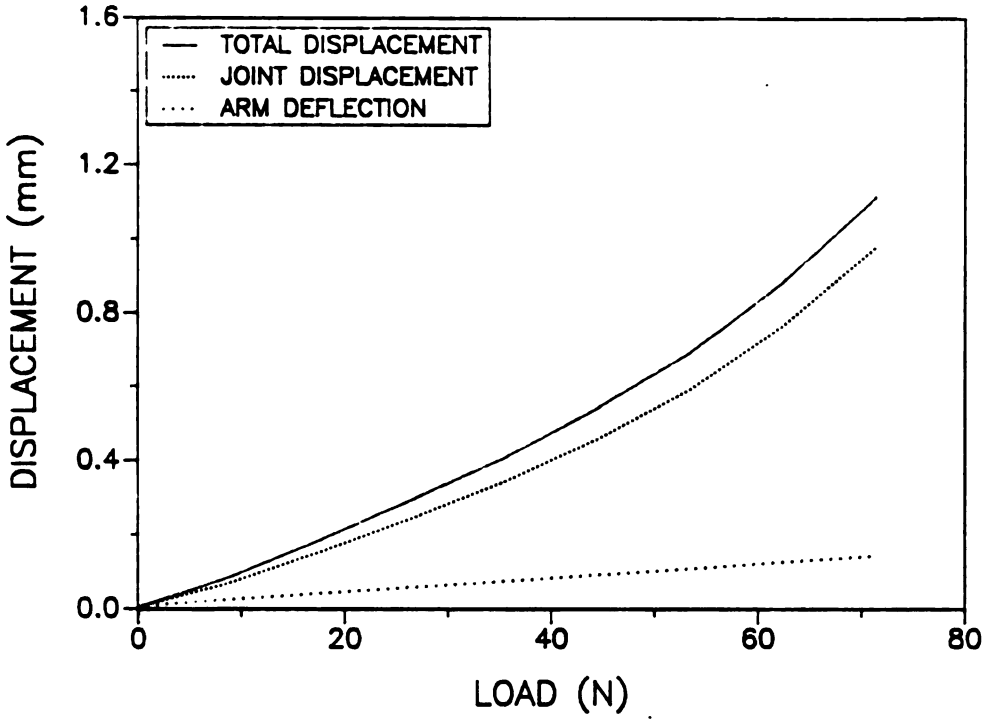

Figure 5.5. Contributions of joint displacement and arm deflection to total end-effector displacement. Configuration 1.

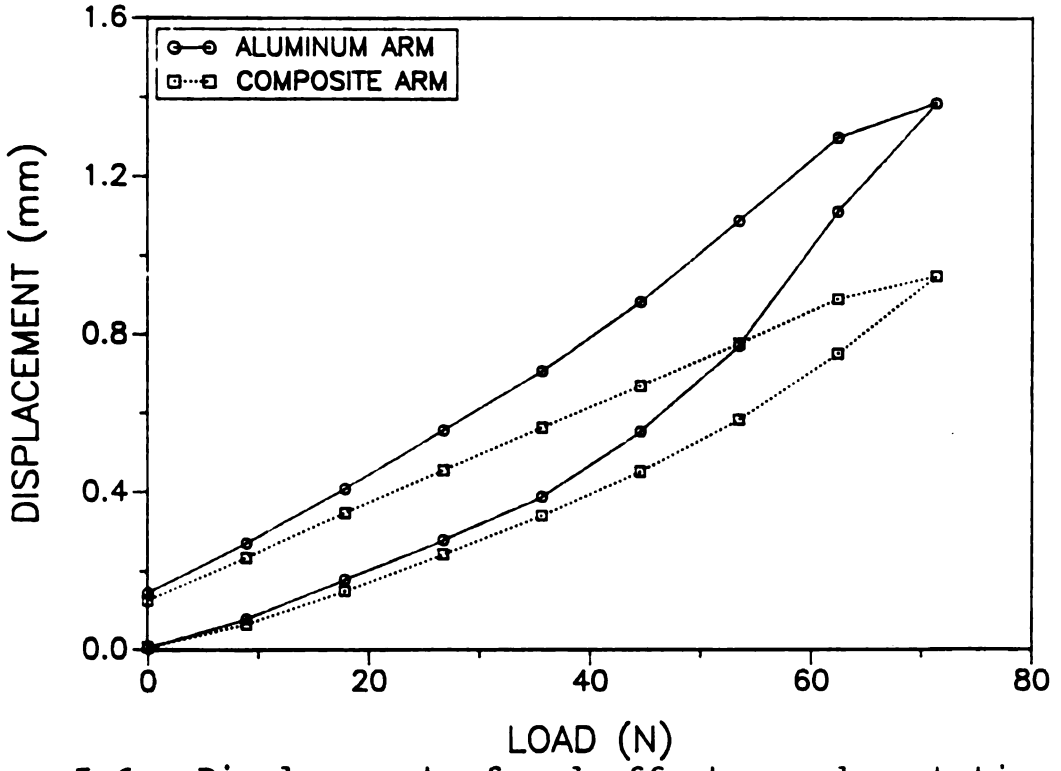

Figure 5.6. Displacement of end-effector under static loading and unloading. Configuration 2.

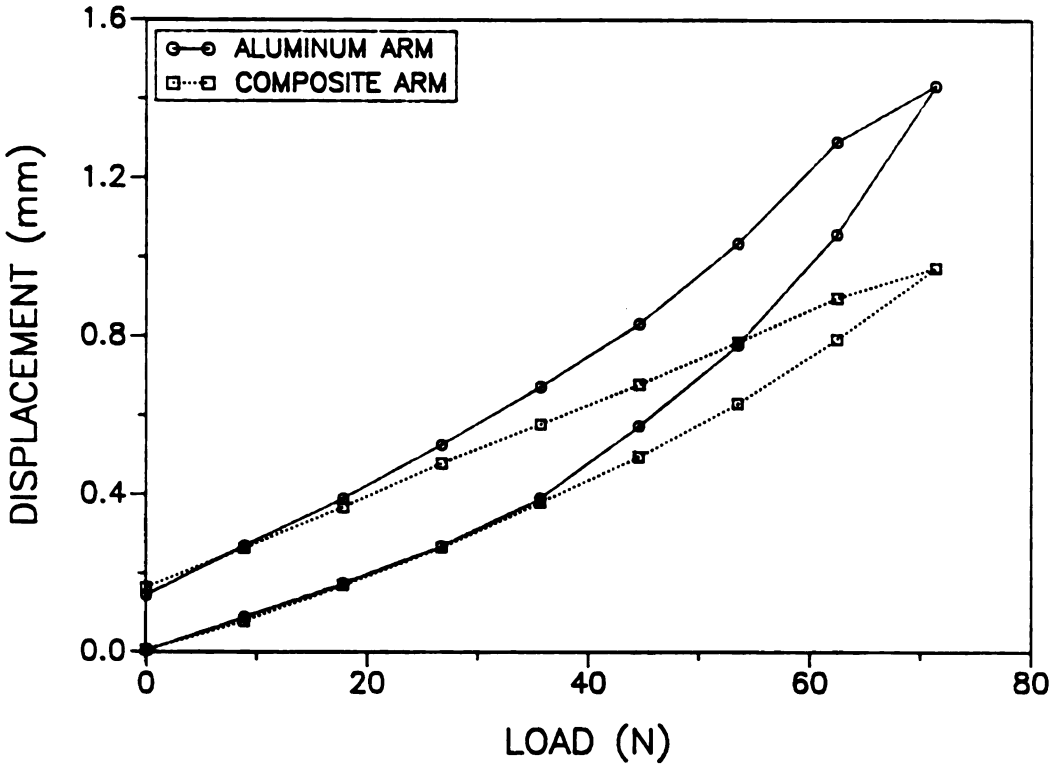

Figure 5.7. Displacement of end-effector under static loading and unloading. Configuration 3.

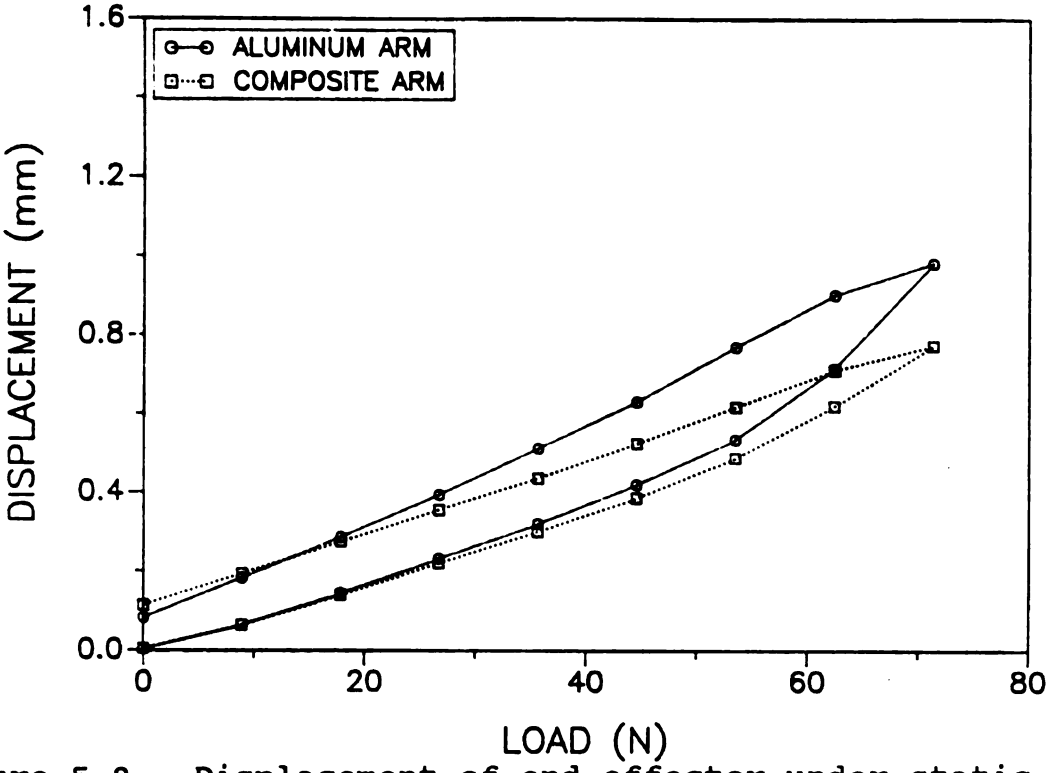

Figure 5.8. Displacement of end-effector under static loading and unloading. Configuration 4.

The P-50 exhibits this effect at a 28 N load for configuration 1. Once again, referring to Figure 5.4, for loads above 28 N, the robot with the aluminum forearm displaced a greater amount than robot with the composite forearm. The maximum displacement values are listed in Table 5.4. The robot with the composite forearm exhibited 30 percent less displacement up to the 70 N maximum load. As mentioned in Section 4.1, the mass of the arm was reduced by 57 percent. In this experiment, the torque on the joints was affected by both the applied load and the mass of the arm. For both cases, the applied load was the same, but mass per unit length of the composite arm was 3.46 kg/m and the mass per unit length of the aluminum arm was 8.13 kg/m. Thus the torques on the joints were larger for the robot with the aluminum arm, which lead to larger displacements.

The reduced total displacement would yield significant advantages for the performance of robotic systems such as

Table 5.4. Maximum deflection for P-50 with aluminum and composite forearms at 71.36 N static load.

	Maximum Deflection (mm)		
Config.	Aluminum	Composite	% Reduction
1	1.537	1.111	28
2	1.381	0.942	32
3	1.430	0.968	32
4	0.979	0.769	21

higher accuracy and higher repeatability. Maximum deviation between the loading and unloading paths was also less for the robot employing the composite arm for all testing configurations (Table 5.5). This result increased the accuracy of the robot; so increased performance was realized by employing the composite arm. It is interesting to observe this characteristic in all configurations.

Table 5.5. Maximum deviation for P-50 with aluminum and composite forearms between loading and unloading paths.

	Maximum Deviation (mm)		
Config.	Aluminum	Composite	% Reduction
1	0.351	0.219	38
2	0.328	0.223	32
3	0.258	0.197	24
4	0.235	0.211	10

5.2 FREQUENCY RESPONSE TESTING

The frequency response experiment was performed on the P-50 robotic system to determine its fundamental frequency of vibration. The fundamental frequency originally determined the bandwidth of the P-50 robot controller. The measured fundamental frequency may provide base-line insight for determining the cut-off frequency used in data filtering.

5.2.1 EXPERIMENTAL APPARATUS AND PROCEDURE

The frequency response was determined using the impulse testing method described in Section 4.2.1. The experimental set-up, presented in Figure 5.9, employed a Hewlett-Packard Model 35660A dynamic signal analyzer to compute the frequency response of the system from inputs of a PCB Piezotronics Model 086B04 impulse force hammer and a B&K Model 4371 accelerometer. The accelerometer was mounted on one side of the forearm next to the end-effector, and the frequency response was obtained by striking the structure on the forearm opposite the accelerometer using the impulse hammer. A considerable striking force was needed to impose proper excitation to the structure, requiring the use of an RTV rubber tip for the impulse hammer. Configurations 1 and 3 were tested, with and without payload.

5.2.2 EXPERIMENTAL RESULTS

The impulse testing method was averaged over ten samples for Configurations 1 and 3 using the RMS averaging process available on the HP signal analyzer. Figures 5.10 to 5.13 represent the frequency response test results for the four configurations. The fundamental frequencies are marked 'x' in the figure. For the first configuration, the P-50 robot had a fundamental frequency of 15.5 Hz, while the P-50 retrofitted with the composite forearm had a

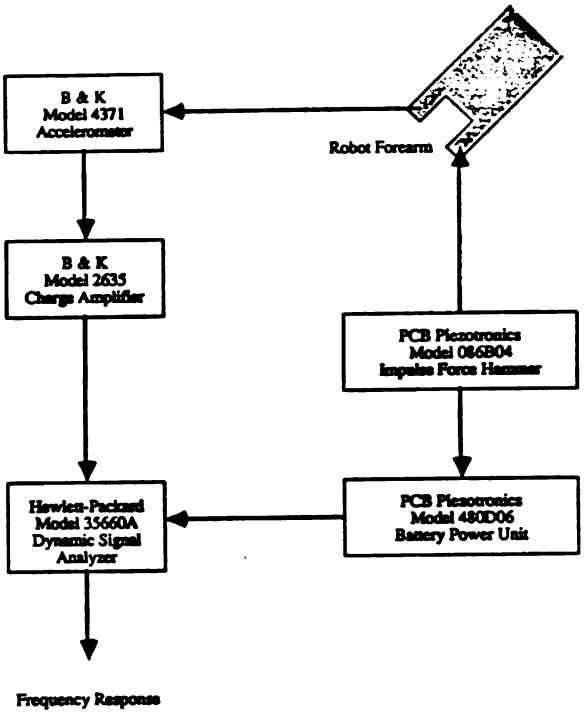

Figure 5.9. Experimental apparatus for frequency response testing.

fundamental frequency of 17.25 Hz. The frequency difference in the two peaks arose because the mass of the composite arm was less than the mass of the aluminum arm. This implied that the robotic system with the composite arm would carry a heavier payload than the original robot while maintaining the same control bandwidth of the system. The fundamental frequencies for various configurations, listed in Table 5.6, indicate only a small dependency on robot configuration, since the values are approximately the same.

Damping ratios were calculated from the frequency response using the half-power bandwidth method (Table 5.7).

The main contributions characteristic of system damping included joint stiffnesses, drive-train compliance, and link mass and compliance. Thus, employing a composite forearm of higher damping would not imply increased damping characteristics of the robotic system. By employing a lighter composite forearm, the damping of the system decreased. Maximum damping occurs with the aluminum arm and maximum payload.

Table 5.6. Fundamental frequencies for the P-50 robot with aluminum and composite forearms from frequency response data.

		Fundamental Frequency (Hz)	
Config.	Payload	Aluminum	Composite
1	0.0 kg	15.50	17.25
3		15.00	17.50
1	7.7 kg	8.75	9.25
3		8.25	10.00

Table 5.7. Damping ratios for the P-50 robot with aluminum and composite forearms from frequency response data.

		Damping Ratio	
Config.	Payload	Aluminum	Composite
1	0.0 kg	0.109	0.061
3		0.066	0.059
1	7.7 kg	0.192	0.125
3		0.142	0.108

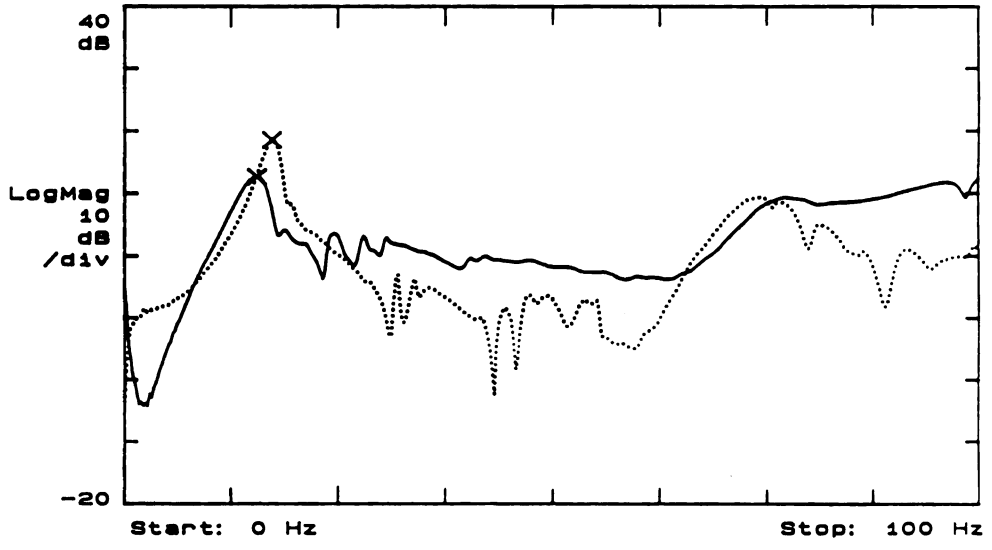

Figure 5.10. Frequency response. Configuration 1, no payload. Solid - aluminum. Dotted - composite.

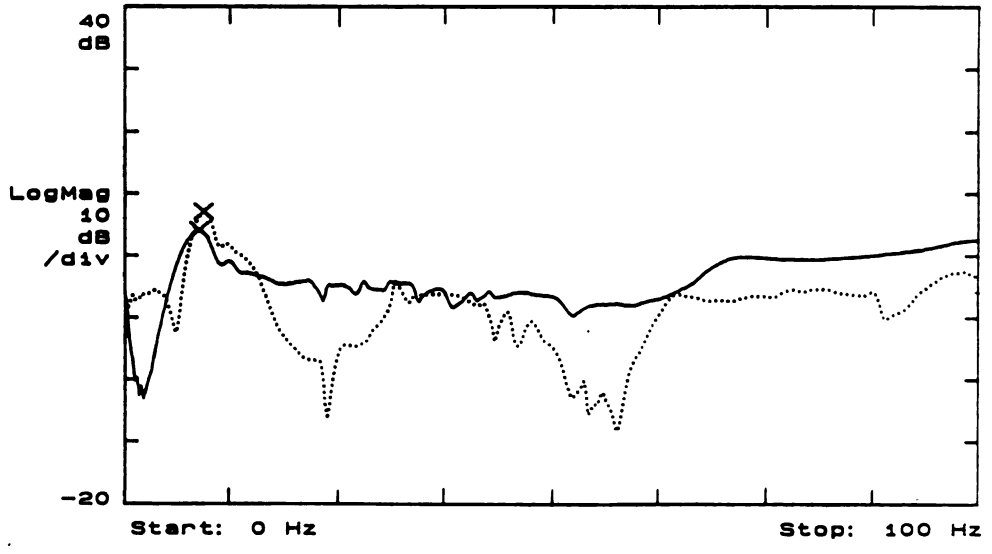

Figure 5.11. Frequency response. Configuration 1, 7.7 kg payload. Solid - aluminum. Dotted - composite.

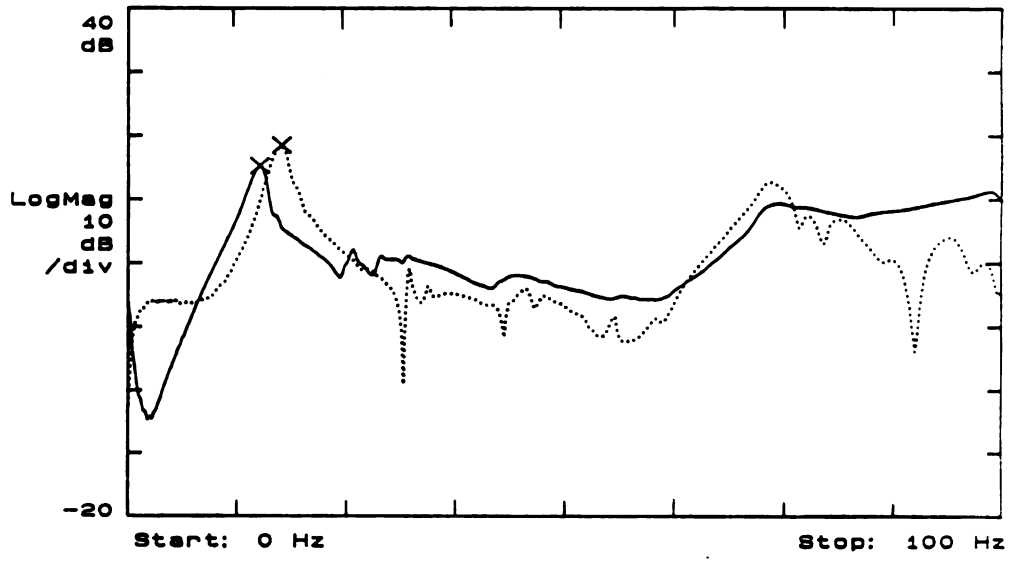

Figure 5.12. Frequency response. Configuration 3, no payload. Solid - aluminum. Dotted - composite.

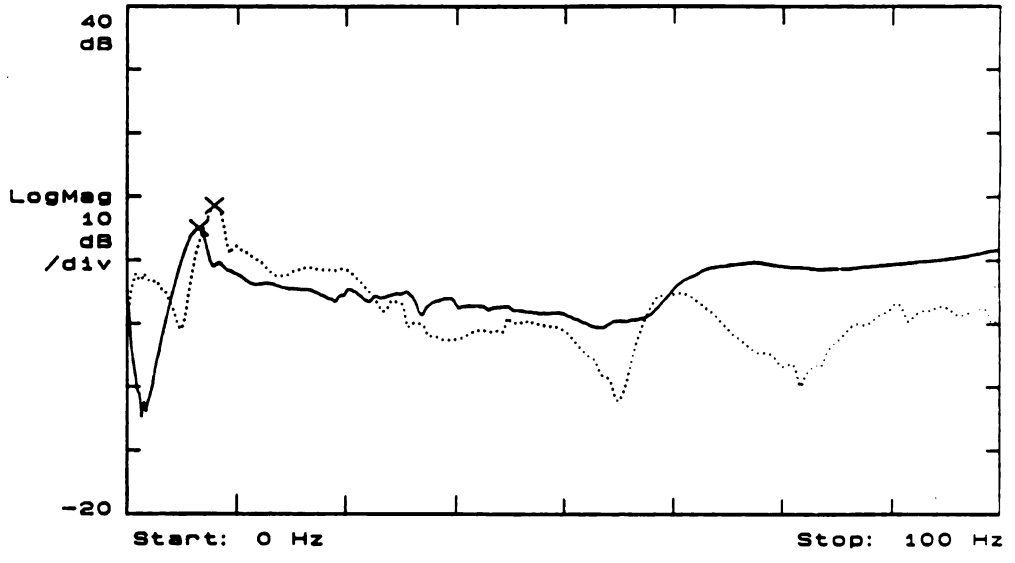

Figure 5.13. Frequency response. Configuration 3, 7.7 kg payload. Solid - aluminum. Dotted - composite.

5.3 TRANSIENT RESPONSE TESTING

The transient response tests determined the fundamental frequencies and damping characteristics for the P-50 robotic manipulator with the P-50 retrofitted with the composite forearm. The test results could be compared with the corresponding frequency response results of Section 5.2, although the frequency response results are much more accurate. In the event that signal analysis equipment would not be available, this method may be used to determine the approximate fundamental frequencies of the robotic system.

5.3.1 EXPERIMENTAL APPARATUS AND PROCEDURE

The test was performed by striking the end-effector by hand while measuring the strain of the forearm using Micro-Measurements Model WD-DY-250BG-350 strain gages in a full-bridge arrangement with a Micro-Measurements Model 2100 strain gage conditioner and amplifier. The strain readings were recorded using a VAXstation II/GPX micro-computer digital data acquisition system. The experimental equipment is diagrammed in Figure 5.14. As in Section 5.2, Configurations 1 and 3 were tested with and without payload.

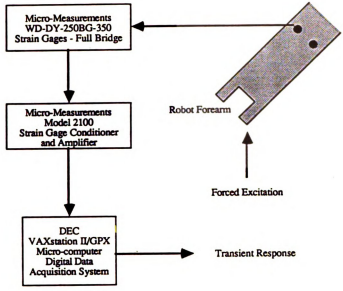

Figure 5.14. Experimental apparatus for transient response testing.

5.3.2 EXPERIMENTAL RESULTS

Figures 5.15 through 5.18 show the transient response data of the P-50 robot and the retrofitted P-50 with the composite arm. Although the fundamental frequencies for configurations with payload were different from the frequency response data by 12 percent, tests without payload in Table 5.8 were within five percent of the values obtained using the frequency analysis. Perhaps through averaging of the transient test results, improved values would be obtained by using this method.

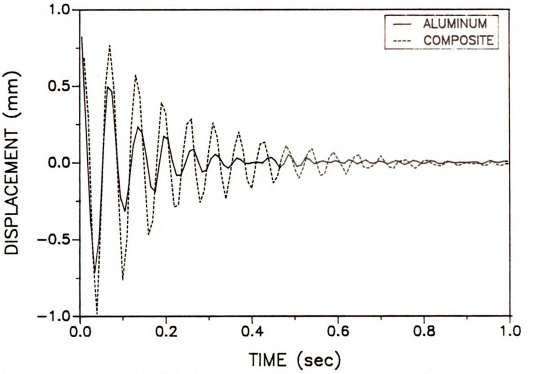

Figure 5.15. Transient response. Configuration 1, no payload.

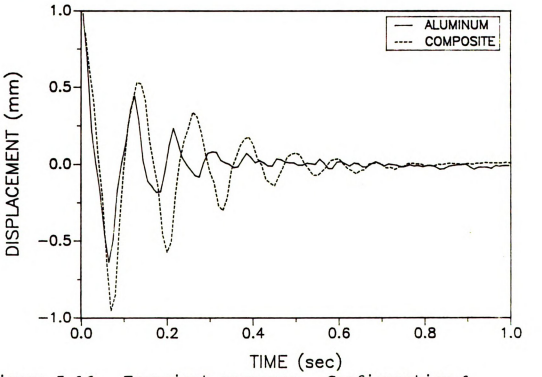

Figure 5.16. Transient response. Configuration 1, 7.7 kg payload.

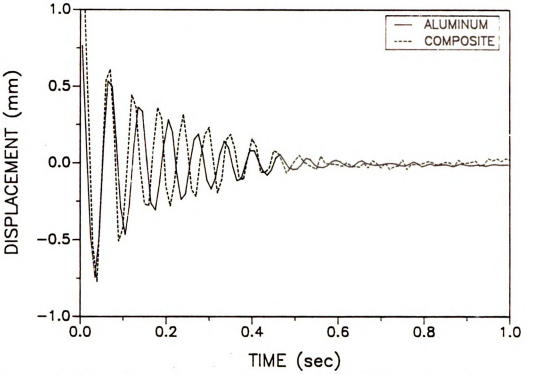

Figure 5.17. Transient response. Configuration 3, no payload.

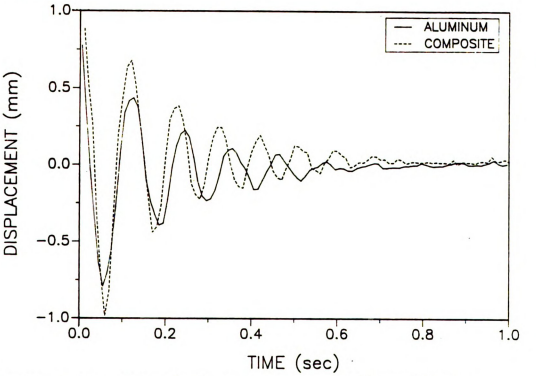

Figure 5.18. Transient response. Configuration 3, 7.7 kg payload.

Table 5.8. Fundamental frequencies for the P-50 robot with aluminum and composite forearms from transient response data.

		Fundamental Frequency (Hz)	
Config.	Payload	Aluminum	Composite
1	0.0 kg	15.5	16.3
3		14.7	17.7
1	7.7 kg	9.7	8.0
3		8.3	9.2

The damping ratios, presented in Table 5.9, were calculated from the logarithmic decrement of the transient response. Differences between Tables 5.7 and 5.9 were as much as 40 percent. The most likely source of error was the transient response of the non-linear behavior which may not have been correctly recorded with the data acquisition system.

Table 5.9. Damping ratios for the P-50 robot with aluminum and composite forearms from transient response data.

		Damping Ratio	
Config.	Payload	Aluminum	Composite
1	0.0 kg	0.094	0.039
3		0.062	0.047
1	7.7 kg	0.129	0.073
3		0.142	0.097

5.4 ANGULAR VELOCITY MEASUREMENTS

The angular velocity measurements were used to verify the testing program maneuvers for proper dwell times and angular positions. The robot tachometers used by the P-50 controller were recorded using the data acquisition system, then converted to angular position and acceleration.

5.4.1 EXPERIMENTAL APPARATUS AND PROCEDURE

Figure 5.19 schematically represents the P-50 controller and robot body. Since the control algorithm was not known, the feedback path was unclear. So the controller was treated as a black-box, with the angular velocity obtained from the servo-drive board within the robot controller. With the VAXstation II/GPX micro-computer digital data acquisition system, the forearm and upper arm velocities were measured for all three test programs of Table 5.2. The SVCT servo controller board was accessed by removing the front cover of the P-50 controller unit. Two Tektronix Model P6105A 10x passive probes were connected in series from the SVCT to the micro-computer. The two probes were used to reduce the controller voltage of more than 100 volts to a measurable range for the data acquisition system.

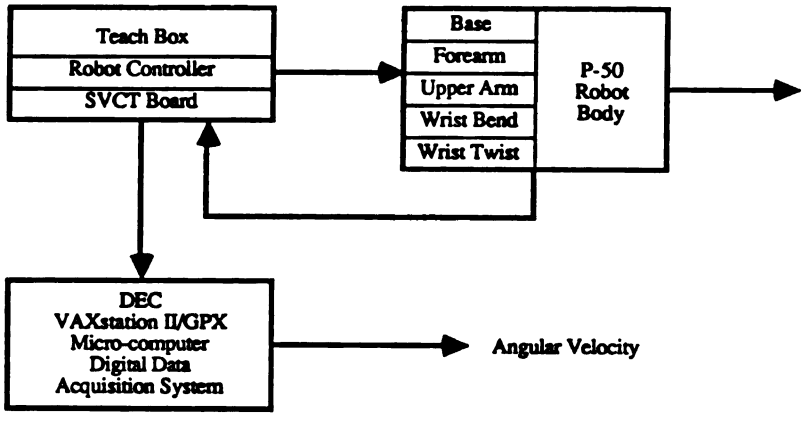

Figure 5.19. Block diagram for obtaining tachometer signals from the SVCT controller board.

5.4.2 EXPERIMENTAL RESULTS

Figure 5.20 presents the angular velocity profiles obtained from test program A for the P-50 robot. Figure 5.21 presents the velocity profiles for the P-50 retrofitted with the composite arm for test program A. Basic similarities were noted between the two figures, although minor differences existed in the sharpness of the corners.

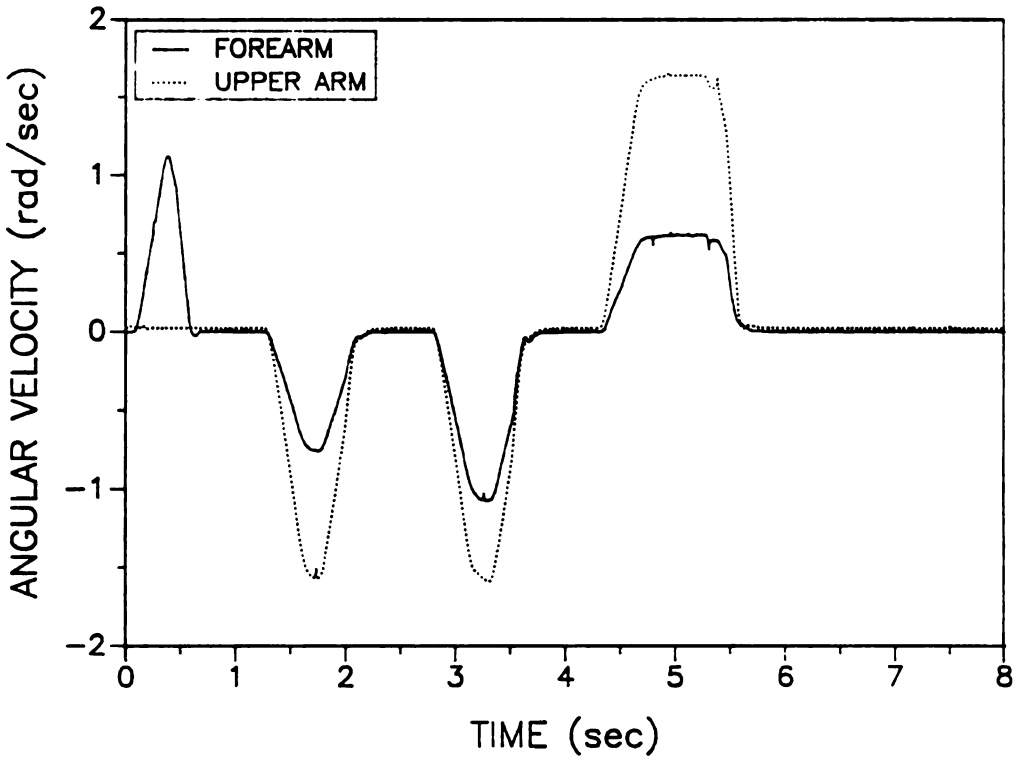

Figure 5.20. Angular velocity obtained from the SVCT controller. Aluminum arm. Test program A.

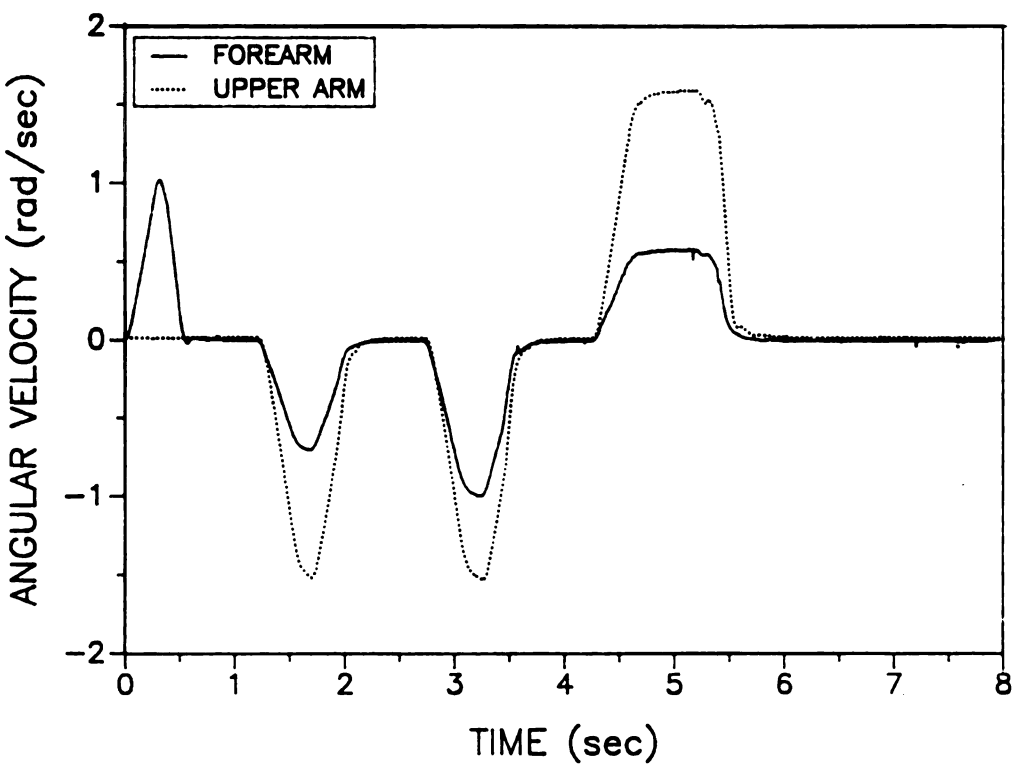

Figure 5.21. Angular velocity obtained from the SVCT controller. Composite arm. Test program A.

Figure 5.22 shows the corresponding angular positions which were obtained by numerically integrating the angular velocity profiles of Figure 5.21 using the trapezoidal integration method. From the angular positions of Figure 5.22, the experimental joint angles and dwell times of 0.8 seconds were found to be in good agreement with the programmed angles and dwell times from Tables 5.1 and 5.2.

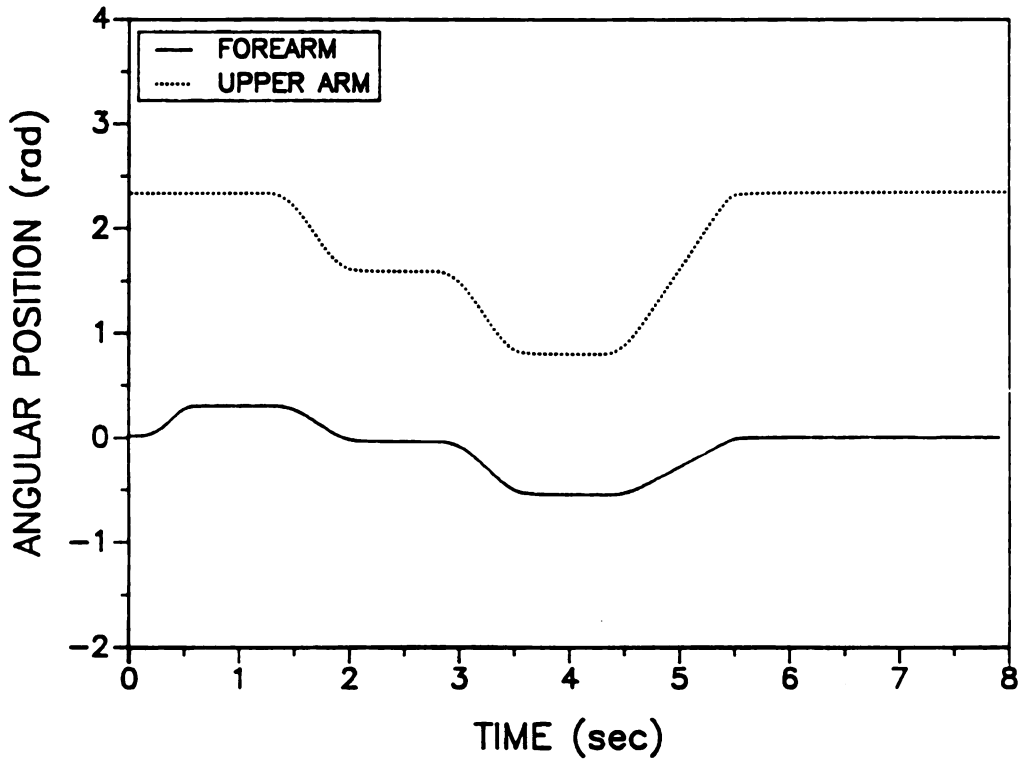

Figure 5.22. Angular position obtained by integrating the angular velocity. Composite arm. Test program A.

The velocities were differentiated using the forward difference method to obtain the angular rigid body acceleration of Figure 5.23. The values of angular position, velocity, and acceleration could also be used to predict the

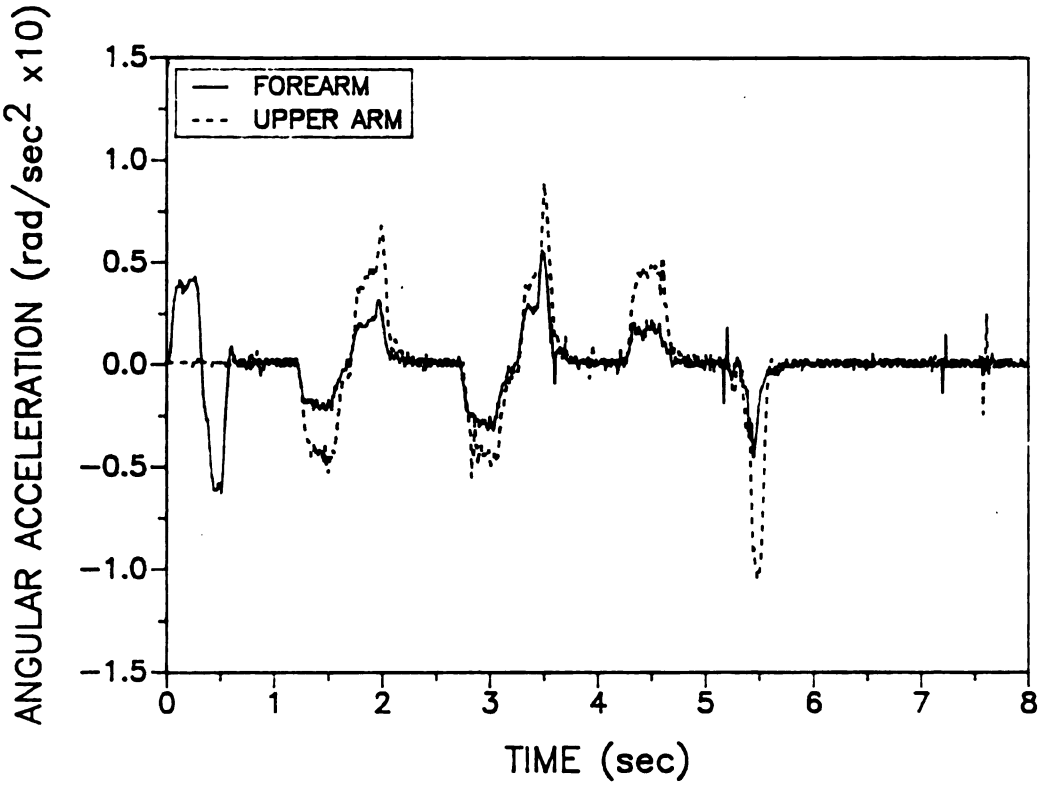

Figure 5.23. Angular acceleration obtained by differentiating the angular velocity. Composite arm. Test program A.

elastodynamic response from the governing equation of motion for the robotic system.

5.5 ACCELERATION TESTING

The objective of the acceleration testing was to compare the acceleration characteristics of the P-50 robot with those of the P-50 retrofitted with the composite forearm. Absolute acceleration may be used to find angular acceleration of the forearm by using the kinematics of the robotic system.

5.5.1 EXPERIMENTAL APPARATUS AND PROCEDURE

The diagram of Figure 5.24 presents the equipment used in the experiment, with both acceleration-time and strain-time components (of Section 5.6) measured simultaneously. The acceleration was measured using a B&K Model 4371 accelerometer and Model 2635 charge amplifier. Strain and acceleration measurement data were recorded using a VAX-station II/GPX micro-computer digital data acquisition system for the three test programs listed in Table 5.2.

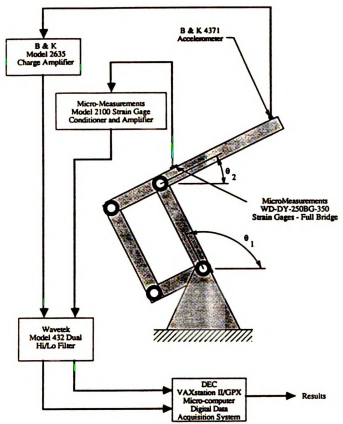

Figure 5.24. Experimental apparatus for acceleration and strain testing.

5.5.2 EXPERIMENTAL RESULTS

The accelerations describing the manipulator response, presented in Figures 5.25, 5.26 and 5.27 were basically the same for the aluminum and composite arms, even though there were small differences in magnitude at certain robot configurations. Thus, the stiffness per unit mass ratio was found not to be the design driver for reducing accelerations. The acceleration data presented may provide information to determine the angular acceleration.

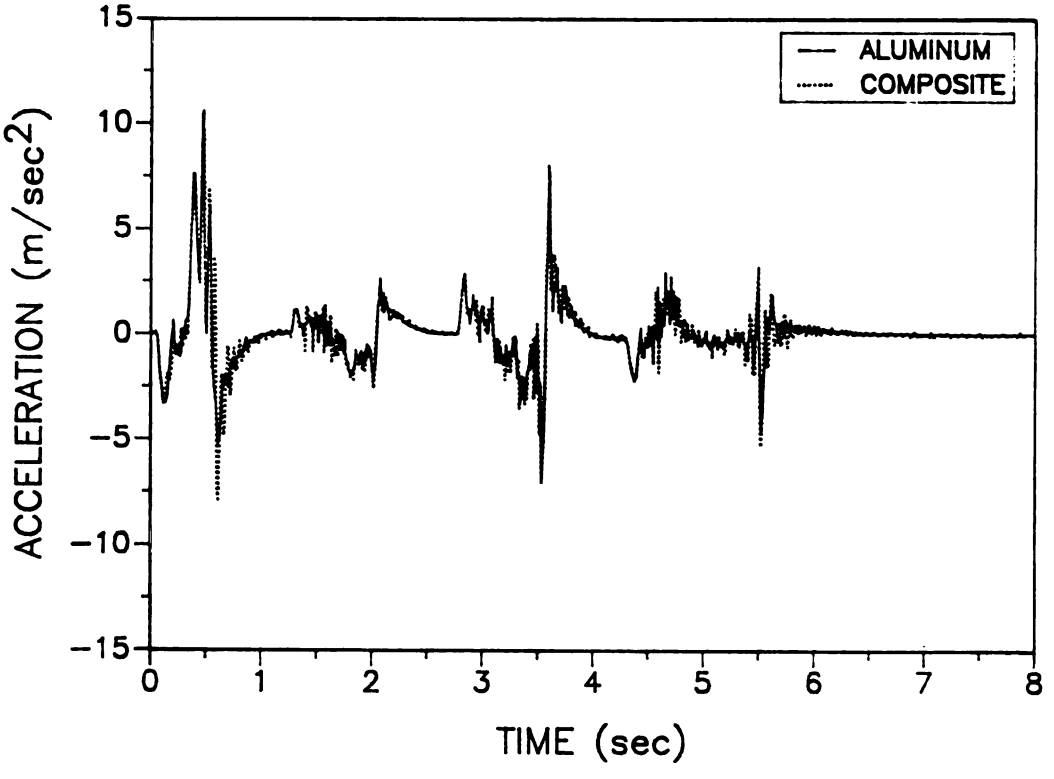

Figure 5.25. Acceleration for test program A.
Speed = 95 cm/s, no payload.

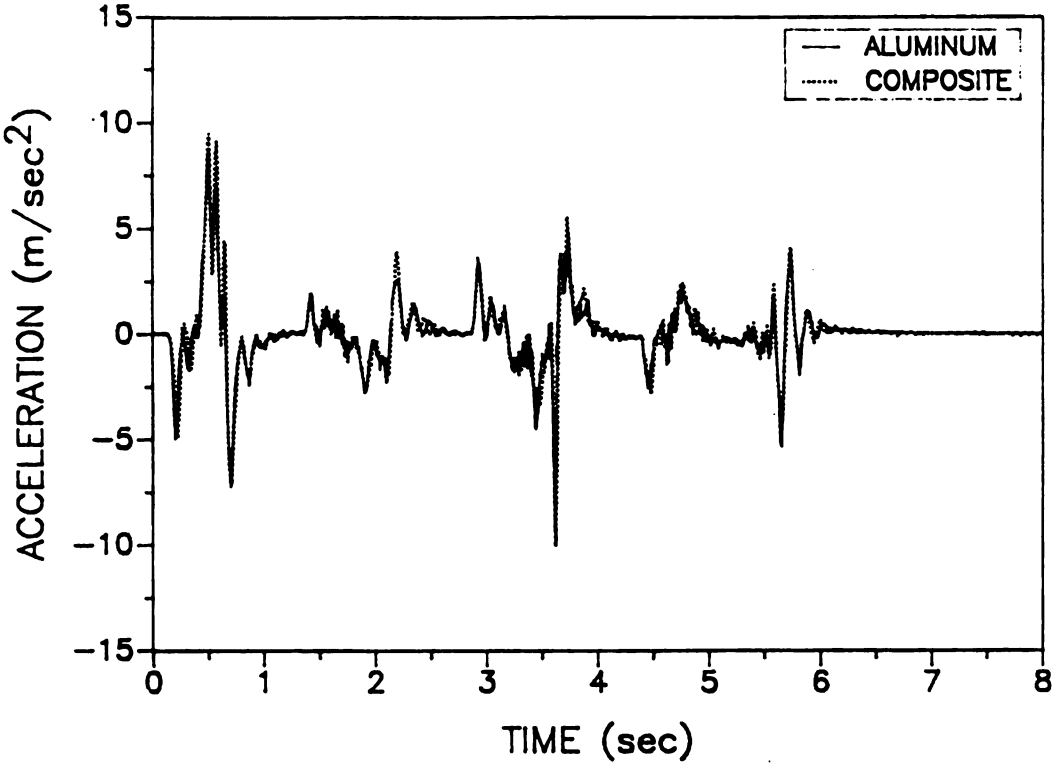

Figure 5.26. Acceleration for test program B.
Speed = 95 cm/s, 7.7 kg payload.

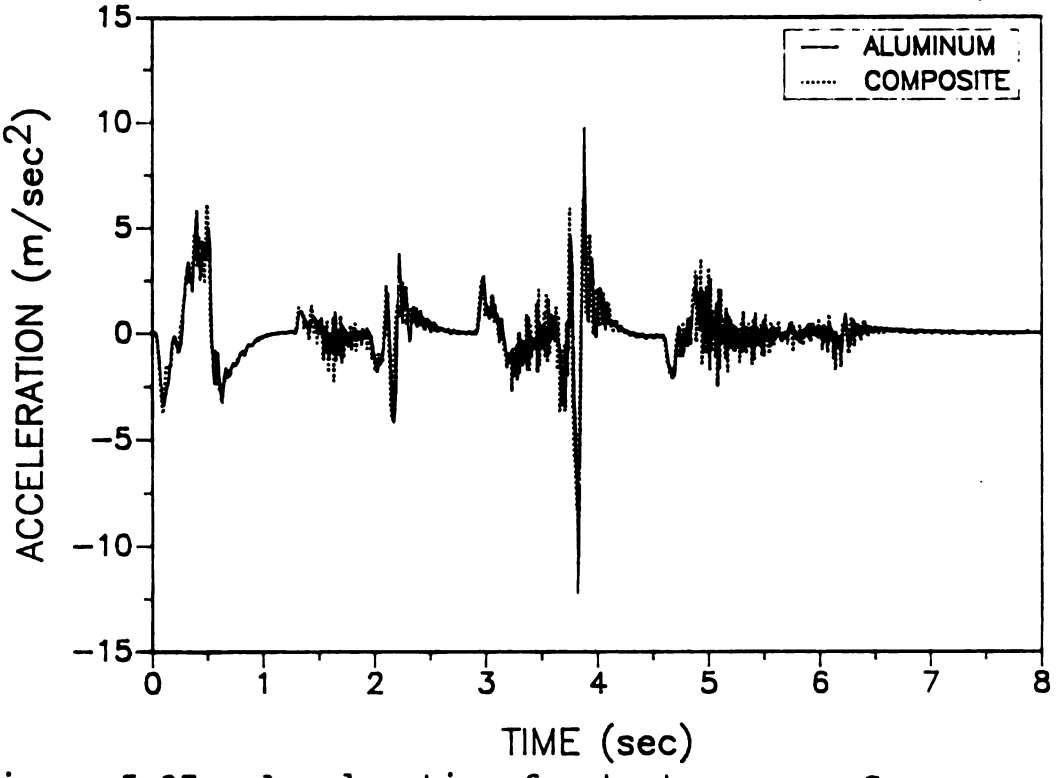

Figure 5.27. Acceleration for test program C.
Speed = 65 cm/s, no payload.

5.6 ELASTODYNAMIC RESPONSE TESTING

The elastodynamic tests were used to evaluate the dynamic behavior of the robotic system. These elastodynamic response tests permit stiffness, damping, and overshoot characteristics to be inferred.

5.6.1 EXPERIMENTAL APPARATUS AND PROCEDURE

The strain test was conducted using Micro-Measurements Model WD-DY-250BG-350 strain gages arranged in a full-bridge configuration located on the arm as in Figure 4.3. The strain signal was amplified using Micro-Measurements Model 2100 strain gage conditioner and amplifier, and recorded simultaneously with the acceleration of Section 5.5 using a VAXstation II/GPX micro-computer digital data acquisition system. The experimental equipment is shown in Figure 5.24. The experiments consisted of the maneuvers of the three test programs listed in Table 5.2.

5.6.2 EXPERIMENTAL RESULTS

Figures 5.28, 5.29, and 5.30 present the results of the strain measurements for the test program. As determined in Chapter 4, the composite forearm possessed 38 percent less effective stiffness. However, by using the composite material, the mass was reduced by 57 percent. The inertial

forces imposed upon the retrofitted P-50 robot were reduced substantially for equivalent elastic deflections of the forearm.

It is seen from the figures that the elastodynamic responses of the two systems were nearly equivalent. For test program B (Figure 5.29), deflections were slightly greater for the composite arm, but the overall responses match. Furthermore, the overshoot and settling-time were nearly identical for both arms. These characteristics were affected by such factors as: the stiffness of the composite arm; the accuracy of the strain calibration factors obtained in Section 4.1; and the chain tension adjustment of the robot during assembly. The figures also provide a

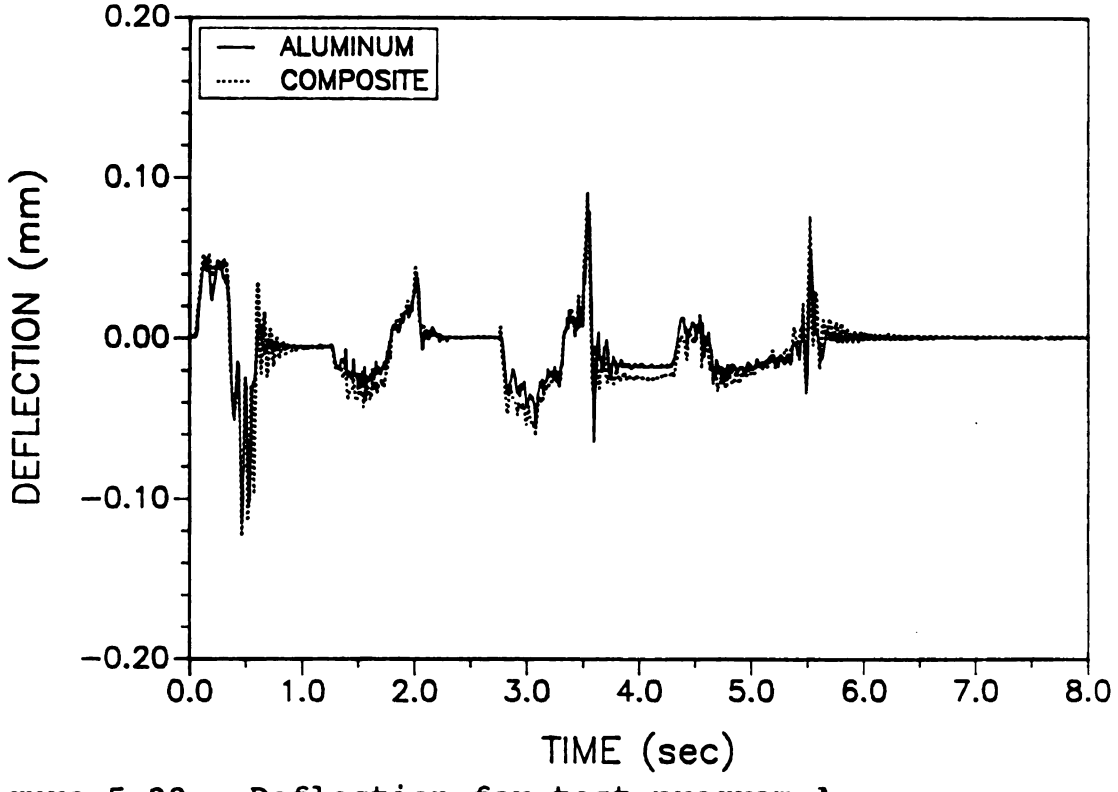

Figure 5.28. Deflection for test program A.
Speed = 95 cm/s, no payload.

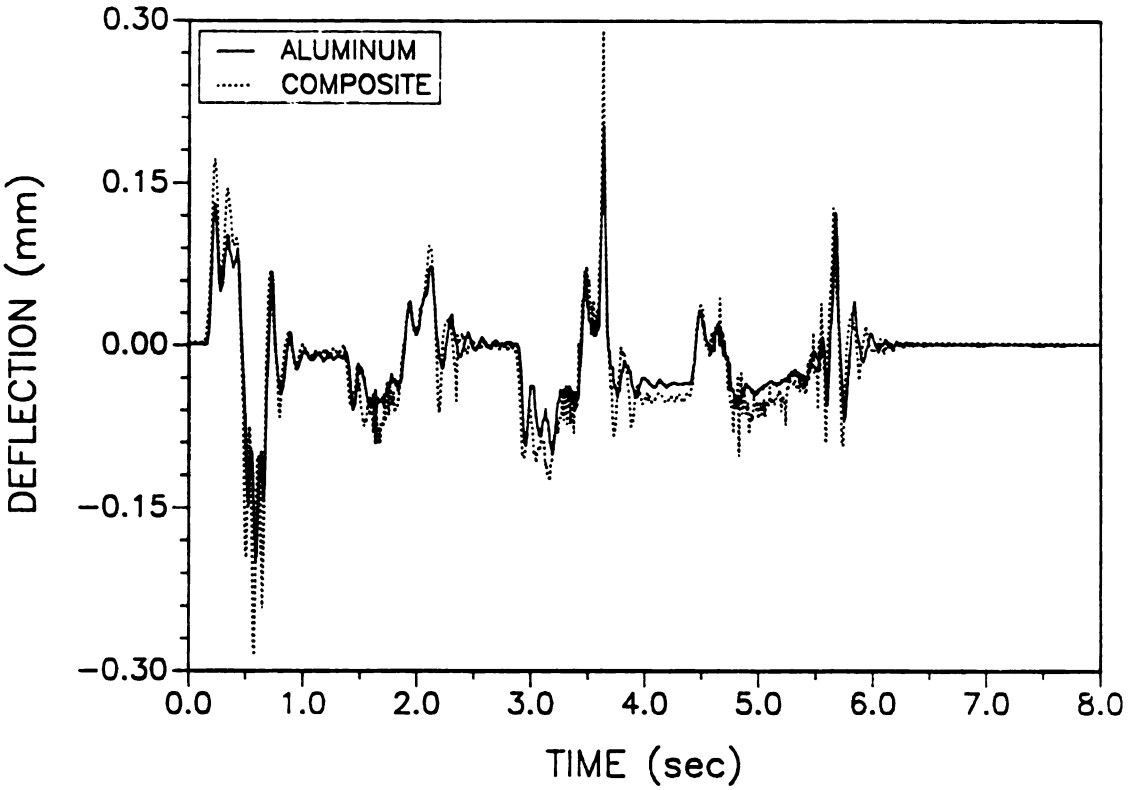

Figure 5.29. Deflection for test program B. Speed = 95 cm/s, 7.7 kg payload.

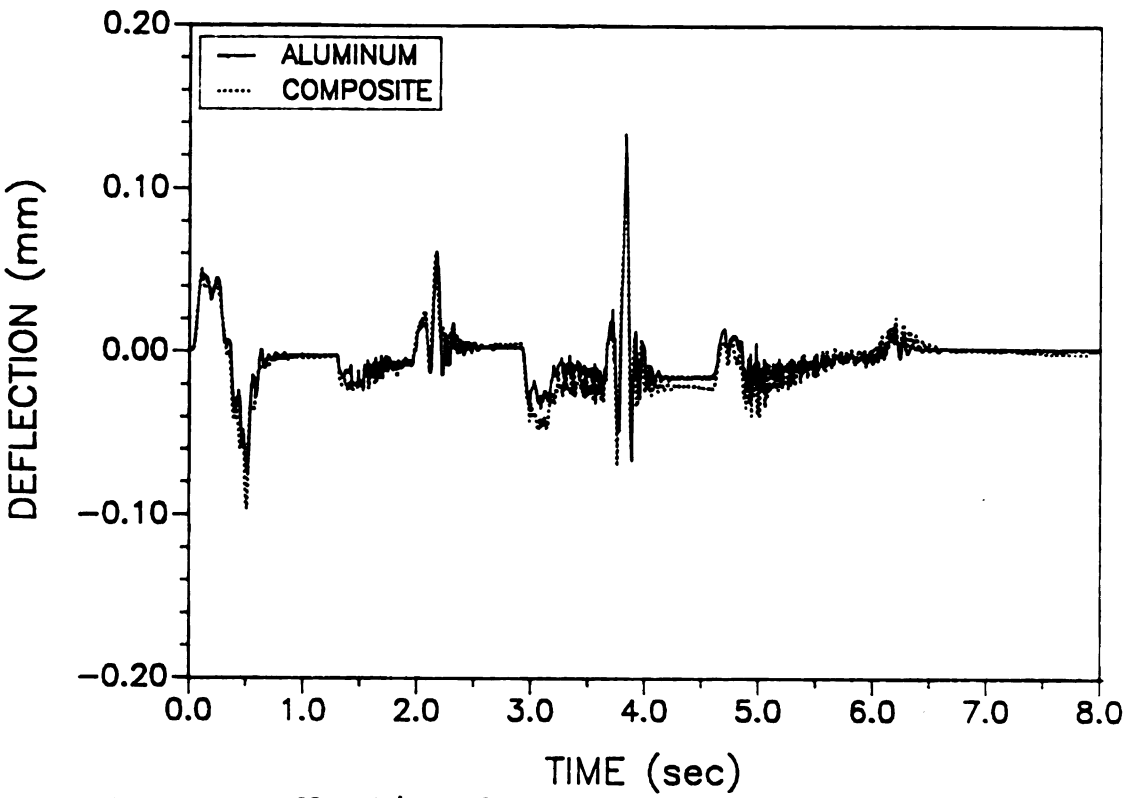

Figure 5.30. Deflection for test program C. Speed = 65 cm/s, no payload.

qualitative measure of the fatigue environment in which the articulating members of robots must operate.

It can be anticipated that if the effective stiffness of the composite arm was the same as the aluminum arm, deflections of the end-effector would be reduced significantly by employing composite materials.

5.7 SUMMARY OF RESULTS

The aluminum and composite arms were installed on the GE P-50 robotic manipulator and the robot systems were tested in both static and dynamic environments. The static tests consisted of hysteresis testing and fundamental frequency testing. The composite forearm exhibited lower hysteresis deviation and less overall deflection upon static loading. The structure with the composite arm also had a greater fundamental frequency over the structure with the original aluminum arm, for configurations with and without maximum payload.

The dynamic tests consisted of test program verification using angular velocity outputs for the forearm and upper arm motions obtained directly from the P-50 controller. Acceleration characteristics between the original P-50 and the retrofitted robot were found to be similar.

Finally, strain curves of the P-50 and the retrofitted P-50 obtained during test program maneuvers were found to have similar characteristics, although the composite arm had 38 percent less effective stiffness and 57 percent less mass than the original aluminum arm.

CHAPTER 6

CONCLUSIONS

A comprehensive study was undertaken to design and fabricate a robot arm for a GE P-50 industrial robotic manipulator from composite materials. The experimental results indicated benefits from implementing the design-for-manufacture approach for employing composite materials. The reduction in weight for the composite forearm was 57 percent without sacrificing any of the dynamic performance in the robotic system. Pay-offs expected from an optimal design of the composite robot arm include reduction of end-effector overshoot and improved settling-times.

6.1 SUMMARY OF RESULTS

The design of the composite robot arm was a process-driven method. Considerations for the constraints of the robotic manipulator were studied, and were maintained in the design of the arm. The use of the finite element method was employed to select the composite laminate sequence required for the lay-up fabrication technique.

The arm was fabricated with graphite-epoxy pre-preg material and autoclave cured. Machining the graphite/epoxy composite arm was an involved project, requiring error-free results.

A comparison between the aluminum and composite arms was completed in isolation tests. The composite arm had 57 percent less mass than the aluminum arm and exhibited a decrease in effective stiffness of 38 percent, predominantly due to the stiffness properties of the cured laminate, which were less than anticipated in the design phase.

The robotic manipulator achieved reduce end-point error due to the lighter mass of the composite arm under static loads. The robotic system employing the composite arm exhibited equivalent dynamic performance during programmed maneuvers with and without maximum payload.

6.2 CONTRIBUTIONS OF STUDY

This pioneering study presented the design and fabrication of an industrial robotic manipulator from composite materials. A comprehensive procedure was followed and documented for the design, analysis, fabrication, and testing. This study provided viable quantification of data for the next generation of industrial robotic manipulators which demand advanced performance properties such as high speed and high accuracy.

6.3 PROBLEMS AND RECOMMENDATIONS

Several problems were encountered in the manufacturing procedure such as the lay-up over the complex geometry of the arm, which did not conform to the finite element model. Also, composite material properties varied between published values and two independent tests performed on composite test panels. Variations may be reduced by performing pre-preg treatment, fabrication, bagging, and cure processes under identical environmental conditions within one facility.

During the experimental testing, the balance of the full-bridge strain gage system was difficult to maintain, most likely due to the high gain of the strain conditioner. The high gain was required for signal amplification for the data acquisition system. The drift may have also been a result of the strain gages bonded to the woven fabric graphite fibers and the epoxy matrix, or of the thermal conductivity of the composite material. A more accurate method for determining the calibration factor for the arm deflection versus strain reading may result in dynamic strain readings which present improvements from using composite materials.

6.4 FURTHER RESEARCH

Automated fabrication should be considered for the composite arm. The fabrication took 50 man-hours to complete; an unacceptable cycle time for high volumes of production. The market for composite arms is large since many earlier generation robotic manipulators with aluminum arms are operating in factories around the world. Since the fabrication of the composite arm in this project was very lengthy, alternative and perhaps highly-automated fabrication methods should be researched to decrease the cycle time of arm fabrication.

Optimal design of the lay-up should be studied, with the anticipation of aligning more fibers along the longitudinal axis of the forearm. By employing an optimal design, the stiffness of the arm (as the objective function) could be increased without altering the mass of the arm. It is anticipated that the pay-offs which accrue from the use of composite materials can be significantly enhanced by optimally selecting the design variables employed in the fabrication of robot arms with composite materials.

The design and fabrication of an entire industrial robotic structure consisting entirely of composite materials should be undertaken. By reducing the weight of the entire structure, advantages such as reduced fixturing, lower noise

levels, and reduced energy consumption become apparent.

The design of a composite robot arm embedding electro-rheological fluids within the layers of the composite member would result in a smart robotic structure capable of responding intelligently to the dynamic demands of the manipulator within the context of the flexible control algorithm.

Composites are excellent materials for dynamic system components which engineers should learn to implement due to the high pay-offs associated with superior dynamic performance. Improvements in the design of the next generation of industrial robotic manipulators can be quantitatively evaluated by reviewing the data presented.

LIST OF REFERENCES

1 S.B. CHOI, M.V. GANDHI, B.S. THOMPSON, C.Y. LEE, "An Experimental Investigation of an Articulating Robotic Manipulator with a Graphite-Epoxy Composite Arm," OSU 10th Annual Conference, Vol. 1, Session 3B, (1987).

2 J.S. ALBUS, "Industrial Robot Technology and Productivity Improvement," Exploration Workshop on the Social Impacts of Robotics: Summary and Issues, Washington, D.C., U.S. Congress, Office of Technology Assessment, Report OTA-BP-CIT-11, pp 62-89, (1982).

3 Computerized Manufacturing Automation: Employment, Education, and the Workplace, Washington, D.C., U.S. Congress, Office of Technology Assessment, Report OTA-CIT-235, pp 77-80, 316-318, (1984).

4 K. SADAMATO, "R & D on Intelligent Robots Being Spurted," The Japan Robot News, Vol. 1, pp 1-6, (1982).

5 F. FUKUCHI and M. AWANE, "Recent Trends and the Future of Hitachi Robots," Hitachi Review, Vol. 34, pp 1-6, (1985).

6 R.M. CHRISTENSEN, "Fiber-Reinforced Composite Materials," ASME Applied Mechanics Reviews, Vol. 38, pp 1267-1269, (1985).

7 W.H. SUNADA and S. DUBOWSKY, "On the Dynamic Analysis and Behavior of Industrial Manipulators with Elastic Members," ASME Journal of Mechanisms, Transmissions and Automation in Design, Vol. 105, pp 42-51, (1983).

8 W.J. BOOK, O. MAIZZA-NETO, and D.E. WHITNEY, "Feedback Control of Two Beam, Two Joint Systems with Distributed Flexibility," ASME Journal of Dynamic Systems, Measurement and Control, Vol. 97, pp 424-441, (1975).

9 F.W. PAUL and F. YOUCEF-TOUMI, Robotics: Theory and Applications, ASME Book DSC-Vol. 3, (1986).

10 R.H. CANNON and E. SCHMITZ, "Initial Experiments on the End-Point Control of a Flexible One-Link Robot," The International Journal of Robotics Research, Vol. 3, pp 61-75, (1984).

11 E. BAYO, "A Finite-Element Approach to Control the End-Point Motion of a Single-Link Flexible Robot," Journal of Robotic Systems, Vol. 4, pp 63-75, (1987).

12 W.J. BOOK, "Recursive Lagrangian Dynamics of Flexible Manipulator Arms," The International Journal of Robotics Research, Vol. 3, pp 87-101, (1984).

13 G.G. LOWEN and C. CHASSAPIS, "The Elastic Behavior of Linkages: An Update," Mechanism and Machine Theory, Vol. 21, pp 33-42, (1986).

14 B.S. THOMPSON and C.K. SUNG, "A Survey of Finite Element Techniques in Mechanism Design," Mechanism and Machine Theory, Vol. 21, pp 351-359, (1986).

15 W.L. CLEGHORN, R.G. FENTON, and B. TABARROK, "Optimum Design of High Speed Flexible Mechanisms," Mechanism and Machine Theory, Vol. 16, pp 399-406, (1981).

16 I. IMAM and G.N. SANDOR, "High-Speed Mechanism Design-A General Analytical Approach," ASME Journal of Engineering for Industry, Vol. 97, pp 609-628, (1975).

17 B.S. THOMPSON and M.V. GANDHI, "The Finite Element Analysis of Flexible Components of Linkage Mechanisms made from Fiber-Reinforced Composite Materials," ASME Paper No. 80-DET-63, (1980).

18 B.S. THOMPSON, "Research Issues in Design: Composite Laminates for Machine Systems," Applied Mechanics Review, Vol. 40, No. 11, (1987).

19 S.B. CHOI, B.S. THOMPSON, and M.V. GANDHI, "Smart Structures Incorporating Electro-Rheological Fluids for Vibration-Control and Active-Damping Applications: An Experimental Investigation," ASME Journal of Vibration, Acoustics, Stress, and Reliability in Design, under review.

20 WALDRON, K.J., "Design of arm," Robotics Encyclopedia, Vol. 1, pp 56-81, (1987).

21 R. VIJAYKUMAR and K.J. WALDRON, "Geometric Optimization of Manipulator Structures for Working Volume and Dexterity," International Journal of Robotics Research, Vol. 5, No. 2, (1986).

22 D. TESAR and M.S. BUTLER, "A Generalized Modular Architecture for Robot Structures," Manufacturing Review, Vol. 2, No. 2, (1989).

23 K.J. WALDRON and J.R. REIDY, "A Study of a Kinematically Redundant Manipulator Structures," 1985 IEEE International Conference on Robotics and Automation, Vol. 1, (1986).

24 G. NAGANATHAN and A.H. SONI, "Coupling Effects of Kinematics and Flexibility in Manipulators," International Journal of Robotics Research, Vol. 6, No. 1, pp 75-84, (1987).

25 H.A. ELMARAGHY and B. JOHNS, "An Investigation into the Compliance of SCARA Robots. Part I: Analytical Model," ASME Journal of Dynamic Systems, Measurement, and Control, Vol. 110, No. 3, pp 18-22, (1988).

26 H.A. ELMARAGHY and B. JOHNS, "An Investigation into the Compliance of SCARA Robots. Part II: Experimental and Numerical Validation," ASME Journal of Dynamic Systems, Measurement, and Control, Vol. 110, No. 3, pp 23-30, (1988).

27 H. KAZEROONI and S. KIM, "Statically-Balanced Direct Drive Robot for Compliance Control Analysis," Modeling and control of Robotic Manipulators and Manufacturing Processes, ASME Book DSC-Vol. 6, pp 193-201, (1987).

28 R.N. STAUFFER, "Robotics Research: What the Labs Might Hold in Store," Manufacturing Engineering, pp 58-64, (1988).

29 D. TESAR, "Thirty-Year Forecast: The Concept of a Fifth Generation of Robotics - The Super Robot," Manufacturing Review, Vol. 2, No. 1, (1989).

30 M.C. LEU, V. DUKOVSKI, and K.K. WANG, "An Analytical and Experimental Study of the Stiffness of Robot Manipulators with Parallel Mechanisms," Robotics and Manufacturing Automation, Vol. 15, pp 137-143, (1985).

31 C.K. SUNG and B.S. THOMPSON, "A Methodology for Synthesizing High-Performance Robots Fabricated with Optimally Tailored Composite Laminates," ASME Journal of Mechanisms, Transmissions, and Design Automation, Vol. 109, No. 1, pp 74-86, March (1987).

32 D.A. SARAVANOS, "Structural Optimum Design of Composite Robotic Manipulators," Ph.D. Thesis, Pennsylvania State University, (1988).

33 B.S. THOMPSON, and M.V. GANDHI, "The Optimally-Tailored Composite Laminate Design of High-Performance Articulating Robotic Systems," Advanced Composites: The Latest Developments, ASM International, pp 15-19, (1986).

34 D.X. LIAO, C.K. SUNG, and B.S. THOMPSON, "The Design of Flexible Robotic Manipulators with Optimal Arm Geometries and Fabricated from Composite Laminates with Optimal Material Properties," International Journal of Robotics Research, Vol. 6, No. 3, (1987).

35 C.K. SUNG, B.S. THOMPSON, P. CROWLEY, and J. CUCCIO, "An Experimental Study to Demonstrate the Superior Response Characteristics of Mechanisms Constructed with Composite Laminates," Mechanism and Machine Theory, Vol. 21, No. 2, (1986).

36 R.B. RAMIREZ, "Design of a High Speed Graphite Composite Robot Arm," ASME Paper No. 84-DET-50, (1984).

37 M.V. GANDHI and B.S. THOMPSON, "The Finite Element Analysis of Flexible Components of Mechanical Systems Using a Bixed Variational Principle," ASME Paper No. 80-DET-64, (1980).

38 W.H. SUNADA and S. DUBOWSKY, "On the Dynamic Analysis and Behavior of Industrial Robotic Manipulators with Elastic Members," ASME Journal of Mechanisms, Transmissions, and Automation in Design, Vol. 105, No. 3, pp 42-51, (1983).

39 D.A. TURCIC and A. MIDHA, "Generalized Equations of Motion for the Dynamic Analysis of Elastic Mechanism Systems," ASME Journal of Dynamic Systems, Measurement, and Control, Vol. 106, No. 6, pp 243-248, (1984).

40 D.A. TURCIC and A. MIDHA, "Dynamic Analysis of Elastic Mechanism Systems. Part I: Applications," ASME Journal of Dynamic Systems, Measurement, and Control, Vol. 106, No. 6, pp 249-254, (1984).

41 D.A. TURCIC, A. MIDHA, and J.R. BOSNIK, "Dynamic Analysis of Elastic Mechanism Systems. Part II: Experimental Results," ASME Journal of Dynamic Systems, Measurement, and Control, Vol. 106, No. 6, pp 255-260, (1984).

42 R. EVANS, and R. SHOURESHI, "Gaining Control over a Manipulator," Mechanical Engineering, Vol. 111, No. 6, pp 76-79, (1989).

43 R.H. CANNON and E. SCHMITZ, "Initial Experiments on the End-Point Control of a Flexible One-Link Robot," Internationl Journal of Robotics Research, Vol. 3, No. 3, pp 62-75, (1984).

44 V. SANGVERAPHUNSIRI and W.J. BOOK, "An Approach to the Minimum Time Control of a Simple Flexible Arm," Robotics Research and Advanced Applications, ASME Booklet, (1982).

45 P.B. USORO, R. NADIRA, and S.S. MAHIL, "Control of lightweight flexible manipulators: a feasibility study," 1984 American Control Conference, Vol. 2, (1984).

46 S.H. WANG, T.C. HSIA, and J.L. WIEDERRICH, "Open-Loop Control of a Flexible Robot Manipulator," International Journal of Robotics and Automation, Vol. 1, No. 2, pp 54-57, (1986).

47 F. MATSUNO, S. FUKUSHIMA, Y. OHSAWA, M. KIYOHARA, and Y. SAKAWA, "Feedback Control of a Flexible Manipulator with a Parallel Drive Mechanism," International Journal of Robotics Research, Vol. 6, No. 4, pp 76-84, (1987).

48 E. NAKANO, "First Approach to the Development of the Patient Care Robot," 11th International Symposium on Industrial Robots, (1981).

49 D.X. LIAO, C.K. SUNG, and B.S. THOMPSON, "The optimal design of symmetric laminated beams considering damping," Journal of Composite Materials, Vol. 20, (1986).

50 C.Y. LEE, B.S. THOMPSON, and M.V. GANDHI, "Temperature-Dependent Dynamic Mechanical Properties of Polymeric Laminated Beams," Journal of Engineering Materials and Technology, Vol. 110, (1988).

51 P.M. GLANCE, "Advances in Computer Aided Engineering Analysis Techniques for the Analysis of Composite Structures," Advanced Composites: The Latest Developments, ASM International, pp 221-227, (1986).

52 G. MENGES, E. SCHMACHTENBERG, and K. KIRBERG, "Techniques to Design, Produce, and Test Composites," Advanced Composites: The Latest Developments, ASM International, pp 163-169, (1986).

53 B.A. WILSON, "Design/Tool/Manufacturing Interfaces," Engineering Materials Handbook: Composites, Vol .1, ASM International, pp 428-431, (1987).

54 K. HUTSON, "High Performance Composite Preform Design," Advanced Composites: The Latest Developments, pp 229-239, (1986).

55 G. MENGES and E. NEISE, "Use of Industrial Robots for Filament Winding," 40th Annual Conference, Reinforced Plastics/Composites Institute, The Society of the Plastics Industry, (1985).

56 W.R. CURRY, "Flat Thermoplastic Tape Laying," Advanced Composites: The Latest Developments, ASM International, pp 45-50, (1986).

57 J.M. MARGOLIS, "Thermoplastics vs. Thermosets Process Economics Aerospace/Aircraft and Automotive Exterior Panels," Advanced Composites: The Latest Developments, ASM International, pp 133-139, (1986).

58 J.V. BUSCH, "Micro-Computer Based Cost Estimation for the SMC Process," Advanced Composites: The Latest Developments, ASM International, pp 141-148, (1986).

59 J.M. MARGOLIS, "Composite Fabricating Economics," Composites in Manufacturing, Vol. 4, No. 1, pp 1-6, (1988).

60 J.D. BUCKLEY, R.L. FOX, and J.R. TYERYAR, "Seam Bonding of Graphite Reinforced Composite Panels," Advanced Composites: The Latest Developments, ASM International, pp 213-216, (1986).

61 R.E. SANDERS, "Bonding Cure Considerations," Engineering Materials Handbook: Composites, Vol. 1, ASM International, pp 702-705, (1987).

62 T.J. REINHART, "Adhesive Bonding Surface Preparation," Engineering Materials Handbook: Composites, Vol. 1, ASM International, pp 681-683, (1987).

63 L.J. HART-SMITH, "Joints," Engineering Materials Handbook: Composites, Vol. 1, ASM International, pp 479-496, (1987).

64 J.L. PHILLIPS, and R.T. PARKER, "Fastener Hole Considerations," Engineering Materials Handbook: Composites, Vol. 1, ASM International, pp 712-715, (1987).

65 R.H. STONE, "Dissimilar Material Separation," Engineering Materials Handbook: Composites, Vol. 1, ASM International, pp 716-719, (1987).

66 J.A. BOLDT, and J.P. CHANANI, "Solid-Tool Machining and Drilling," Engineering Materials Handbook: Composites, Vol. 1, ASM International, pp 667-672, (1987).

67 G. SPUR, and U.E. WUNSCH, "Turning of Fiber-Reinforced Plastics," Manufacturing Review, Vol. 1, No. 2, (1988).

68 M.V. GANDHI, B.S. THOMPSON, and F. FISHER, "Design-for-Manufacture Issues for Composite-Based Components of Articulating Mechanism and Robotic Systems," Trends and Developments in Mechanisms, Machines, and Robotics, DE-Vol. 15-3, Vol. III, pp 105-112, (1988).

69 D. HULL, An Introduction to Composite Materials, Cambridge University Press, (1981).

70 D.L. NELSON, "Structural Composites from RIM Mat Molding," SAE Paper No. 870528, (1987).

71 A.M. SHRIBLEY, Handbook of Composites, Van Nostrand Reinhold Company, (1982).

72 T.J. REINHART, Engineering Materials Handbook: Composites, Vol. 1, ASM International, (1987).

73 M.M. SCHWARTZ, Composite Materials Handbook, McGraw-Hill, (1984).

74 M. GRAYSON, Encyclopedia of Composite Materials and Components, John Wiley & Sons, (1983).

75 S.W. TSAI and H.T. HAHN, Introduction to Composite Materials, Technomic Publishing Company, (1988).

76 R.M. CHRISTENSEN, Mechanics of Composite Materials, John Wiley & Sons, (1979).

77 R.M. JONES, Mechanics of Composite Materials, Scripta Book Company, (1975).

78 J.R. VINSON and R.L. SIERAKOWSKI, The Behavior of Structures Composed of Composite Materials, Kluwer Academic Publishers, (1985).

79 F.M. SWEENEY, Introduction to Reaction Injection Molding, Technomic Publishing Company, (1979).

80 B. MILLER, "Preforms Pave the Way for Lower-Cost Structurals," Plastics World, pp 26-31, January Issue, (1988).

81 L.M. SHEPPARD, "The Revolution of Filament Winding," Metal Progress, Advanced Materials & Processes, (1987).

82 Auto Air Industries, 5640 Enterprise Drive, Lansing, Michigan, 48911.

83 E.J. KUBEL, "A Composites Wish List," Metal Progress, Advanced Materials & Processes, pp 47-54, (1987).

84 R.C. JUVINALL, Fundamentals of Machine Component Design, John Wiley & Sons, (1983).

85 G. KRETSIS, "A Review of the Tensile, Compressive, Flexural, and Shear Properties of Hybrid Fiber-Reinforced Plastics," Composites, Vol. 18, No. 1, (1987).

86 H. FUKUDA, "An Advanced Theory of the Strehgth of Hybrid Composites," Journal of Materials Science, (1983).

87 C. ZWEBEN, "Tensile Strength of Hybird Composites," Journal of Materials Science, (1977).

88 H.D. WAGNER, I. ROMAN, AND G. MAROM, "Hybrid Effects in the Bending Stiffness of Graphite/Glass-Reinforced Composites," Journal of Materials Science, (1982).

89 Hercules Incorporated, Graphite Fibers Business Center, P.O. Box 98, Magna, Utah, 84044.

90 N.J. PAGANO, "Exact Solutions for Composite Laminates in Cylindrical Bending," Journal of Composite Materials, Vol. 3, No. 7, pp 398-411, (1969).

91 J.M. WHITNEY, "Cylindrical Bending of Unsymmetrically Laminated Plates," Journal of Composite Materials, Vol. 3, No. 10, pp 715-719, (1969).

92 S.W. TSAI and E.M. WU, "General Theory of Strength for Anisotropic Materials," Journal of Composite Materials, Vol. 5, No. 1, pp 58-80, (1971).

93 H.J. WARNECKE and R.D. SCHRAFT, Industrial Robots: Applications Experience, IFS Publications Ltd, (1982).

94 F. FISCHER, "The Basis for a Design-for-Manufacture Methodology Pertaining to the Fabrication of a General Electric P-50 Robot Forearm in a Composite Material," Studienarbeit Thesis, Institut fuer Getriebetechnik und Maschinendynamik, RWTH-Aachen, Aachen, West Germany, undertaken in the Machinery Elastodynamics Laboratory, Michigan State University, East Lansing, Michigan, (1987).

95 General Electric P-50 Process Robot - Operators Manual, General Electric Corporation, (1983).

96 J.N. REDDY, An Introduction to the Finite Element Method, McGraw-Hill, (1984).

97 K.J. BATHE and E.L. WILSON, Numerical Methods in Finite Element Analysis, Prentice-Hall, (1976).

98 S.S. RAO, The Finite Element Method in Engineering, Pergamon Press, (1982).

99 Engineering Mechanics Research Corporation, P.O. Box 696, Troy, Michigan, 48099.

100 D.J. NOVOTNY, Technical Communications, NSK Corporation, Bearing Division, P.O. Box 1507, Ann Arbor, Michigan, 48106.

101 D.J. EWINS, Modal Testing: Theory and Practice, Research Studies Press, (1986).

102 W.G. HALVORSEN and D.L. BROWN, "Impulse Testing for Structural Frequency Response Testing," Sound and Vibration, pp 8-21, November, (1977).

103 D. HALLIDAY and R. RESNICK, Fundamentals of Physics, John Wiley & Sons, (1981).